

CHARACTERIZATION OF PGAM5

A Dissertation

presented to

the Faculty of the Graduate School
at the University of Missouri-Columbia

In Partial Fulfillment

of the Requirements for the Degree

Doctor of Philosophy

by

JORDAN WILKINS

Dr. Mark Hannink, Dissertation Supervisor

JULY 2013

The undersigned, appointed by the dean of the Graduate School,
have examined the dissertation entitled
PGAM5 CHARACTERIZATOIN
presented by
Jordan M. Wilkins,
a candidate for the degree of
Doctor of Philosophy of Biochemistry
and hereby certify that, in their opinion, it is worthy of acceptance.

Dr. Mark Hannink

Dr. Steve Alexander

Dr. Brenda Peculis

Dr. Richard Tsika

DEDICATIONS

I want to thank my mother, Jillian. If it were not for my mother, I would not have gotten this far. Mom, thank you for your support and guidance. I owe a lot of my success to you for being such a great mother. I love you mom and thank you for everything. Thank you to my brothers, Joel and Justin, for being supportive and doing what brothers do best, looking out for one another. Grandma Jan and Grandpa Jack, thank you for all the support, love, and encouragement you have given me. To my family, thank you for everything. You have all played a large role in my life and I have been so lucky to have a good family. I love all of you and thank you.

I also want to thank my dearest Fernanda Plucani Amaral for your love and support, for standing by my side, bringing me happiness, and always encouraging me through any situation. I love you and thank you.

To all my close friends, Josh, John, Ala, Jim, Severin, Jamie, Victoria, Laurent, Matt, Raghav, Ying, Carina, Jonathan, Khalid, Mette, Ashutosh, Vinit, Tommi, Bruno, Nick, Tiffinay, Erkan, Geoff, Christina, and my besties on 4 east Maggie and Terri and many more friends. Your friendships have meant a lot to me and made my time here in MO very enjoyable. Thank you.

Thank you to everyone else who did not make it on here but has helped me in the past.

ACKNOWLEDGEMENTS

First I would like to thank my advisor Dr. Mark Hannink. Dr. Hannink has been patient, provided guidance, and imparted knowledge to me that will help me become a successful researcher. One thing I have always appreciated with Dr. Hannink is that our discussions were two ways. Not only did we communicate as friends, but more importantly as scientists. Our meaningful discussions always challenged me to think critically, which is a skill I will always use to my advantage as a researcher in the future. Dr. Hannink, thank you for guiding me through graduate school and for all of your support.

I would also like to thank all of my committee members. Dr. Steve Alexander, Dr. Mike Henzl, Dr. Marc Johnson, Dr. Brenda Peculis, Dr. Peter Tipton, and Dr. Richard Tsika, thank you for taking time out of your busy schedules to provide me with your insight and thoughtful criticism to help shape and guide me towards becoming a better scientist. I have enjoyed all of you serving on my committee and appreciate your commitments to me.

Thank you Dr. Shrikesh Sachdev for all of your help. You were always very willing to help no matter the situation. I have really enjoyed our friendship and I appreciate all the techniques and equipment that you helped train me on. Thank you Dr. Stefan Sarafianos for all of your support and the time you have taken to teach and train me in several techniques and for the use of the equipment in your lab. Thank you Dr. Sam Waters for all of the useful discussions we had and for use of your laboratory equipment. Thank you Jim Bixby for all of your help in the LSC. I have also enjoyed our friendship and all of our conversations.

TABLE OF CONTENTS

| | |
|-----------------------------|-----|
| ACKNOWLEDGEMENTS | ii |
| LIST OF FIGURES | vii |
| LIST OF TABLES | ix |
| LIST OF ABBREVIATIONS | x |
| ABSTRACT | xii |

CHAPTERS

| | |
|---|---|
| 1. INTRODUCTION AND BACKGROUND | 1 |
| 1.1 Generation of mitochondrial reactive oxygen species | |
| 1.2 Mitochondrial membrane potential | |
| 1.3 Control of oxidative stress by NRF2 and KEAP1 | |
| 1.4 Cell death by apoptosis | |
| 1.4.1 Extrinsic pathway | |
| 1.4.2 Intrinsic pathway | |
| 1.4.3 Control of mitochondrial membrane permeability | |
| 1.5 Necrosis | |
| 1.6 Autophagy | |
| 1.7 Mitochondrial fusion | |
| 1.7.1 Mitofusins | |
| 1.7.2 Optic atrophy 1 | |
| 1.8 Mitochondrial fission | |
| 1.8.1 Dynamin-related protein 1 | |
| 1.8.2 DRP1 recruitment to mitochondria | |

| | |
|--|----|
| 1.9 Mitochondrial movement | |
| 1.9.1 Mitochondrial anterograde transport along microtubules | |
| 1.9.2 Mitochondrial retrograde movement along microtubules | |
| 1.9.3 Transport along actin cables | |
| 1.10 Phosphoglycerate mutase 5 review | |
| 1.10.1 PGAM5 is targeted by KEAP1 for degradation | |
| 1.10.2 PGAM5 activation of ASK1 | |
| 1.10.3 PGAM5 alleviates symptoms of Parkinson's disease in flies | |
| 1.10.4 PGAM5 in apoptosis | |
| 1.10.5 PGAM5 in necrosis | |
| 1.11 Summary of chapters | |
| 1.11.1 Chapter 2 - PGAM5 crystallization | |
| 1.11.2 Chapter 3 - Multimerization of PGAM5 is necessary for PGAM5 phosphatase activity and mitochondrial morphology | |
| 1.11.3 Chapter 4 - PGAM5 gene-trap mice: Microarray analysis and characterization | |
| 2. CRYSTALLIZATION OF PGAM5 | 24 |
| 2.1 Purification of PGAM5 protein | |
| 2.2 Phosphatase activity of PGAM5 proteins | |
| 2.3 Solubility of PGAM5 proteins | |
| 2.4 Crystallization of Δ N89-PGAM5 | |
| 2.5 Crystallization of Δ N49-PGAM5 | |
| 2.6 Crystallization of Δ N30-dPGAM5 | |
| 2.7 Crystallization of drosophila selenomethionine-PGAM5 | |

| | |
|---|----|
| 2.8 Optimization of SEM-dPGAM5 | |
| 2.9 Cryoprotectants and x-ray diffraction of SEM-dPGAM5 | |
| 2.10 X-ray diffraction of SEM-dPGAM5 crystals using the dry method | |
| 2.11 Discussion | |
| 3. MULTIMERIZATION OF PGAM5 IS NECESSARY FOR PGAM5 PHOSPHATASE ACTIVITY AND MITOCHONDRIAL MORPHOLOGY | 51 |
| 3.1 Characterization of PGAM5's phosphatase activity | |
| 3.2 PGAM5's N-terminus is required for phosphatase activity | |
| 3.3 The conserved WDxNWD motif is required for PGAM5's phosphatase activity | |
| 3.4 PGAM5 multimerization requires the WDxNWD motif | |
| 3.5 Two populations of PGAM5 exists in MEFs | |
| 3.6 A4-PGAM5 causes mitochondrial fragmentation | |
| 3.7 Discussion | |
| 4. PGAM5 GENE-TRAP MICE: MICROARRAY ANALYSIS AND CHARACTERIZATION | 73 |
| 4.1 Generation and characterization of a mouse containing a gene-trap disruption in the PGAM5 locus. | |
| 4.1.1 Gene trap vectors are tools for generation of loss of function mutations. | |
| 4.1.2 Characterization of a gene-trap insertion into the mPGAM5 locus | |
| 4.1.3 An intact PGAM5 locus is required for embryonic development in the mouse | |
| 4.1.4 Genotype analysis of embryos | |
| 4.2 Generation and characterization of a PGAM5-deficient mouse embryo fibroblast cell line | |
| 4.2.1 Identification of a PGAM5-deficient mouse embryo fibroblast cell line | |

| | |
|---|-----|
| 4.2.2 Reconstitution of PGAM5 expression into the MEF 666A cell line | |
| 4.2.3 PGAM5-deficient cells have increased sensitivity to staurosporine-induced apoptosis | |
| 4.3 Identification of genes and pathways that are differentially regulated in PGAM5-deficient mouse embryo fibroblasts | |
| 4.3.1 Microarray analysis to identify genes that are differentially expressed in PGAM5-deficient mouse embryo fibroblasts | |
| 4.3.2 Identification of genes that are differentially expressed between the MEF 666 A and MEF 666 B cell lines | |
| 4.3.3 Analysis of differential gene expression using DAVID | |
| 4.4 Discussion | |
| 5. DISCUSSION | 98 |
| 5.1 Summary of the key findings of this dissertation | |
| 5.2 Involvement of PGAM5 in cell death pathways | |
| 5.2.1 PGAM5 and necrosis | |
| 5.2.2 PGAM5 in apoptosis | |
| 5.2.3 PGAM5 in autophagy/mitophagy | |
| 5.3 Future directions | |
| MATERIALS AND METHODS..... | 111 |
| REFERENCES | 118 |
| VITA | 131 |

LIST OF FIGURES

| | Page |
|--|------|
| Figure 2.1: HIS-PGAM5 constructs | 26 |
| Figure 2.2: Purification of PGAM5 by FPLC..... | 27 |
| Figure 2.3: Crystallization of ΔN30-dPGAM5 using MbClass Suite I..... | 34 |
| Figure 2.4: Crystallization of ΔN30-dPGAM5 at 8mg/ml..... | 35 |
| Figure 2.5: Comparison of ΔN30-dPGAM5 and SEM-PGAM5 crystallization | 37 |
| Figure 2.6: Optimized conditions for MbClassII-71..... | 39 |
| Figure 2.7: Crystallization of SEM-dPGAM5 with Additive screen..... | 40 |
| Figure 2.8: Crystals used for screening cryoprotectants and x-ray diffraction..... | 44 |
| Figure 2.9: Crystallization of SEM-dPGAM5 using JBScreen | 45 |
| Figure 2.10: Diagram depicting dry method..... | 46 |
| Figure 2.11: Diffraction of SEM-dPGAM5 crystals using dry method..... | 47 |
| Figure 3.1: N-terminally truncated PGAM5 proteins | 57 |
| Figure 3.2: Phosphatase activity of truncated PGAM5 | 58 |
| Figure 3.3: Phosphatase activity of PGAM5 against BCL-XL in cells | 59 |
| Figure 3.4: Alignment of PGAM5 WDxNWD motif across various species..... | 60 |
| Figure 3.5: PGAM5 exists as a multimeric complex..... | 62 |
| Figure 3.6: Molar mass determination of PGAM5 complexes..... | 63 |
| Figure 3.7: PGAM5 exists in two distinct pools in MEFs..... | 65 |
| Figure 3.8: PGAM5 multimerization is required for proper mitochondrial morphology..... | 67 |
| Figure 4.1: Gene disruption by gene-trap | 76 |
| Figure 4.2: The mPGAM5 locus..... | 79 |
| Figure 4.3: Genotyping results of MEF cell lines..... | 83 |
| Figure 4.4: PGAM5 protein levels in MEF cell lines | 84 |

| | |
|--|----|
| Figure 4.5: MEF A cells do not express detectable levels of the wild-type PGAM5 transcript | 84 |
| Figure 4.6: Reconstitution of PGAM5 expression..... | 85 |
| Figure 4.7: Cell death assay | 86 |
| Figure 4.8: Caspase 3/7 activity during staurosporine-induced cell death | 87 |
| Figure 4.9: Scatter plot of genes differentially expressed in MEF 666A vs MEF 666B cells | 89 |
| Figure 4.10: Purine metabolism..... | 92 |
| Figure 4.11: Focal adhesion pathway | 93 |

LIST OF TABLES

| | Page |
|---|------|
| Table 2.1: Phosphatase activity of PGAM5 | 29 |
| Table 2.2: Crystallization screens used in crystal trials with Δ N89-PGAM5 | 30 |
| Table 2.3: Summary of results for Δ N89-PGAM5 crystal trials..... | 31 |
| Table 2.4: Screens tested against Δ N49-PGAM5 | 32 |
| Table 2.5: Crystal trials using Δ N30-dPGAM5 with various screens | 35 |
| Table 2.6: Optimization of MbClass II solution 71 | 38 |
| Table 2.7: Crystallization of SEM-dPGAM5 | 42 |
| Table 2.8: Comparison of MbClassII-71 with PEGII-28 | 43 |
| Table 2.9: Cryoprotectants tested with crystals | 45 |
| Table 3.1: Kinetic parameters of PGAM5 phosphatase activity against model phosphopeptides..... | 54 |
| Table 3.2: Kinetic parameters of PGAM5 phosphatase activity against candidate substrates | 54 |
| Table 4.1: Primer sets used to genotype PGAM5 gene-trap mice..... | 79 |
| Table 4.2: Genotype results in a mixed C57/129 background..... | 80 |
| Table 4.3: Genotype results in a 129 background | 81 |
| Table 4.4: Genotyping results of embryos derived from het x het matings | 82 |
| Table 4.5: Up regulated pathways in MEF 666 A | 91 |
| Table 4.6: Up regulated genes involved in purine metabolism | 92 |
| Table 4.7: Down regulated genes in MEF 666A | 92 |
| Table 4.8: Down regulated genes in focal adhesion pathway | 93 |

LIST OF ABBREVIATIONS

ROS: Reactive Oxygen Species

ARE: Antioxidant Responsive Element

NRF2: Nuclear factor erythroid 2-Related Factor 2

KEAP1: Kelch-like ECH-Associated Protein 1

CUL3: Cullin 3

BTB: Bric-a-brac

DISC: Death-Inducing Signaling Complex

TNF α : Tumor Necrosis Factor –alpha

TNFR: Tumor Necrosis Factor Receptor

DD: Death Domain

FADD: Fas-Associated protein with Death Domain

DED: Death Effector Domain

IMS: Inter Membrane Space

APAF1: Apoptotic Protease-Activating Factor 1

CARD: Caspase-Recruitment Domain

MMP: Mitochondrial Membrane Permeability

OMM: Outer Mitochondrial Membrane

TRADD: TNFR1- Associated Death Domain

RIPK1: Receptor-Interacting Ser/Thr Kinases 1

RIPK3: Receptor-Interacting Ser/Thr Kinases 3

TRAF2: TNFR-Associated Factor 2

PINK1: PTEN Induced Putative Kinase 1

PARKIN: Parkinson protein 2

MTS: Mitochondrial Targeting Sequence

MPP: Mitochondrial Processing Protease

PARL: Presenilins-Associated Rhomboid-Like

CCCP: Carbonyl Cyanide 3-Chlorophenylhydrazone

MFN 1: or 2: Mitofusin 1 or 2

OPA1: Optic Atrophy 1

DRP1: Dynamin Related Protein 1

MEF: Mouse Embryonic Fibroblasts

ASK1: Apoptosis Signaling Kinase 1

SEC: Size Exclusion Chromatography

ABSTRACT

Programmed cell death (PCD) is a naturally occurring event that is highly regulated and required for normal development. The protein phosphoglycerate mutase 5 (PGAM5) has been implicated in apoptosis, necrosis, and autophagy of mitochondria, known as mitophagy. However, the mechanisms by which PGAM5 contributes to cell death are poorly understood. In this dissertation, we provide new insight into the function and regulation of PGAM5 and how PGAM5 may be contributing to cell death. Current models suggest that PGAM5 promotes cell death via necrosis and apoptosis. Our data, however, suggests that PGAM5 is necessary for development and protects cells from apoptosis. Our studies in mice demonstrate that disruption of the PGAM5 gene is embryonic lethal. We derived PGAM5-deficient mouse embryonic fibroblasts (MEFs) from a heterozygous mouse containing one disrupted PGAM5 allele. PGAM5-deficient MEFs were more prone to staurosporine-induced cell death, which was accompanied by a two-fold increase in caspase activity when compared to wild-type MEFs. Reconstitution of PGAM5 in PGAM5-deficient MEFs increased their resistance to cell death. These data provide evidence that PGAM5 is protecting the cells from apoptosis. Furthermore, we discovered a highly conserved WDxNWD motif across various species of PGAM5 protein, which we demonstrate is necessary for both the phosphatase activity of PGAM5 and normal mitochondrial morphology. Mutation of the WDxNWD motif abolished PGAM5's phosphatase activity, while overexpression in cells of PGAM5 with mutations in the WDxNWD motif caused fragmentation of mitochondria. We show that PGAM5 forms a multimeric complex, which is necessary for phosphatase activity. Multimerization of PGAM5 is disrupted when mutations are made within the WDxNWD motif. Taken together, we suggest that multimerization of PGAM5 is required for PGAM5's phosphatase activity and maintaining normal mitochondrial morphology, while disruption of the PGAM5 complex inactivates PGAM5's phosphatase activity, leading to fragmentation of mitochondria, and ultimately cell death by apoptosis.

Chapter 1

Introduction and background

The topic of this dissertation is PGAM5. PGAM5 is a member of the phosphoglycerate mutase family of enzymes, several of which are well known for their roles in metabolism. PGAM5, however, is a poorly characterized protein that does not appear to be a metabolic enzyme. Work in our lab and other labs have provided evidence that PGAM5 is a mitochondrial localized protein with possible functional roles in mitochondrial reactive oxygen species production, apoptosis, necrosis, and mitophagy.

Mitochondria are essential organelles that participate in metabolism, signaling, ATP production, calcium homeostasis, and apoptosis. Mitochondria undergo cycles of fission and fusion and are transported throughout the cell. Disruption of proper mitochondrial function has been implicated in several processes including generation of reactive oxygen species, increased cellular death, aging, and neurodegenerative diseases such as Huntington's, Alzheimer's, and Parkinson's disease.

1.1 Generation of mitochondrial reactive oxygen species

One of the major sources for reactive oxygen species (ROS) in a cell originates from mitochondria during oxidative phosphorylation [1]. During transport of electrons along the electron transport chain, electrons leak predominately from complex I (NADH dehydrogenase) and complex III (ubiquinone-cytochrome c reductase) [2]. Leaked electrons are transferred to molecular oxygen forming the radical superoxide. Superoxide is highly reactive and leads to the formation of other molecules associated with increased oxidative stress such as the hydroxyl radical and hydrogen peroxide. Increases in oxidative stress can result in damage to DNA, lipids, and proteins and has been associated with neurodegenerative diseases, aging, and cellular death [2-4].

1.2 Mitochondrial membrane potential

Transport of electrons through the electron transport chain is coupled to the pumping of protons from the mitochondrial matrix into the mitochondrial intermembrane space. This proton gradient establishes a mitochondrial membrane potential giving the intermembrane space a net positive charge, while the matrix has a net negative charge [5]. The potential energy established by the proton gradient is used by the mitochondrial complex V (ATP synthase) to generate ATP [6]. Changes in electron transport, loss of mitochondrial potential, and altered ATP production have all been implicated in oxidative stress and cell death [7-9].

1.3 Control of oxidative stress by NRF2 and KEAP1

In general, the degree of cellular oxidative stress is determined by the balance between levels of ROS and the mechanisms used by cells to decrease cellular ROS. One major mechanism used to counteract oxidative stress is through the induction of cytoprotective genes known as phase 2 genes, which include detoxifying enzymes such as NQO1 (NADPH: quinone oxidoreductase 1), GSTA2 (glutathione S-transferase A2), and HO1 (heme oxygenase 1) [10, 11]. Phase 2 genes are under tight transcriptional control through a cis-acting element known as the antioxidant responsive element (ARE) [12]. During increased oxidative stress, the transcription factor nuclear factor erythroid 2-related factor 2 (referred to as NRF2 from here on) binds to AREs, which leads to increased transcription of phase 2 genes [13-15].

Once oxidative stress levels are reduced, NRF2 is negatively regulated by the kelch-like ECH-associated protein 1 (KEAP1) in order to prevent unnecessary

transcription of phase 2 genes [16]. KEAP1 acts as a substrate adaptor allowing for efficient ubiquitination of NRF2 by the CUL3-E3 ubiquitin ligase complex [17]. The N-terminal Bric-a-brac (BTB) domain of KEAP1 binds to CUL3, while the C-terminal kelch domain of KEAP1 binds to NRF2 [17, 18]. Structural analysis of KEAP1 and NRF2 revealed a conserved DxETGE motif in NRF2 and NRF2-related proteins that was required for binding of KEAP1 to NRF2 [19, 20]. Formation of the NRF2/KEAP1/CUL3 complex allows for efficient conjugation of ubiquitin onto NRF2, which targets NRF2 for degradation by the proteasome [21].

ROS and electrophilic compounds react with distinct cysteine residues in KEAP1, which allows KEAP1 to act as a sensor for oxidative stress [22]. Modification of distinct cysteine residues in KEAP1 is thought to either hinder transfer of ubiquitin to NRF2 or cause dissociation of KEAP1 from CUL3 [23].

1.4 Cell death by apoptosis

Apoptosis and necrosis are two major forms of cellular death. While apoptosis is a form of programmed cell death, requiring ATP, necrosis is generally regarded as a consequence of a sudden insult, and is a rapid process that can occur with minimal changes in intracellular ATP levels [8]. Two major pathways of apoptosis have been well characterized, termed extrinsic and intrinsic. The extrinsic pathway is activated through binding of death-inducing ligands to receptors on the plasma membrane, which leads cell death, while the intrinsic pathway involves changes in mitochondrial permeability causing the release of apoptotic factors that trigger cell death. In both cases, formation of a death-inducing complex leads to the activation of caspases, which leads to

the execution of apoptosis. Caspases are a class of cysteinyl aspartases that can be grouped either as initiator caspases (caspases -1, -2, -4, -5, -8, -9, -10, -11, and -12) or effector caspases (caspases -3, -6, and -7) [24]. Caspases are synthesized as zymogens (also known as procaspases) that require proteolytic cleavage prior to activation.

Typically, initiator procaspases are activated upstream of effector procaspases, and upon activation, initiator caspases cleave and activate effector caspases. Activated effector caspases in turn cleave multiple cellular components, which leads to the execution of apoptosis [24].

1.4.1 Extrinsic pathway

Activation of caspases through the extrinsic pathway requires the formation of the death-inducing signaling complex (DISC) [25]. Formation of the DISC begins with the binding of cell surface death receptors with their respective ligands. Death receptors (such as TNFR1 and FAS) belong to the tumor necrosis factor receptor (TNFR) family and bind to ligands (such as TNF α and FASL) belonging to the tumor necrosis factor (TNF) family [26]. Ligand binding to the TNFR promotes oligomerization of these receptors on the cell surface [26]. These receptors contain a death domain (DD) on their cytoplasmic side, which recruits adaptor molecules through their cognate DDs. For example, the adaptor protein Fas-associated protein with death domain (FADD) contains a C-terminal DD that interacts with the DD of the FAS receptor, which completes the formation of the DISC [26]. FADD also contains an N-terminal death effector domain (DED), which is required for recruitment of an initiator procaspase (such as procaspase-8). Upon recruitment of procaspase-8 to the DISC, procaspase-8 is cleaved and activated,

which leads to apoptosis through activation of effector caspases (such as caspase -3 and -7) [27].

1.4.2 Intrinsic pathway

The intrinsic pathway is a mitochondrial-mediated process in which cytochrome c is released from the intermembrane space (IMS) of mitochondria into the cytosol and forms a complex with apoptotic protease-activating factor 1 (APAF1) and procaspase-9 called the apoptosome [28]. Cytochrome c release is triggered by a change in mitochondrial membrane permeability (discussed further below). APAF1 contains an N-terminal caspase-recruitment domain (CARD), an ATPase domain, and a C-terminal WD40 repeat region [29]. APAF1 binds to procaspase-9 through CARD-CARD interactions, while the ATPase domain and WD40 repeat bind to ATP and cytochrome c, respectively [28]. Formation of the apoptosome results in procaspase-9 cleavage and activation, which in turn activates caspase-3, resulting in apoptosis [30].

1.4.3 Control of mitochondrial membrane permeability

In healthy cells, the mitochondrial membrane permeability (MMP) is tightly regulated, which is necessary to establish a mitochondrial membrane potential for oxidative phosphorylation [5]. During apoptosis, however, MMP is increased to allow the release of cytochrome c and other apoptotic factors [31]. Members of the BCL2 family are largely responsible for modulating MMP [32].

The BCL2 family can be classified as either pro-apoptotic (such as BAX, BAK, BCL-XS, BID, BAD, and BIK) or anti-apoptotic (such as BCL-XL, BCL-2, and MCL-1). Each member of the BCL2 family contains one or more BCL-2 homology (BH1, BH2, BH3, and BH4) domain. Depending on the composition of their BH domains, the BCL2

family can be further subdivide into multidomain proteins (BCL-XL, BCL-2, MCL-1, BAX, BAK, and BCL-XS) or BH3-only proteins (BID, BAD, and BIK) [33].

BCL-XL and BCL-2 have been shown to prevent cellular apoptosis, though the exact mechanism is unclear [34-36]. Both BCL-XL and BCL-2 are thought to primarily exert their anti-apoptotic affects by binding to pro-apoptotic factors (such as BAX, BAK, BIM, and BID) and prevent them from activating apoptosis.

BAX and BAK have been identified as key components in regulating MMP. In mouse embryonic fibroblasts (MEFs), double knockout of BAX and BAK prevented intrinsic cell death, while single knockout of either BAX or BAK did not provide protection against cell death [37]. Under basal conditions, BAX is predominately found in the cytosol. Upon induction of apoptosis, BAX redistributes from the cytosol to punctate regions of mitochondria where it is inserted into the outer mitochondrial membrane (OMM) [38]. Once inserted into the mitochondrial membrane, BAX is believed to form supramolecular openings in the OMM, which can facilitate the release of cytochrome c [39].

The BH3-only members are critical for initiating the release of cytochrome c by BAX and BAK. In one model, the BH3-only members were classified as sensitizers (BAD and BIK) or activators (BID or BIM) [40]. Binding of the activators to BAX or BAK induced a conformational change in BAX and BAK, which initiated BAX and BAK oligomerization and insertion into the OMM where they mediate the release of cytochrome c. During normal conditions, however, the activators are sequestered by BCL-2 and BCL-XL. Death inducing signals increase binding of the sensitizers to BCL-

2 and BCL-XL, which liberates the activators and allows their binding to BAX and BAK, inducing apoptosis [40].

1.5 Necrosis

Necrosis is largely characterized by certain morphological characteristics including swelling, decreased plasma membrane integrity, organelle damage, and ultimately bursting of the cell [41]. Traditionally, necrosis was thought to occur in an uncontrolled manner due to severe insult to the cell. However, there is increasing evidence to support the notion that caspase-independent cell death pathways exist, which regulate necrosis [42]. Studies in which caspase activity was blocked have identified the receptor-interacting serine-threonine kinases -1 and subsequently -3 (RIPK1 and RIPK3) as key regulators of necrosis [43-45].

Similar to the extrinsic pathway for apoptosis, necrosis begins with the oligomerization of death receptors, including TNFR1, CD95, and TRAIL [46]. TNF α induces the trimerization of TNFR1 and recruitment of TNFR1-associated death domain (TRADD) [47]. This provides a docking station for the recruitment of RIPK1, FADD and TNFR-associated factor 2 (TRAF2). In the presence of caspase inhibitors, such as z-VAD, RIPK1 is released from the docking station and associates with RIPK3 through the interaction of RIP homotypic interaction motifs (RHIMs) found in both RIPK1 and RIPK3 [48-50]. The kinase activity of RIPK1/RIPK3 is thought to be necessary to induce necrosis [43, 51, 52]. One candidate substrate for RIPK1/RIPK3 is PGAM5. RIPK1/RIPK3 phosphorylation of PGAM5 is thought to activate PGAM5 as a phosphatase, which leads to dephosphorylation of DRP1 at Ser-637 and activation of

DRP1. Active DRP1 mediates mitochondrial fission, which leads to necrosis (reviewed below and [53]).

1.6 Autophagy

Autophagy is another recognized form of programmed cell death [54].

Autophagy is an organized process for degradation of proteins and organelles.

Autophagic vesicles (autophagosomes) engulf cytoplasmic material containing proteins or damaged organelles and fuse with lysosomes in order to recycle cellular material [55].

Degradation of mitochondria by autophagy is referred to as mitophagy.

Mitophagy is thought to occur in response to damage of mitochondria in order to remove defective mitochondria. The proteins PTEN induced putative kinase 1 (PINK1) and parkinson protein 2 (PARKIN) have been identified as key players in targeting damaged mitochondria for autophagy [56].

In humans, newly synthesized PINK1 exists as a 63KDa protein. PINK1 contains an N-terminal mitochondrial localization signal (MTS) and transmembrane domain, which targets PINK1 for insertion into the inner mitochondrial membrane (IMM). In healthy cells, the N-terminal MTS of PINK1 is cleaved by the mitochondrial processing protease (MPP), forming a 60KDa product of PINK1 [57]. Further processing of PINK1 by presenilins-associated rhomboid-like (PARL) protein generates a 52KDa form of PINK1, which is rapidly degraded [58]. Mechanisms by which PINK1 is released from the IMM into the cytosol, though, remains unclear. Treatment of cells with proteasome inhibitors or carbonyl cyanide 3-chlorophenylhydrazone (CCCP) results in the accumulation of the 60KDa form of PINK1[59-61].

CCCP is a protonophore that is commonly used to uncouple mitochondria. Upon loss of MMP by CCCP, PINK1 is stabilized and accumulates on the outer mitochondrial membrane (OMM), though the exact mechanism of PINK1 accumulation is not understood. One study identified the OMM receptor protein TOM70 to be necessary for PINK1 recognition and import/insertion of PINK1 into the OMM, though the exact mechanism for import and insertion was not determined [62]. One possible mechanism may be through lateral release of OMM proteins by the TOM complex [63].

PINK1 accumulation and stabilization on the OMM promotes recruitment of PARKIN to mitochondria [61], though the exact mechanism is not fully understood. PARKIN is an E3-ubiquitin ligase that participates in ubiquitination of mitochondrial proteins, which results in mitophagy [56, 64, 65]. While the exact mechanism of PINK1/PARKIN-mediated mitophagy is not known, several studies have demonstrated a role for PARKIN-mediated ubiquitination of proteins that regulate mitochondrial dynamics, which is thought to help mediate mitochondrial degradation.

Prior to targeting mitochondria for degradation, it is believed that damaged mitochondria are separated from healthy mitochondria through mitochondrial fission [66]. Mitofusin-1 and mitofusin-2 (MFN1/MFN2) are mitochondrial proteins that help facilitate mitochondrial fusion and have been shown to be targets for PARKIN-mediated ubiquitination [67-69]. It was demonstrated that CCCP treatment of cells caused ubiquitination of MFN1 and MFN2, which was reduced upon silencing of PARKIN or PINK1 [67]. Although the downstream effects of MFN1/MFN2 ubiquitination is not known, it was speculated that ubiquitination of MFN1/MFN2 would promote fission

either by degradation of MFN1/MFN2 or by interfering with dimerization of the MFN1/MFN2 proteins.

Mitochondrial Rho GTPase (MIRO) is an adaptor protein that links kinesin heavy chain (KHC) with mitochondria to mediate anterograde microtubule-based movement [70]. MIRO has been identified as a substrate for PINK1 and phosphorylation of MIRO by PINK1 has been implicated in PARKIN-mediated degradation of MIRO [71, 72]. Degradation of MIRO by PINK1/PARKIN is thought to help facilitate removal of damaged mitochondria from microtubule tracks, enabling the damaged mitochondria to undergo mitophagy [73].

1.7 Mitochondrial fusion

Fission and fusion of mitochondria constantly occurs in healthy cells to promote proper function and health of mitochondria. In mammalian cells, three proteins have been identified as crucial components in mitochondrial fusion. These include MFN1, MFN2, and optic atrophy 1 (OPA1). MFN1 and MFN2 mediate OMM fusion, while OPA1 mediates IMM fusion [74].

1.7.1 Mitofusins

Mitofusins are GTPases that contain two transmembrane domains that span the OMM, leaving both the N- and C- terminal of MFN-1/2 exposed to the cytosol [68]. MEFs lacking either MFN1 or MFN2 show an increase in fragmentation of mitochondria while proving lethal during mouse midgestation [69, 75]. The N-terminal GTPase domain of MFN-1/2 is necessary for mitochondrial fusion, though the underlying mechanism is not understood [76]. It was demonstrated that purified MFN1 protein had

an 8-fold higher GTPase activity compared to MFN2 and that GTPase activity correlated to the oligomeric state of MFN, suggesting functional differences between MFN1 and MFN2 [76].

MFNs contain a C-terminal coiled-coil region containing a heptad repeat region (HR2) domain. MFN proteins on adjacent mitochondria interact through their HR2 domains, tethering adjacent mitochondria. Through MFN GTPase activity, a conformational change occurs that is thought to facilitate fusion of two adjacent mitochondria [77, 78].

1.7.2 Optic atrophy 1

OPA1 is an IMM protein that belongs to the dynamin family [79]. OPA1 is exposed to the intermembrane space, though some splice variants of OPA1 have different localization patterns [80-82]. Similar to MFN1/2, OPA1 contains an N-terminal GTPase domain and a C-terminal coiled-coil domain [83]. In mammalian cells, over-expression OPA1 promotes fusion and elongation of mitochondria while its repression drives fragmentation of mitochondria [83-85]. OPA1 mediates fusion of the inner membrane, though inner membrane fusion is not well understood.

1.8 Mitochondrial fission

The key player in mitochondrial fission in mammals appears to be the protein dynamin-related protein 1 (DRP1). Several mitochondrial proteins, however, have been reported to recruit DRP1 to mitochondria.

1.8.1 Dynamin-related protein 1

Under normal conditions DRP1 is found largely in the cytosol [86]. DRP1 contains an N-terminal GTPase domain and a C-terminal GTPase effector domain (GED). Contact between these domains is important for GTPase activity and mitochondrial fission [87]. During fission, DRP1 forms ring like structures, which are thought to constrict around dividing mitochondria [88, 89].

While DRP1-mediated mitochondrial fission has been implicated in cell death, DRP1 also has an important role in normal development as DRP1-null mice die by embryonic day 11.5 [53, 90, 91]. Mitochondria in MEFs lacking DRP1, however, are still able to undergo fission after treatment with etoposide or actinomycin D, suggesting that there are other mediators of mitochondrial fission that remain to be identified [90, 92].

1.8.2 DRP1 recruitment to mitochondria

The protein fission 1 (FIS1) was identified as a mitochondrial protein involved in recruitment of DRP1 to mitochondria. Overexpression studies of FIS1 in mammalian cells resulted in increased fragmentation of mitochondria while RNAi knockdown of FIS1 decreases fission [93]. FIS1 is located on the cystolic side of the OMM where it is thought to facilitate recruitment of DRP1 during mitochondrial fission, though the underlying mechanism is not well understood.

Mitochondrial fission factor (MFF) is another receptor for DRP1 that is anchored to the OMM. MFF was identified in *Drosophila* using siRNA studies, which showed that knockdown of dMFF resulted in increased fusion of mitochondria [94]. Furthermore, knockdown of MFF reduced mitochondrial recruitment of DRP1 in mammalian cells, while conditional knockout of FIS1 appeared to be dispensable for mitochondrial fission

[95]. These results suggest that MFF is the principal protein that recruits DRP1 to mitochondria.

1.9 Mitochondrial movement

Mitochondria are constantly transported throughout the cell in response to cellular needs. Much of what we have learned about mitochondrial movement in mammalian systems comes from studies in neurons. Neurons are ideal models for studying mitochondrial movement due to their lengthy axons. Mitochondria originating from the cell body are transported along the axon to the axon terminal where they are needed to supply ATP and modulate calcium levels to help maintain synaptic transmission [96]. Mitochondria are transported long distances along microtubules and short distances along actin filaments. Mitochondrial movement also switches between anterograde movement (towards the plus end of microtubules) and retrograde movement (towards the minus end of microtubules) [97].

1.9.1 Mitochondrial anterograde transport along microtubules

Anterograde movement of mitochondria is towards the plus ends of microtubules [98]. In mammals, the kinesin-1 family of proteins (referred to as KIF5) mediate anterograde movement of mitochondria along microtubules [99]. Three KIF5 isoforms (KIF5A, KIF5B, and KIF5C) have been identified in mammals [100]. KIF5B knockout mice were shown to be embryonic lethal while KIF5B null extraembryonic cells displayed abnormal clustering of mitochondria in the perinuclear region [101]. Furthermore, perinuclear clustering was reversed with ectopic expression of KIF5B.

KIF5 motor proteins contain an N-terminal domain that binds to and hydrolyzes ATP, converting the chemical energy released into mechanical movement towards the plus ends of microtubules [102]. The C-terminal domain of KIF5 interacts with kinesin light chains (KLCs), which mediates binding of KIF5 to its cargo [103].

In *Drosophila*, Milton and Miro, known as trafficking kinesin-binding protein milt and mitochondrial rho, respectively, were identified as adaptor proteins that link mitochondria to the C-terminus of KIF5 [104-106]. Mutation of Milton or Miro in *Drosophila* results in abnormal distribution of mitochondria [105, 106]. Miro contains a C-terminal mitochondrial transmembrane domain, which inserts Miro into the OMM [107]. Miro then binds Milton, which in turn binds to KIF5 to facilitate mitochondrial anterograde movement [70, 105]. The mammalian orthologues of Milton (TRAK1 and TRAK2) and Miro (MIRO1 and MIRO2) were also shown to interact with KIF5 and mediate mitochondrial movement [108, 109].

1.9.2 Mitochondrial retrograde movement along microtubules

The mechanisms that regulate retrograde movement of mitochondria are not well understood. Movement of mitochondria in the retrograde direction is presumed to rely mainly on cytoplasmic dynein [110, 111]. Dynein consists of two heavy chains, three intermediate chains, and four light chains. The heavy chains form a globular head that is involved in binding to microtubule tracks and ATP hydrolysis. The intermediate and light chains interact with the protein complex dynactin, which is thought to facilitate cargo binding [110, 112, 113].

1.9.3 Transport along actin cables

Little is known about mitochondrial transport along actin cables in mammals. Members of the myosin family are known to be motor proteins that facilitate movement along actin filaments [114]. Recently, the myosin motor protein MYO19 has been identified as a mitochondrial localized protein that mediates actin-based mitochondrial movement [115]. MYO19 contains a motor domain, three IQ motifs, and a short tail. Recombinant GFP-MYO19 constructs revealed that the tail region was necessary for colocalization with mitochondria. They found that overexpression of GFP-MYO19 increased the motility of mitochondria in 40% of the cells expressing the construct. The motor domain of MYO19 was required for increased motility for expression of GFP-MYO19-tail was not sufficient enough to increase motility. Furthermore, disruption of microtubule tracks did not alter GFP-MYO19 motility, while F-actin disruption by latrunculin B prevented GFP-MYO19 movement [115].

1.10 Phosphoglycerate mutase 5 review

The protein phosphoglycerate mutase 5 (PGAM5) is a mitochondrial localized protein that has been implicated in the regulation of mitochondrial function and cellular homeostasis. PGAM5 is a member of the PGAM family, which consists of several evolutionarily conserved enzymes that have metabolic roles in glycolysis [116]. The PGAM family proteins share a conserved catalytic motif (PGAM motif) that is involved in the transfer of phosphate (mutase) or removal of phosphate (phosphatase) on their substrates, which include 3-phosphoglycerate and 2-phosphoglycerate. The PGAM motif contains a highly conserved RHG region where the histidine residue is crucial for

catalysis. The catalytic pocket consists of two histidine and two arginine residues that are involved in catalysis [116].

1.10.1 PGAM5 is targeted by KEAP1 for degradation

PGAM5 was originally identified as an interacting partner with the apoptotic factor BCL-XL [117]. PGAM5 was later identified as a substrate for KEAP1 [118]. The KEAP1 protein acts as a sensor for oxidative stress. During redox homeostasis, the KEAP1-E3 ligase complex binds to transcription factor NRF2 and targets it for ubiquitination and degradation by the proteasome [119]. NRF2 plays a key role in maintaining redox homeostasis by up-regulating the transcription of phase 2 enzymes that help reduce oxidative stress [119]. KEAP1 forms a dimer through its BTB domain and was shown to act as a scaffold to form a ternary complex containing both PGAM5 and NRF2 on mitochondria [120]. These data suggest that the PGAM5/NRF2/KEAP1 complex is involved in responding to and/or regulating mitochondrial ROS.

1.10.2 PGAM5 activation of ASK1

PGAM5 contains a highly conserved RHG motif, which is conserved in the PGAM family and is required for catalysis [116]. It was demonstrated that PGAM5 was capable of dephosphorylating phosphopeptides, while lacking any mutase activity [121]. Mutation of H105 (within the RHG region) abolished all phosphatase activity of PGAM5. Furthermore, PGAM5 phosphatase activity was specific for phospho-Ser/Thr residues, while it lacked the ability to dephosphorylate phospho-Tyr residues [121].

PGAM5 was identified as an interacting partner of the apoptosis signal-regulating kinase 1 (ASK1) protein and reported to activate ASK1 via dephosphorylation, though the exact site(s) of dephosphorylation was not determined [121]. ASK1 is a member of

the mitogen-activated protein kinase kinase kinase (MAPKKK) family that is activated by several stress signals, such as oxidative stress, leading to JNK and p38 activation and cell death [122]. Since PGAM5 is localized to the mitochondria and ASK1 is found in the cytosol, PGAM5 is most likely only acting on a fraction of ASK1. Since oxidative stress is known to activate ASK1 [123], and PGAM5 is found in complex with KEAP1 [120, 124], this may suggest another level of control for mitochondrial oxidative stress. It is possible that KEAP1's association with PGAM5 modulates the phosphatase activity of PGAM5 through conformational changes or ubiquitination. Upon increased oxidative stress and dissociation of KEAP1 from PGAM5, PGAM5 might become activated and dephosphorylate ASK1. Though PGAM5 would only be acting on a fraction of ASK1, this may provide a feed-forward mechanism enhancing the ASK1 pathway and cell death.

1.10.3 PGAM5 alleviates symptoms of Parkinson's disease in flies

Drosophila are used as models to study human disease due to their conservation of genes and cellular processes that are found in humans [125]. One such disease is Parkinson's disease (PD). PD is characterized by loss of dopaminergic neurons (neurodegeneration) resulting in motor defects causing muscle stiffness, tremors, and locomotive issues [126]. Similar phenotypes can be seen in PD flies including loss of dopaminergic neurons, muscle degeneration that affects wing posture, reduced lifespan, and difficulties in climbing [125].

In *Drosophila*, dPGAM5 was found as an interacting partner of dPINK1 [127]. In this study, dPINK1 inactivation was associated with a shorter lifespan, motor defects, and muscle degeneration in flies. Loss of dPGAM5 alleviated the symptoms of dPINK1

inactivation in flies. Overexpression of dPGAM5 enhanced these defects flies, likely by negatively regulating PINK1. [127].

Mitochondrial depolarization reduced PARL-mediated cleavage of PINK1 while cleavage of PGAM5 was increased, however, the physiological reasons for PGAM5 cleavage is unknown [128]. These studies may provide insight into a mechanism by which loss of MMP results in the stabilization of PINK1 and cleavage of PGAM5 by PARL, inactivating PGAM5 and increasing PINK1/PARKIN activity.

1.10.4 PGAM5 in apoptosis

Mitochondria are highly implicated in cell death [4, 7, 8, 129]. Recently, PGAM5 has been implicated in both necrotic and apoptotic functions [53, 124]. It was suggested that PGAM5 formed a complex on mitochondria containing both KEAP1 and BCL-XL, similar to that of the KEAP1-NRF2-PGAM5 ternary complex [120, 124]. In this model, PGAM5's ESGE motif interacted with KEAP1's kelch domain [124]. BCL-XL was then recruited to the complex through binding to PGAM5 [118, 124]. The BCL-XL/PGAM5/KEAP1 complex led to ubiquitination and degradation of both PGAM5 and BCL-XL [124]. Overexpression of KEAP1 increased PGAM5/BCL-XL degradation and increased etoposide-mediated accumulation of BAX, causing release of cytochrome c and activation of caspase-3/7, which in turn resulted in apoptosis [124].

1.10.5 PGAM5 in necrosis

PGAM5 was found to be activated by the RIPK1/RIPK3 pathway [53]. In these experiments, necrosis was achieved by treating cells with both z-VAD and a SMAC-mimetic. SMAC (Second mitochondria-derived activator of caspase) and mimetics of smac bind to and block inhibitors of apoptosis proteins (IAPs) [130]. Preventing the

activity of IAPs allows for complete TNF activation of RIPK1/Caspase-8 [131]. z-VAD is a cell-permeable inhibitor of caspases [132]. When used simultaneously, z-VAD and smac-mimetics allows for TNF activation of RIPK1 while inhibiting caspase-8-mediated apoptosis, thereby promoting necrosis.

Under conditions that promote necrosis, TNF induces oligomerization of TNFR and promotes activation of RIPK1 [43]. Activated RIPK1 binds to RIPK3 through RHIM motifs found in both RIPK1 and RIPK3 [50]. The RIPK1/RIPK3 complex then associates with the mixed lineage kinase domain-like (MLKL) protein to form a functional complex referred to as the necrosome [133].

The necrosome complex (RIPK1/RIPK3/MLKL) has been reported to bind to PGAM5 and activate PGAM5 through phosphorylation. The necrosome inhibitor, necrosulfonamide, disrupted necrosome-PGAM5 interactions [53]. Phosphorylation of PGAM5 resulted in the recruitment of DRP1 to mitochondria, followed by dephosphorylation of DRP1 at Ser-637. While dephosphorylation of DRP1 at Ser-637 was used to indicate activation of DRP1, direct dephosphorylation of this residue by PGAM5 was not established. Activation of DRP1 led to increased mitochondrial fission and cell death by necrosis [53].

1.11 Summary of chapters

This dissertation characterizes the protein PGAM5. Our results show that gene disruption of PGAM5 in mice is embryonic lethal and that PGAM5-deficient MEFs exhibit increased sensitivity to staurosporine-induced apoptosis. Multimerization of PGAM5 is necessary for both PGAM5 phosphatase activity and proper mitochondrial

maintenance. Taken together, our data would suggest that PGAM5 is necessary for survival and proper mitochondrial maintenance and cellular function as opposed to being a pro-apoptotic factor that induces cell death through necrosis or apoptosis [53, 124].

1.11.1 Chapter 2 – PGAM5 crystallization

To date, there is a partial structure of human PGAM5 consisting of amino acids 98-289 [134]. The crystal structure shows that PGAM5 dimerizes through its PGAM domain. However, studies from our lab demonstrates that PGAM5 is inactive as a phosphatase when truncated by more than 55 amino acids at PGAM5's N-terminus. Our goal was to crystalize an active form of PGAM5.

We tested the solubility of several PGAM5 proteins and screened them in crystal trials. We were able to purify *Drosophila* PGAM5 up to 13mg/mL. After optimizing the crystallization conditions for *Drosophila* PGAM5, we found that *Drosophila* PGAM5 best crystallized at 6mg/mL in drops containing 0.1M Lithium Sulfate, 0.1M ADA pH 6.5, 12% (w/v) PEG 4000, and 0.1M Hexamine cobalt(III) chloride. We were able to demonstrate that these crystal do diffract, however, further studies will need to be conducted to determine appropriate freezing conditions that would allow us to obtain better diffraction data.

1.11.2 Chapter 3 – Multimerization of PGAM5 is necessary for PGAM5 phosphatase activity and mitochondrial morphology

In an attempt to crystallize an active structure of PGAM5, we discovered that PGAM5 multimerizes into a higher order complex. Multimerization of PGAM5 is mediated through what we refer to as the multimerization domain, which is conserved across all PGAM5 species. The multimerization domain facilitates formation of a stable

PGAM5 dodecamer and a higher order multimeric structure for which the size appears to be greater than 600KDa. The multimerization domain is also crucial for PGAM5 phosphatase activity both in vitro and in vivo. Furthermore, in mammalian cells, overexpression of PGAM5 harboring mutations in the multimerization domain caused fragmentation of mitochondria. These results may suggest that PGAM5's phosphatase activity may contribute to the regulation of mitochondrial morphology.

1.11.3 Chapter 4 – PGAM5 gene-trap mice: Microarray analysis and characterization

We characterized a mouse containing a loss-of-function gene-trap insertion in the PGAM5 locus. We genotyped over 200 mice and 70 embryos and did not identify any homozygous PGAM5 gene-trap mice. Therefore, we determined that PGAM5 was crucial for development and that PGAM5 gene disruption was embryonic lethal.

MEFs were generated from ten embryos of a single heterozygous mouse. One embryo was deficient of PGAM5. We show that PGAM5-deficient MEFs are more prone to staurosporine-induced apoptosis. Increased sensitivity to staurosporine was accompanied with an increase in caspase-3/7 activity. Furthermore, reconstitution of PGAM5 in PGAM5-deficient MEFs partially alleviate increased staurosporine sensitivity.

Using microarrays, we identified differentially expressed genes between wild-type MEFs and PGAM5-deficient MEFs that were generated from PGAM5 heterozygous embryos. About 2800 differentially expressed genes were identified. The bioinformatics software DAVID suggests that PGAM5 may have a role in purine/pyrimidine metabolism

and in regulation of focal adhesion, providing insight into possible biological roles for PGAM5.

Chapter 2

Crystallization of PGAM5

In this chapter, I review my efforts to crystallize PGAM5. To date, there is no structure resolved for PGAM5 that is active as a phosphatase. There is a partial structure for PGAM5 (human) reported on the Protein Data Bank (PDB) website [134]. This partial structure only contains the residues 90-289 of PGAM5. As determined in our lab, PGAM5 lacks phosphatase activity when the N-terminus of PGAM5 is truncated by more than 55 amino acids. Therefore, we sought to solve the structure of an active form of PGAM5. We tested several PGAM5 constructs in order to optimize solubility of PGAM5. We achieved the greatest solubility using *Drosophila* PGAM5 (residues 30-289; Δ N30-dPGAM5), which was soluble up to 13mg/mL. Δ N30-dPGAM5 crystalized under several conditions with 0.1M Lithium Sulfate, 0.1M ADA pH 6.5, 12% (w/v) PEG 4000, and 0.1M Hexamine cobalt(III) chloride providing the sharpest and most symmetrical crystals observed with a size of about 0.1mm. We verified that Δ N30-dPGAM5 crystals grown under this condition are capable of diffraction up to 4.5 angstroms. However, diffraction of 4.5 angstroms was achieved without freezing of the crystals. Normally, crystals are frozen to prevent degradation of the crystal upon the exposure of the crystal to x-rays. Identifying optimal freezing conditions would allow us to increase the exposure time of our crystals to the x-ray source in order to obtain better diffraction data from the crystals. We might then be able to elucidate a structure for the active form of PGAM5.

2.1 Purification of PGAM5 protein

The general purification scheme for the different PGAM5 proteins was identical regardless of the PGAM5 construct used. PGAM5 was cloned into the pET-15b vector.

The pET-15b vector encodes for an N-terminal HIS-tag sequence followed by a multiple cloning site into which PGAM5 was cloned into using the NdeI/BamHI sites (Figure 2.1). pET-15b-HIS-PGAM5 (HIS-PGAM5) is under the control of bacteriophage T7 transcription and translation signals. The HIS-PGAM5 vector was transformed into the bacterial host Rosetta cells (BL21-LysS) and expression of HIS-PGAM5 was induced by addition of isopropyl β -D-1-thiogalactopyranoside (IPTG). Bacterial cultures were lysed by freeze/thaw cycles carried out in the presence of protease inhibitors. HIS-PGAM5 purification is facilitated using a Ni-NTA column. Bound HIS-PGAM5 was washed several times with 500mM NaCl and 60mM imidazole and eluted with 500mM NaCl and 500mM imidazole. Using Fast Protein Liquid Chromatography (FPLC), the eluted protein was desalted using desalting columns (GE) to a final salt concentration of 100mM NaCl and 20mM Hepes pH 7.2 (Figure 2.2A). At pH 7.2, PGAM5 carries a net positive charge, therefore, desalted HIS-PGAM5 was passed over a cation exchange column (GE) and eluted using a salt gradient (Figure 2.2B). Bound HIS-PGAM5 eluted from the cation exchange columns around 300mM-400mM NaCl. Finally, HIS-PGAM5 is desalted back to 100mM NaCl, 20mM Hepes pH 7.2 for use in crystal trials (Figure 2.2C).

Figure 2.1: HIS-PGAM5 constructs

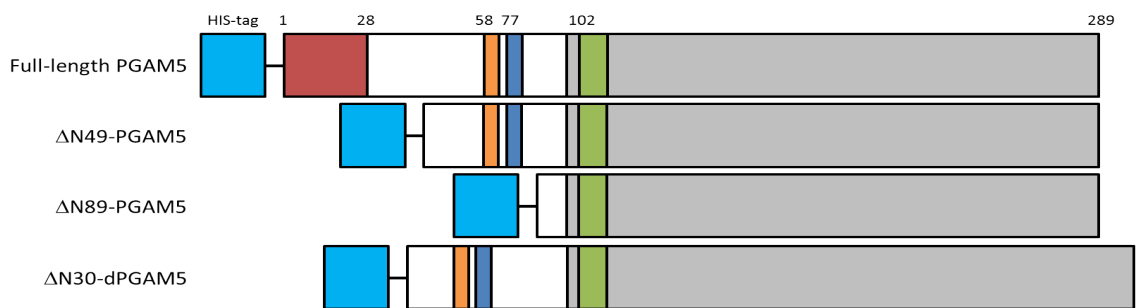
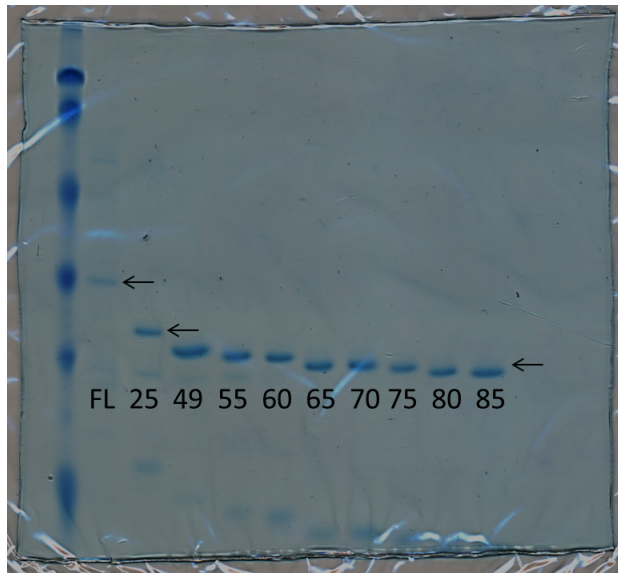


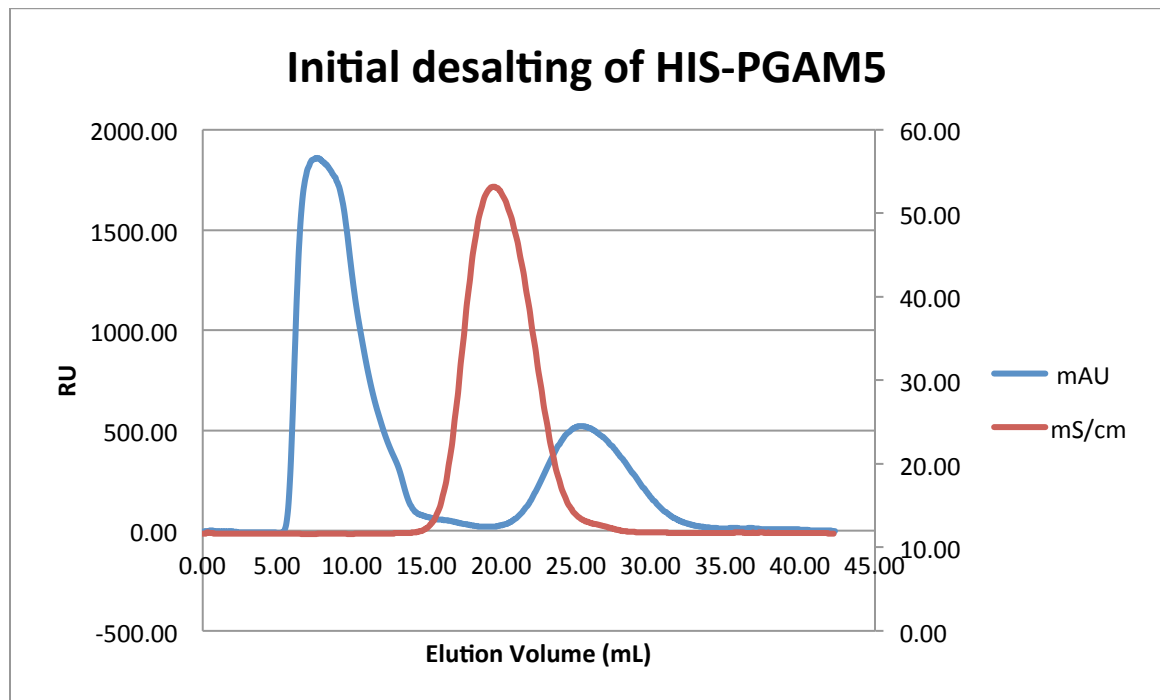
Figure 2.1: Line diagrams depicting constructs used for PGAM5 protein purification. The HIS-tag (light blue) is indicated with 1 being the first amino acid position of PGAM5. The N-terminus of PGAM5 contains the mitochondrial targeting sequence (Red). Orange/Blue indicate WDxxWD motif. The PGAM5 domain is depicted in gray. The PGAM motif containing the catalytic residues RHG is indicated in green.

Figure 2.2: Purification of PGAM5 by FPLC

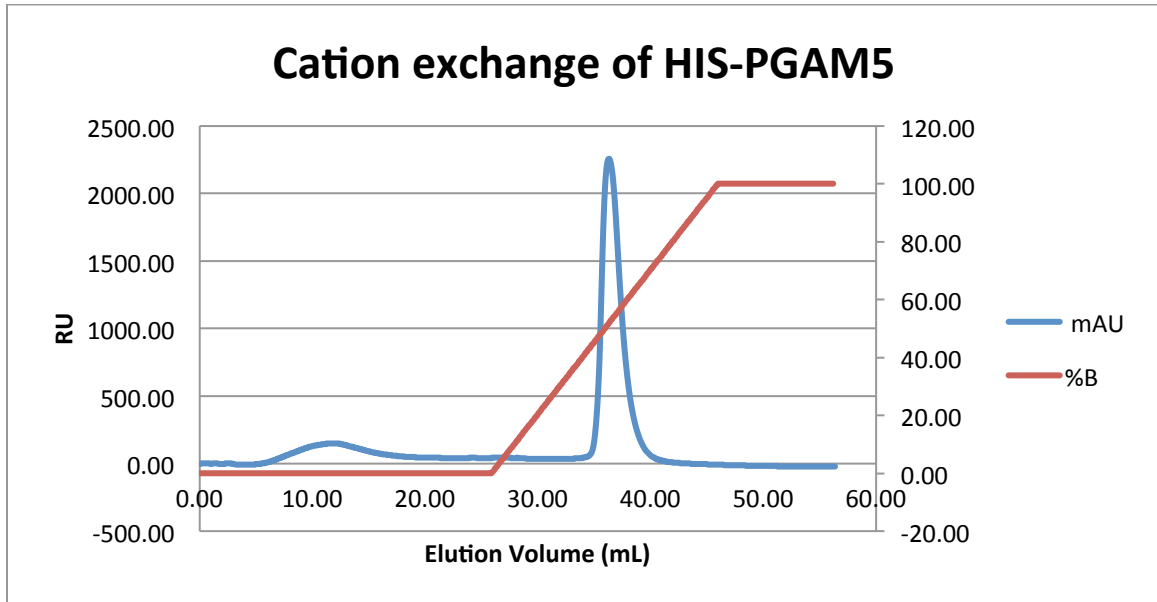
A) Coomassie stained gel of purified HIS-PGAM5 PGAM5



B) Initial desalting of HIS-PGAM5



C) Cation exchange of HIS-PGAM5



D) Final desalting of HIS-PGAM5

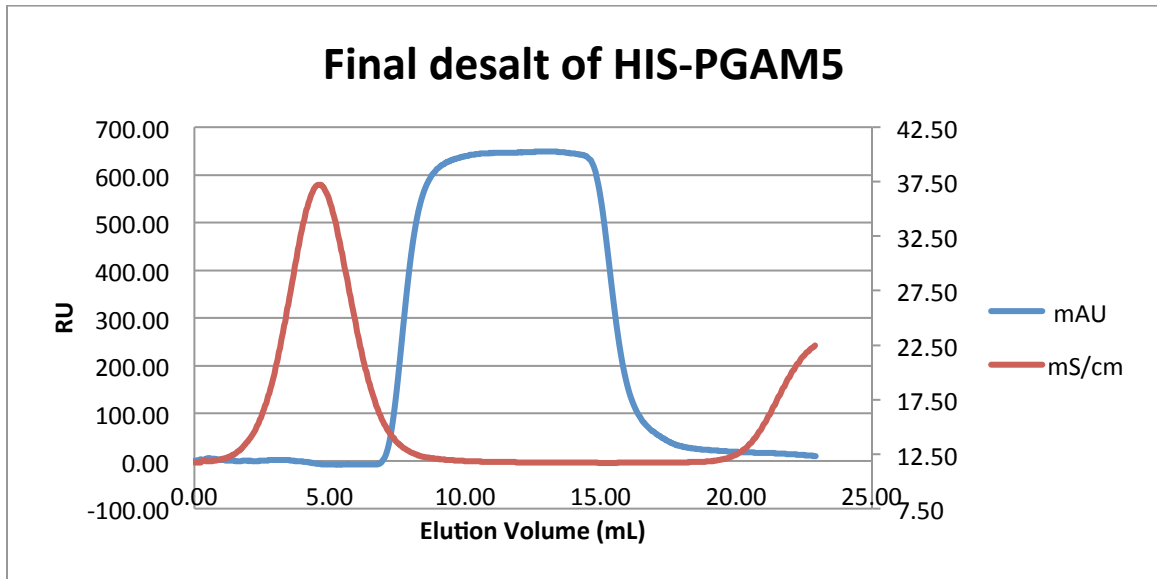


Figure 2.2: Purification scheme for HIS-PGAM5 proteins. (A) Coomassie stained HIS-PGAM5 proteins eluted from Ni-NTA column. Proteins in order from left to right: Ladder, full-length PGAM5, Δ N25-PGAM5, Δ N49-PGAM5, Δ N55-PGAM5, Δ N60-PGAM5, Δ N65-PGAM5, Δ N70-PGAM5, Δ N75-PGAM5, Δ N80-PGAM5, Δ N85-PGAM5. Arrows indicate position of PGAM5 proteins. (B) Proteins eluted from the Ni-NTA column were desalted into 100mM NaCl and 20mM Hepes pH 7.2 in order to allow binding to the cation exchange column. (C) Protein bound to the cation exchange column was subjected to a NaCl gradient (100mM-1M). PGAM5 protein eluted at approximately 0.3-0.4M NaCl. (D) Purified PGAM5 protein was desalted back down to 100mM NaCl and 20mM Hepes pH 7.2 for use in phosphatase assays and crystal trials.

2.2 Phosphatase activity of PGAM5 proteins

PGAM5 is a Ser/Thr phosphatase [121]. To determine which PGAM5 proteins had phosphatase activity, we assayed the PGAM5 proteins for phosphatase activity against the phosphopeptide BCL-XL-pSer62 with the following sequence of WHLAD(pS)PAVNG (Table 2.1). We measured the phosphatase activity using the malachite green assay kit from R&D research. Briefly, PGAM5 was incubated in phosphatase assay buffer with the BCL-XL-pSer62 phosphopeptide. The reaction was quenched with a strong acid and free-phosphate was detected by addition of malachite green. Upon binding of malachite green to free-phosphate, an absorbance shift occurs that we measure at 630nm. Of the proteins in figure 2.1, the only inactive protein was Δ N89-PGAM5. Full-length, Δ N49-PGAM5, and Δ N30-dPGAM5 had comparable K_m values ranging from 28uM-52uM.

Table 2.1: Phosphatase activity of PGAM5

| Construct | Species | Amino Acids | K_m (\pm error), uM | V_{max} (\pm error), uM | Solubility |
|---------------------|------------|-------------|--------------------------|------------------------------|------------|
| Full-length PGAM5 | Human | 1-289 | 28.5 (1.7) | 2053.9 (39.1) | 1 mg/ml |
| Δ N49-PGAM5 | Human | 49-289 | 51.0 (3.3) | 3128.2 (60.9) | 1 mg/ml |
| Δ N89-PGAM5 | Human | 89-289 | ND | ND | 5 mg/ml |
| Δ N30-dPGAM5 | Drosophila | 30-289 | 52.2 (10.5) | 927.5 (51.5) | 13 mg/ml |

Table 2.1: 100nM purified PGAM5 protein was tested for phosphatase activity against various concentrations of the phosphopeptide BCL-XL-pSer62 (WHLAD(pS)PAVNG). Phosphatase activity was determined using the malachite green assay. Kinetic parameters were determined using Kaleidagraph software. Solubility of PGAM5 proteins were determined by absorbance at 280nm in 100mM NaCl and 20mM Hepes pH 7.2.

2.3 Solubility of PGAM5 proteins

Δ N49-PGAM5 could only be purified to 1mg/ml before it would begin precipitating out of solution. While Δ N89-PGAM5 was not an active phosphatase, we could achieve protein concentrations up to 4mg/ml. With the Drosophila construct Δ N30-dPGAM5 construct, we were able to achieve up to 13mg/ml of purified protein.

2.4 Crystallization of Δ N89-PGAM5

Our initial crystal trials with Δ N89-PGAM5 were set up utilizing the screens shown in Table 2.2. Each screen was set up using Δ N89-PGAM5 at 4mg/ml or 5mg/ml. Of all the screens tested, only one solution produced crystals; A5 of Qiagen Nextal Classics Suite (Table 2.3). The Classics Suite solution A5 has the following formulation: 0.2M Ammonium Acetate, 0.1M Tris-HCl pH 8.5, and 30% (v/v) isopropanol. The crystals formed were rod shaped, symmetrical, and small. The A5-solution would have been a good candidate for optimization, however, we wanted to crystalize the active form of PGAM5 so we did not pursue optimizing this condition.

Table 2.2: Crystallization screens used in crystal trials with Δ N89-PGAM5

| | |
|------------------------------|------------------------------|
| Precipitant Synergy Block I | Precipitant Synergy Block II |
| Qiagen Nextal Classics Suite | Crystal Screen 1 and 2 |
| JCSG Core I Suite | PACT Suite |
| MBClass Suite I | MBClass Suite II |

Table 2: Crystal screens used to help define conditions for crystallizing Δ N89-PGAM5.

Table 2.3: Summary of results for ΔN89-PGAM5 crystal trials.

| Screen ¹ | [Protein] ² , mg/ml | Ratio ³ (Protein:Drop) | Clear ⁴ | Precipitate ⁵ | Wells Crystallized ⁶ |
|---------------------------------|-----------------------------------|--------------------------------------|--------------------|--------------------------|------------------------------------|
| Precipitant Synergy Block I | 4 | 1:3 | 46 | 50 | |
| Precipitant Synergy Block I | 4 | 1:1 | 46 | 50 | |
| Precipitant Synergy Block I | 4 | 3:1 | 54 | 42 | |
| Precipitant Synergy Block II | 4 | 1:3 | 76 | 20 | |
| Precipitant Synergy Block II | 4 | 1:1 | 73 | 23 | |
| Precipitant Synergy Block II | 4 | 3:1 | 72 | 24 | |
| Qiagen Nextal Classics Suite | 4 | 1:3 | 63 | 33 | |
| Qiagen Nextal Classics Suite | 4 | 1:1 | 62 | 34 | |
| Qiagen Nextal Classics Suite | 4 | 3:1 | 62 | 34 | A5 |
| Crystal Screen 1 and 2 | 5 | 1:3 | 55 | 41 | |
| Crystal Screen 1 and 2 | 5 | 1:1 | 52 | 44 | |
| Crystal Screen 1 and 2 | 5 | 3:1 | 56 | 40 | |
| JCSG Core I Suite | 5 | 1:3 | 29 | 67 | |
| JCSG Core I Suite | 5 | 1:1 | 44 | 52 | |
| JCSG Core I Suite | 5 | 3:1 | 66 | 30 | |
| MBClass Suite I | 5 | 1:3 | 65 | 31 | |
| MBClass Suite I | 5 | 1:1 | 68 | 28 | |
| MBClass Suite I | 5 | 3:1 | 70 | 26 | |
| MBClass Suite II | 5 | 1:3 | 50 | 46 | |
| MBClass Suite II | 5 | 1:1 | 54 | 42 | |
| MBClass Suite II | 5 | 3:1 | 69 | 27 | |
| PACT Suite | 5 | 1:3 | 22 | 74 | |
| PACT Suite | 5 | 1:1 | 36 | 60 | |
| PACT Suite | 5 | 3:1 | 69 | 27 | |

Table 2.3: Purified ΔN89-PGAM5 was concentrated to 4mg/ml and setup for crystal trials using various screens.

¹The crystal screen used for trials.

²Concentration of ΔN89-PGAM5 used in screen.

³Indicates the ratio of protein to solution used per screen.

⁴Indicates number of wells that had clear drops.

⁵Indicates number of wells that formed precipitation.

⁶Indicates wells that formed crystals in the respective screen.

2.5 Crystallization of ΔN49-PGAM5

We set up similar trials using ΔN49-PGAM5 at a concentration of 1mg/ml. The trials consisted of the screens found in Table 2.4. From these trials, approximately 32% of the drops precipitated and no crystals were formed. The lack of crystal formation was likely due to the poor solubility ΔN49-PGAM5. However, other factors that may have affected crystal growth include temperature, purity of protein, and the crystallization solution.

Table 2.4: Screens tested against ΔN49-PGAM5.

| Screen ¹ | Ratio ² (Protein:Drop) | Clear ³ | Precipitate ⁴ | % Precipitation ⁵ |
|--------------------------------|-----------------------------------|--------------------|--------------------------|------------------------------|
| MB Class Suite | 1:1 | 86 | 10 | 10 |
| Hamptom Crystal Screen 1 and 2 | 1:3 | 78 | 18 | 19 |
| Hamptom Crystal Screen 1 and 2 | 1:1 | 79 | 17 | 18 |
| Hamptom Crystal Screen 1 and 2 | 3:1 | 74 | 22 | 23 |
| JCSG Core I Suite | 1:3 | 38 | 58 | 60 |
| JCSG Core I Suite | 1:1 | 32 | 64 | 67 |
| JCSG Core I Suite | 3:1 | 38 | 58 | 60 |
| PACT Suite | 1:3 | 76 | 20 | 21 |
| PACT Suite | 1:1 | 72 | 24 | 25 |
| PACT Suite | 3:1 | 67 | 29 | 30 |
| Qiagen Nextal Classics Suite | 1:3 | 76 | 20 | 21 |
| Qiagen Nextal Classics Suite | 1:1 | 67 | 29 | 30 |
| Qiagen Nextal Classics Suite | 3:1 | 58 | 38 | 40 |

Table 2.4: Screens tested against ΔN49-PGAM5.

¹The crystal screen used for trials.

²Indicates the ratio of protein to solution used per screen.

³Indicates number of wells that had clear drops.

⁴Indicates number of wells that formed precipitation.

⁵Ratio of precipitated wells to clear wells.

2.6 Crystallization of Δ N30-dPGAM5

After testing the human PGAM5 proteins in crystal trials, we had only identified one condition in which the PGAM5 proteins could crystallize. We believe this is due to the low solubility (1mg/ml) of the human PGAM5 proteins. Several methods can be utilized to help improve protein stability, solubility, and crystallization. One method is to crystallize your protein as a complex, which may help stabilize your protein through binding partners [135]. Point mutations in proteins are often used to change the polarity or charge of amino acids on the surface of the protein [136]. Lastly, trying homologous proteins from other species may dramatically improve the crystallization of your protein simply due to the variations in surface exposed amino acids [137]. We utilized *Drosophila* PGAM5 (Δ N30-dPGAM5) in our experiments and found that the phosphatase activity was conserved and that the solubility of Δ N30-dPGAM5 improved. We could achieve higher concentrations of Δ N30-dPGAM5 (up to 13mg/ml) as compared to the human PGAM5 proteins (up to 1mg/ml).

We set up crystal trials with the MBClass Suite I screen using purified Δ N30-dPGAM5 protein concentrated to 4mg/ml, 6mg/ml, or 8mg/ml. About 56% of the drops precipitated, while 5% formed crystals. Four of the wells that formed crystals looked like good candidates for optimization. Each of the four wells contained crystals hexagonal in shape that had semi-sharp edges and were symmetrical (Figure 2.3).

Figure 2.3: Crystallization of Δ N30-dPGAM5 using MbClass Suite I

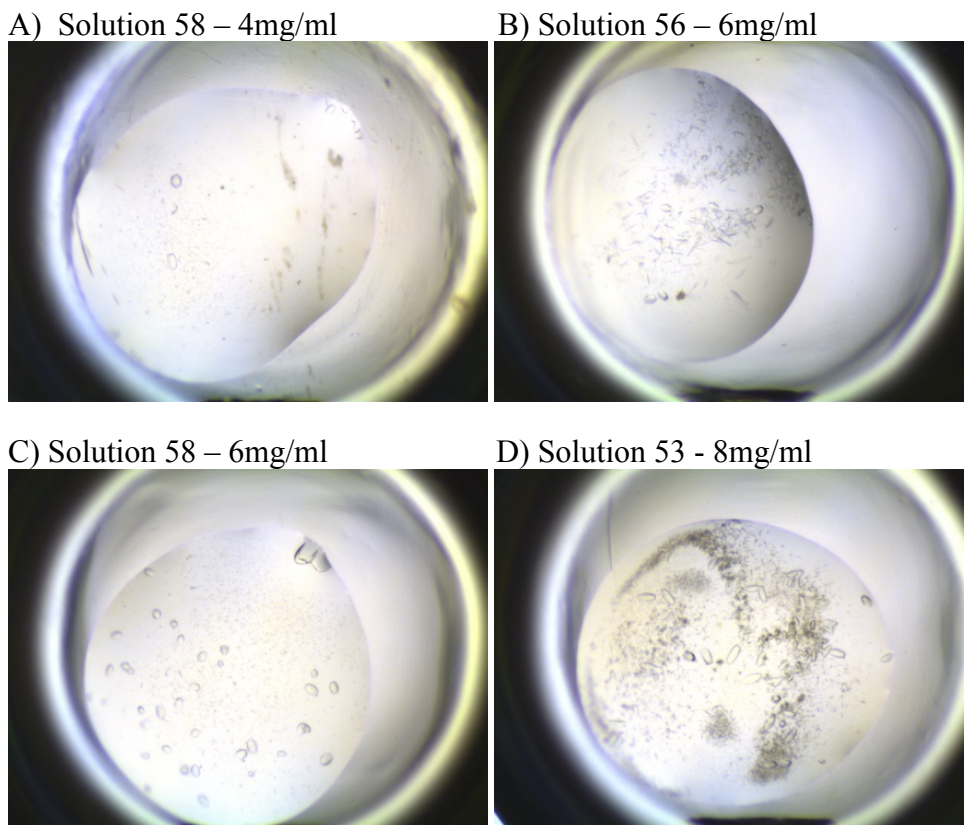


Figure 2.3: Crystallization of Δ N30-dPGAM5 using MbClass Suite I. (A) 4mg/ml, 1:1, solution 58(E10) - 0.05M Tris-HCl pH 7.5, 2%(w/v) PEG 4000. (B) 6mg/ml, 1:3, solution 56(E8) - 0.5M Sodium Chloride, 0.05M Tris-HCl pH 7.5, 12%(w/v) PEG 2000 MME. (C) 6mg/ml, 1:1, solution 58(E10) - 0.05M Tris-HCl pH 7.5, 2%(w/v) PEG 4000. (D) 8mg/ml, 1:1, solution 53(E5) - 0.3M Magnesium Chloride, 0.1M Bicine pH 9.0, 25%(w/v) PEG 2000, 15%(w/v) Glycerol.

We further expanded our crystal trials of Δ N30-dPGAM5 using several screens at 8mg/ml (Table 2.5). Of these trials, solutions A11 of JCSG Suite I and F11 of MbClassII may be good candidates for optimization (Figure 2.4). Solution A11 consisted mostly of plates. Plates are more difficult to analyze by x-ray diffraction due to the thinness of plates, but these plates were more ideal than other plates found because they were larger, thicker, and polarized. Solution F11 contained several crystals that were symmetrical and hexagonal in shape.

Table 2.5: Crystal trials using Δ N30-dPGAM5 with various screens

| Screen ¹ | Ratio ² (Protein:Drop) | Clear ³ | Precipitate ⁴ | % Precipitation ⁵ | Wells Crystallized ⁶ |
|----------------------|--------------------------------------|--------------------|--------------------------|---------------------------------|------------------------------------|
| JCSG Core I | 1:3 | 10 | 86 | 90 | 0 |
| JCSG Core I | 1:1 | 9 | 87 | 91 | 1 |
| JCSG Core I | 3:1 | 5 | 91 | 95 | 10 |
| MbClass Suite I | 1:3 | 47 | 49 | 51 | 0 |
| MbClass Suite I | 1:1 | 44 | 52 | 54 | 4 |
| MbClass Suite I | 3:1 | 57 | 39 | 41 | 5 |
| MbClass Suite II | 1:3 | 39 | 57 | 59 | 2 |
| MbClass Suite II | 1:1 | 35 | 61 | 64 | 4 |
| MbClass Suite II | 3:1 | 29 | 67 | 70 | 0 |
| Qiagen Classics I | 1:3 | 47 | 49 | 51 | 0 |
| Qiagen Classics I | 1:1 | 49 | 47 | 49 | 0 |
| Qiagen Classics I | 3:1 | 39 | 57 | 59 | 1 |

Table 2.5: Purified Δ N30-dPGAM5 was concentrated to 8mg/ml and setup for crystal trials.

¹The crystal screen used for trials.

²Indicates the ratio of protein to solution used per screen.

³Indicates number of wells that had clear drops.

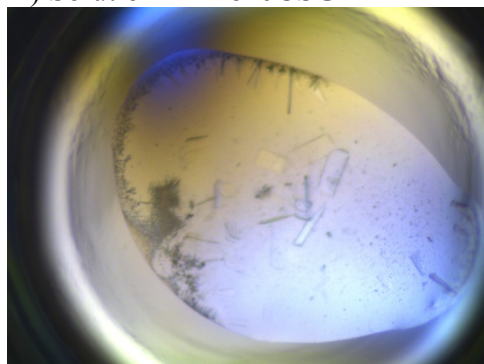
⁴Indicates number of wells that formed precipitation.

⁵Ratio of precipitated wells to clear wells.

⁶Indicates wells that formed crystals in the respective screen.

Figure 2.4: Crystallization of Δ N30-dPGAM5 at 8mg/ml

A) Solution A11 of JCSG I



B) Solution F11 of MbClass II

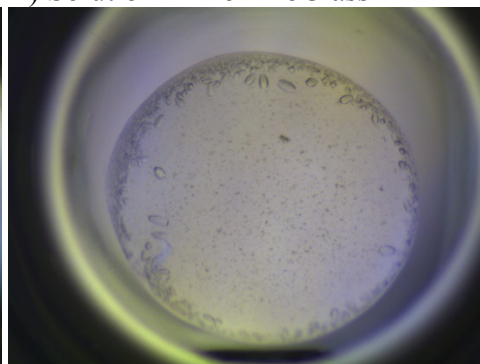


Figure 2.4: Purified Δ N30-dPGAM5 was concentrated to 8mg/ml and setup in crystal trials. (A) Solution A11 of JCSG Suite I (0.2M potassium acetate, 20%(w/v) PEG 3350) at a 3:1 (protein:solution) ratio. (B) Solution F11 of MbClass II Suite (0.1M lithium sulfate, 0.1M ADA pH 6.5, 12%(w/v) PEG 4000) at a 1:1 (protein:solution) ratio.

2.7 Crystallization of *Drosophila* selenomethionine-PGAM5

One of the biggest challenges in crystallography is determining the phase of the diffracted x-rays. This is commonly known as the phase problem. To address the phase problem, we incorporated an analog of methionine, selenomethionine, by growing our bacterial cultures in the presence of selenomethionine instead of methionine. Most selenomethionyl protein crystals are isomorphous with that of the native protein crystals differing at each selenium atom by 18 electrons [138]. This difference in electron density helps to determine the proper phase of diffracted x-rays through the use of multiwavelength anomalous diffraction (MAD) phasing method [139]. Within Δ N30-dPGAM5, there are three methionine groups at amino acid positions 29, 139, and 272. This constitutes about 1% of all the amino acids in dPGAM5. It is estimated that one out of every 75-100 amino acids needs to be a selenomethionine residue in order to solve the phase problem [140], which makes HIS-tag-selenomethionine-dPGAM5 (30-289) (SEM-dPGAM5) an ideal candidate for solving the phase problem.

We utilized SEM-dPGAM5 in several screens including MbClass II Suite, JBScreen, and PEG II Suite. MbClass II produced crystals under multiple conditions. More importantly, MbClassII-71 solution produced optimizable crystals under the same conditions that which produced ideal crystals for Δ N30-dPGAM5 (Figure 2.5). This is important for it shows that incorporation of selenomethionine into Δ N30-dPGAM5 minimally perturbed the crystallization conditions. We would then be able to compare

the diffraction data of the non-incorporated and incorporated selenomethionine crystals to help solve the phase problem.

Figure 2.5: Comparison of Δ N30-dPGAM5 and SEM-PGAM5 crystallization

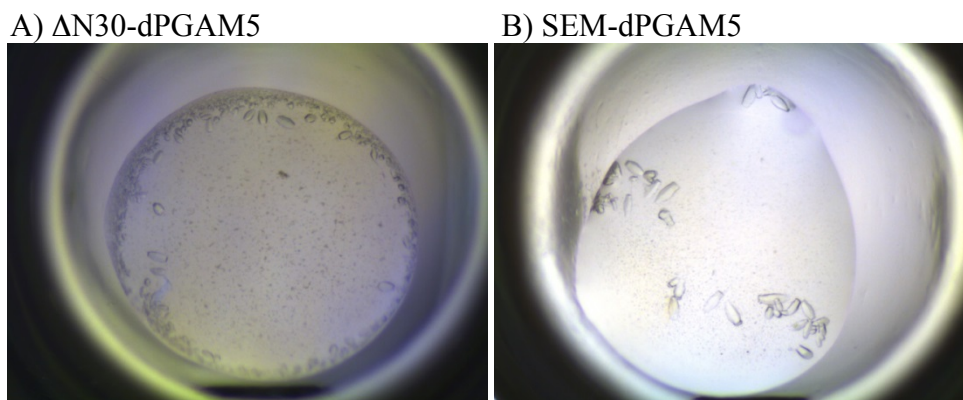


Figure 2.5: Comparison of Δ N30-dPGAM5 and SEM-dPGAM5 using MbClassII-71 solution (0.1M Lithium Sulfate, 0.1M ADA pH 6.5, 12% (w/v) PEG 4000). (A) Crystals formed using Δ N30-dPGAM5 at 8mg/ml, 1:1 ratio. (B) Crystals formed using SEM-dPGAM5 at 8mg/ml, 1:1 ratio.

2.8 Optimization of SEM-dPGAM5

We tested SEM-dPGAM5 using the optimization screen seen in Table 2.6. We set up screens using concentrations of 4mg/ml, 6mg/ml, and 8mg/ml SEM-dPGAM5. We set up ratios of protein:well solution at either 1:3, 1:1, or 3:1. Screens set up using 4mg/ml protein produced no crystals. At 6mg/ml protein, three wells produced crystals at a ratio of 1:3. Of these three, solution F12 (0.1M NaCl, 0.1M NH₄SO₄, 12% PEG 4000) had crystals that were fairly symmetrical and sharp-edged, making them ideal candidates for optimization (Figure 2.6A). At 8mg/ml protein and a ratio of 1:1, solution E5 (0.3M Magnesium Chloride, 0.1M Bicine pH 9.0, 25%(w/v) PEG 2000, 15%(w/v) Glycerol) produced some precipitant and small crystals but also produced crystals of decent size and shape, making a good candidate for optimization (Figure 2.6B). Glycerol is a common cryoprotectant and may be an appropriate cryoprotectant for dPGAM5

crystals, given that solution E5 produced decent crystals in the presence of 15% (w/v) glycerol.

Table 2.6: Optimization of MbClass II solution 71.

| | 1 | 2 | 3 | 4 | 5 | 6 | 7 | 8 | 9 | 10 | 11 | 12 |
|--|--|--|--|--|---|---|---|--|--|--|---|---|
| A - 0.1M MES (pH 6.0) | 0M NaCl, 0.1M LiSO ₄ , 8% PEG 4000 | 0M NaCl, 0.1M LiSO ₄ , 10% PEG 4000 | 0M NaCl, 0.1M LiSO ₄ , 12% PEG 4000 | 0.1M NaCl, 0.1M LiSO ₄ , 8% PEG 4000 | 0.1M NaCl, 0.1M LiSO ₄ , 10% PEG 4000 | 0.1M NaCl, 0.1M LiSO ₄ , 12% PEG 4000 | 0M NaCl, 0.1M NH ₄ SO ₄ , 8% PEG 4000 | 0M NaCl, 0.1M NH ₄ SO ₄ , 10% PEG 4000 | 0M NaCl, 0.1M NH ₄ SO ₄ , 12% PEG 4000 | 0.1M NaCl, 0.1M NH ₄ SO ₄ , 8% PEG 4000 | 0.1M NaCl, 0.1M NH ₄ SO ₄ , 10% PEG 4000 | 0.1M NaCl, 0.1M NH ₄ SO ₄ , 12% PEG 4000 |
| B - 0.1M Bis- Tris (pH 6.5) | 0M NaCl, 0.1M LiSO ₄ , 8% PEG 4000 | 0M NaCl, 0.1M LiSO ₄ , 10% PEG 4000 | 0M NaCl, 0.1M LiSO ₄ , 12% PEG 4000 | 0.1M NaCl, 0.1M LiSO ₄ , 8% PEG 4000 | 0.1M NaCl, 0.1M LiSO ₄ , 10% PEG 4000 | 0.1M NaCl, 0.1M LiSO ₄ , 12% PEG 4000 | 0M NaCl, 0.1M NH ₄ SO ₄ , 8% PEG 4000 | 0M NaCl, 0.1M NH ₄ SO ₄ , 10% PEG 4000 | 0M NaCl, 0.1M NH ₄ SO ₄ , 12% PEG 4000 | 0.1M NaCl, 0.1M NH ₄ SO ₄ , 8% PEG 4000 | 0.1M NaCl, 0.1M NH ₄ SO ₄ , 10% PEG 4000 | 0.1M NaCl, 0.1M NH ₄ SO ₄ , 12% PEG 4000 |
| C - 0.1M Imida zol (pH 7.0) | 0M NaCl, 0.1M LiSO ₄ , 8% PEG 4000 | 0M NaCl, 0.1M LiSO ₄ , 10% PEG 4000 | 0M NaCl, 0.1M LiSO ₄ , 12% PEG 4000 | 0.1M NaCl, 0.1M LiSO ₄ , 8% PEG 4000 | 0.1M NaCl, 0.1M LiSO ₄ , 10% PEG 4000 | 0.1M NaCl, 0.1M LiSO ₄ , 12% PEG 4000 | 0M NaCl, 0.1M NH ₄ SO ₄ , 8% PEG 4000 | 0M NaCl, 0.1M NH ₄ SO ₄ , 10% PEG 4000 | 0M NaCl, 0.1M NH ₄ SO ₄ , 12% PEG 4000 | 0.1M NaCl, 0.1M NH ₄ SO ₄ , 8% PEG 4000 | 0.1M NaCl, 0.1M NH ₄ SO ₄ , 10% PEG 4000 | 0.1M NaCl, 0.1M NH ₄ SO ₄ , 12% PEG 4000 |
| D - 0.1M Hepe s (pH 7.5) | 0M NaCl, 0.1M LiSO ₄ , 8% PEG 4000 | 0M NaCl, 0.1M LiSO ₄ , 10% PEG 4000 | 0M NaCl, 0.1M LiSO ₄ , 12% PEG 4000 | 0.1M NaCl, 0.1M LiSO ₄ , 8% PEG 4000 | 0.1M NaCl, 0.1M LiSO ₄ , 10% PEG 4000 | 0.1M NaCl, 0.1M LiSO ₄ , 12% PEG 4000 | 0M NaCl, 0.1M NH ₄ SO ₄ , 8% PEG 4000 | 0M NaCl, 0.1M NH ₄ SO ₄ , 10% PEG 4000 | 0M NaCl, 0.1M NH ₄ SO ₄ , 12% PEG 4000 | 0.1M NaCl, 0.1M NH ₄ SO ₄ , 8% PEG 4000 | 0.1M NaCl, 0.1M NH ₄ SO ₄ , 10% PEG 4000 | 0.1M NaCl, 0.1M NH ₄ SO ₄ , 12% PEG 4000 |
| E - 0.1M Tris (pH 8.0) | 0M NaCl, 0.1M LiSO ₄ , 8% PEG 4000 | 0M NaCl, 0.1M LiSO ₄ , 10% PEG 4000 | 0M NaCl, 0.1M LiSO ₄ , 12% PEG 4000 | 0.1M NaCl, 0.1M LiSO ₄ , 8% PEG 4000 | 0.1M NaCl, 0.1M LiSO ₄ , 10% PEG 4000 | 0.1M NaCl, 0.1M LiSO ₄ , 12% PEG 4000 | 0M NaCl, 0.1M NH ₄ SO ₄ , 8% PEG 4000 | 0M NaCl, 0.1M NH ₄ SO ₄ , 10% PEG 4000 | 0M NaCl, 0.1M NH ₄ SO ₄ , 12% PEG 4000 | 0.1M NaCl, 0.1M NH ₄ SO ₄ , 8% PEG 4000 | 0.1M NaCl, 0.1M NH ₄ SO ₄ , 10% PEG 4000 | 0.1M NaCl, 0.1M NH ₄ SO ₄ , 12% PEG 4000 |
| F - 0.1M Tris (pH 8.5) | 0M NaCl, 0.1M LiSO ₄ , 8% PEG 4000 | 0M NaCl, 0.1M LiSO ₄ , 10% PEG 4000 | 0M NaCl, 0.1M LiSO ₄ , 12% PEG 4000 | 0.1M NaCl, 0.1M LiSO ₄ , 8% PEG 4000 | 0.1M NaCl, 0.1M LiSO ₄ , 10% PEG 4000 | 0.1M NaCl, 0.1M LiSO ₄ , 12% PEG 4000 | 0M NaCl, 0.1M NH ₄ SO ₄ , 8% PEG 4000 | 0M NaCl, 0.1M NH ₄ SO ₄ , 10% PEG 4000 | 0M NaCl, 0.1M NH ₄ SO ₄ , 12% PEG 4000 | 0.1M NaCl, 0.1M NH ₄ SO ₄ , 8% PEG 4000 | 0.1M NaCl, 0.1M NH ₄ SO ₄ , 10% PEG 4000 | 0.1M NaCl, 0.1M NH ₄ SO ₄ , 12% PEG 4000 |
| G - 0.1M ADA (pH 6.5) | 0M NaCl, 0.1M LiSO ₄ , 8% PEG 4000 | 0M NaCl, 0.1M LiSO ₄ , 10% PEG 4000 | 0M NaCl, 0.1M LiSO ₄ , 12% PEG 4000 | 0.1M NaCl, 0.1M LiSO ₄ , 8% PEG 4000 | 0.1M NaCl, 0.1M LiSO ₄ , 10% PEG 4000 | 0.1M NaCl, 0.1M LiSO ₄ , 12% PEG 4000 | 0M NaCl, 0.1M NH ₄ SO ₄ , 8% PEG 4000 | 0M NaCl, 0.1M NH ₄ SO ₄ , 10% PEG 4000 | 0M NaCl, 0.1M NH ₄ SO ₄ , 12% PEG 4000 | 0.1M NaCl, 0.1M NH ₄ SO ₄ , 8% PEG 4000 | 0.1M NaCl, 0.1M NH ₄ SO ₄ , 10% PEG 4000 | 0.1M NaCl, 0.1M NH ₄ SO ₄ , 12% PEG 4000 |

Table 2.6: Optimization of MbClass II solution 71. Solutions listed in table were varied around MbClass II solution 71: 0.1M Lithium Sulfate, 0.1M ADA pH 6.5, 12% (w/v) PEG 4000.

Figure 2.6: Optimized conditions for MbClassII-71

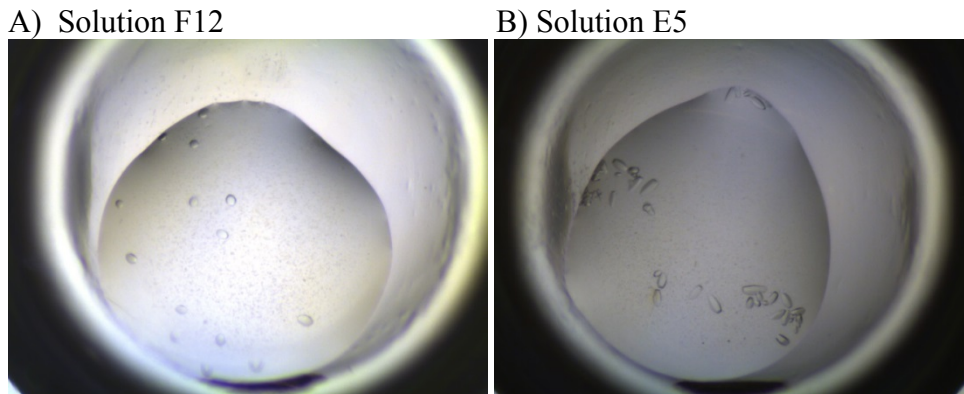


Figure 2.6: Crystals produced using optimization screen found in table 6 using SEM-dPGAM5 at 8mg/ml. (A) Crystals formed in solution F12 (0.1M NaCl, 0.1M NH₄SO₄, 12% PEG 4000). (B) Crystals formed in solution E5 (0.3M Magnesium Chloride, 0.1M Bicine pH 9.0, 25%(w/v) PEG 2000, 15%(w/v) Glycerol).

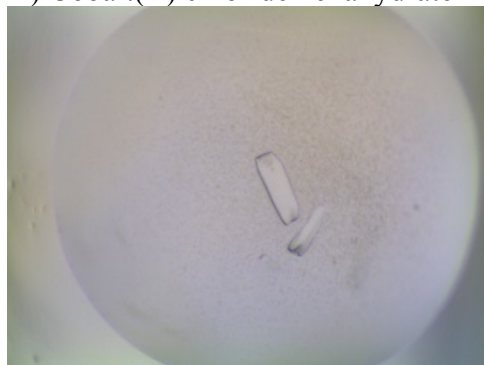
The optimized conditions for MbClassII-71 (Table 2.6) proved difficult to reproduce crystals even in the control solution that is formulated to be the same as MbClassII-71 solution (G3 in optimized screen, Table 2.6). This may be due to small variations in the pH, stock solutions used, and concentrations of components between the solution made from Qiagen and the solution made in lab. To minimize the variations in future screens, we used Qiagen's refill solution for MbClassII-71 for additional screening.

We setup a screen using MbClassII-71 in combination with an Additive screen (Hampton Research, HR2-428) (Figure 2.7). SEM-dPGAM5 was concentrated to 8mg/ml and used at a 1:1 ratio in the trials. Only 4 wells precipitated while 51 wells formed crystals. Ten of the wells produced larger and/or sharper crystals while the remaining 41 wells consisted primarily of showers of small crystals or thin plates that were clustered together. We found that addition of the polyamine Hexamine Cobalt(III) Chloride (HCC) had the best overall improvement in crystal quality (Figure 2.7F).

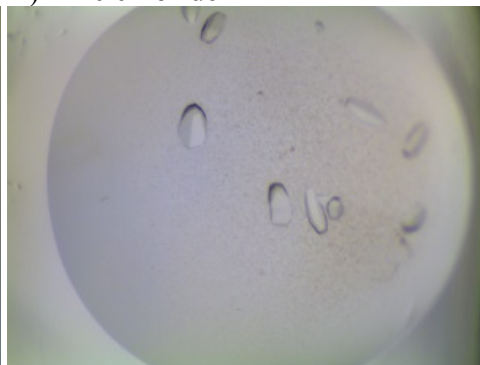
Figure 2.7: Crystallization of SEM-dPGAM5 with Additive screen

| Image ¹ | Final concentration ² | Additive ³ | Description ⁴ |
|--------------------|----------------------------------|---------------------------------|--------------------------|
| A | 0.01M | Cobalt(II) chloride hexahydrate | Multivalent |
| B | 0.01M | Zinc chloride | Multivalent |
| C | 0.01M | Nickel(II) chloride hexahydrate | Multivalent |
| D | 0.1M | Ammonium sulfate | Salt |
| E | 0.01M | Phenol | Dissociating Agent |
| F | 0.01M | Hexamine cobalt(III) chloride | Polyamine |
| G | 0.01M | Trimethylamine hydrochloride | Chaotrope |
| H | 4% (v/v) | Acetonitrile | Organic, Volatile |
| I | 0.5% (v/v) | Ethyl acetate | Organic, Volatile |
| J | 0.7% (v/v) | 1-Butanol | Organic, Volatile |

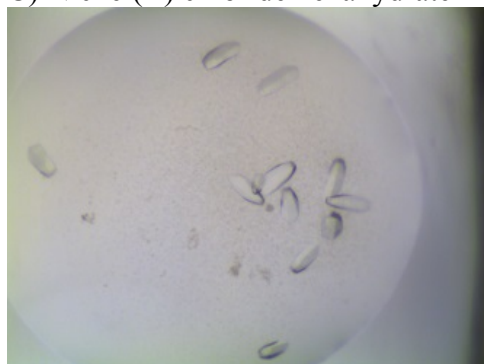
A) Cobalt(II) chloride hexahydrate



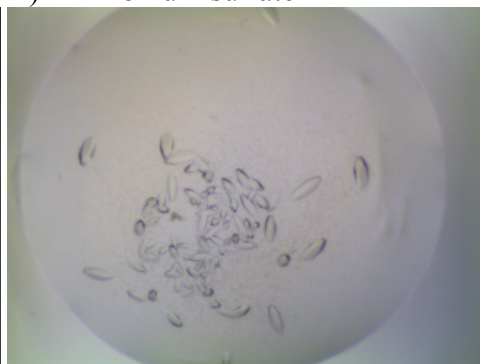
B) Zinc chloride



C) Nickel(II) chloride hexahydrate



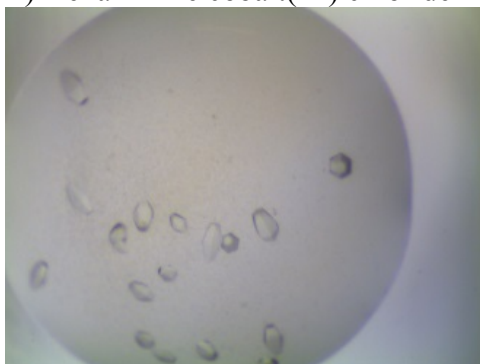
D) Ammonium sulfate



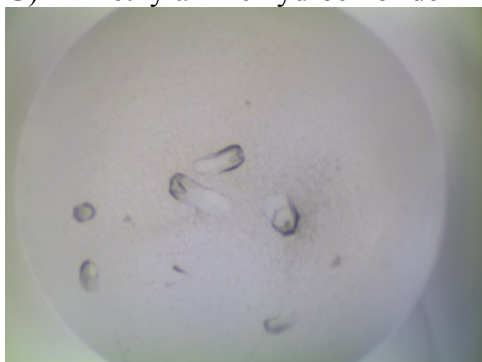
E) Pheno



F) Hexammine cobalt(III) chloride



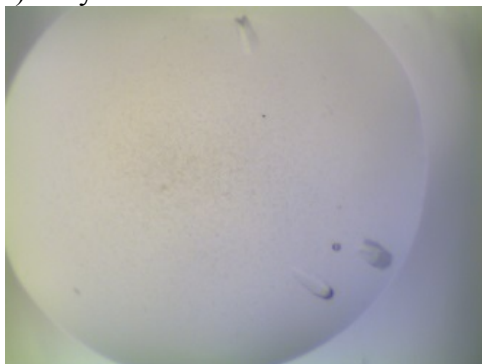
G) Trimethylamine hydrochloride



H) Acetonitrile



I) Ethyl acetate



J) 1-Butanol

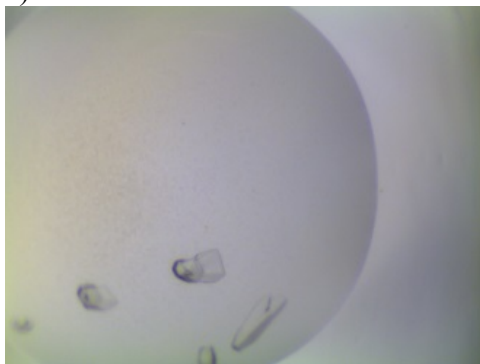


Figure 2.6: Crystallization of SEM-dPGAM5 with Additive screen. Crystal trials were set up using SEM-dPGAM5 at 8mg/ml in MbClassII-71 solution at a 1:1 ratio (A-J). Additives were added to a final concentration as indicated in the table.

¹Letter designations for the corresponding pictures found below the table.

²Final concentration of the additive within the drop.

³Name of the additive used.

⁴Description of the additive used.

We set up three additional screens using 6mg/ml or 8mg/ml SEM-dPGAM5 protein. For each screen, we used ratios of protein:solution of 1:3, 1:1, and 3:1. Table

2.7 outlines the results of each screen. Of the three screens tested, PEGII-28 solution produced crystals similar to those found with MbClassII-78.

Table 2.7: Crystallization of SEM-dPGAM5

| Screen ¹ | [Protein] ² | Ratio ³ | Well(s) ⁴ | Notes ⁵ | Condition ⁶ |
|---------------------|------------------------|--------------------|--|--|---|
| PEG II Suite | 8mg/ml | 1:3 | C4, H6 | C4 is sharp, hexagonal, about 0.06mm | C4 = 0.2M Magnesium Chloride, 0.1M MES pH 6.5, 10% PEG 4000 |
| PEG II Suite | 8mg/ml | 1:1 | C4, C7, H6, H9 | H6 is good shape, about 0.08-0.09mm in size | H6 = 0.1M Tris pH 8.5, 8% PEG 8000 |
| PEG II Suite | 8mg/ml | 3:1 | B9, B11, C8, C11, D1, E8, E12, G9, G10, G11, H11 | C8 good size, relatively sharp, some clustering of crystals. | C8 = 0.2M Sodium Acetate, 0.1M Tris pH 8.5, 16% PEG 4000 |
| Compas Suite | 6mg/ml | 1:1 | A2, A6 | A6: Crystal size of 0.09-0.12mm, ok shape | A6 = 0.05M NH4SO4, 0.1M Sodium Citrate, 15% PEG 8000 |
| Compas Suite | 6mg/ml | 3:1 | A8-12, B1, B6 | A8: Crystal size of 0.09-0.12mm, ok shape | A8 = 0.1M Sodium Acetate, 0.1M Hepes pH 7.5, 18% PEG 8000, 2% Isopropanol |
| Compas Suite | 8mg/ml | 1:1 | A1, A2, A5, C3 | no ideal crystals for optimization | |
| Compas Suite | 8mg/ml | 3:1 | A2, A7, A8, B1, B5-7, C3 | no ideal crystals for optimization | |
| JCSG Suite I | 8mg/ml | 1:1 | E5 | no ideal crystals for optimization | |
| JCSG Suite I | 8mg/ml | 3:1 | A7, C9, D6, E7, F11 | C9 was decent shape, about 0.07-0.08mm | C9 = 10% Glycerol, 0.1M Hepes pH 7.5, 5% PEG 3000, 30% PEG 4000 |

Table 2.7: Crystallization of SEM-dPGAM5 using PEG II, Compas Suite, and JCSG Suite I screens.

¹The crystal screen used for trials.

²Concentration of SEM-dPGAM5 used in screen.

³Indicates the ratio of protein to solution used per screen.

⁴Indicates wells within screen containing crystals.

⁵Notes on crystals that may be good candidates for optimization.

⁶Composition of solution to generate crystals mention in column 5.

We set up two trays to compare MbClassII-71 with PEGII-28. Crystals were generated using MbClassII-71 or PEGII-28 alone or in the presence of an additive (either sodium bromide, hexammine cobalt(III) chloride, or polyvinylpyrrolidone K15). In tray 1 (Table 2.8), larger drops (10uL) and 6mg/ml protein was used in attempt to slow down the crystallization rate and get larger crystals. While crystals still formed within one to

two days, the crystals were slightly larger in size compared with that of a 2uL drop (Table 2.9). However, most of the crystals in the 10uL drop formed off the surface of the plate or had multiple nucleation sites within one crystal, making it difficult to work with the crystals.

Table 2.8: Comparison of MbClassII-71 with PEGII-28

| Tray 1 Wells | Base Solution | Additive |
|--------------|---------------|-------------------------------|
| A1-A2 | MBClassII-71 | Sodium Bromide |
| A3-A4 | MBClassII-71 | Hexamine Cobalt(III) Chloride |
| A5-A6 | MBClassII-71 | PVP K15 |
| B1-B2 | PEG II | Sodium Bromide |
| B3-B4 | PEG II | Hexamine Cobalt(III) Chloride |
| B5-B6 | PEG II | PVP K15 |
| | | |
| Tray 2 Wells | Base Solution | Additive |
| A1-A2 | MBClassII-71 | None |
| A3-A4 | MBClassII-71 | None |
| A5-A6 | MBClassII-71 | None |
| B1-B2 | MBClassII-71 | Sodium Bromide |
| B3-B4 | MBClassII-71 | Hexamine Cobalt(III) Chloride |
| B5-B6 | MBClassII-71 | PVP K15 |
| C1-C2 | PEGII-28 | None |
| C3-C4 | PEGII-28 | None |
| C5-C6 | PEGII-28 | None |
| D1-D2 | PEGII-28 | Sodium Bromide |
| D3-D4 | PEGII-28 | Hexamine Cobalt(III) Chloride |
| D5-D6 | PEGII-28 | PVP K15 |

Table 2.8: Layout of trays 1 and 2 solutions comparing MbClassII-71 with PEGII-28.

Tray 1: Drop size of crystal trials was 10uL. The concentration of SEM-dPGAM5 was 6mg/ml. The final concentration of the additives was 10mM final. The ratio of protein to well solution was 1:1.

Tray 2: Drop size of crystal trials was 2uL. The concentration of SEM-dPGAM5 was 8mg/ml. The final concentration of the additives was 10mM final. The ratio of protein to well solution was 1:1.

Tray 2 consisted of a 2uL drop size. The protein concentration was 8mg/ml using a 1:1 ratio of protein:well solution. The additives were kept at 10mM final. Wells A1-C6 all formed very small crystals. Wells D1-D6 showed improved crystal size and shape, while D1/D2 were the best. Overall, crystals in MbClassII-71 with Hexamine Cobalt(III) Chloride consistently produced crystals of ideal shape. While the size was still small, it was slightly improved in 10uL drops at 6mg/ml (Figure 2.8).

Figure 2.8: Crystals used for screening cryoprotectants and x-ray diffraction

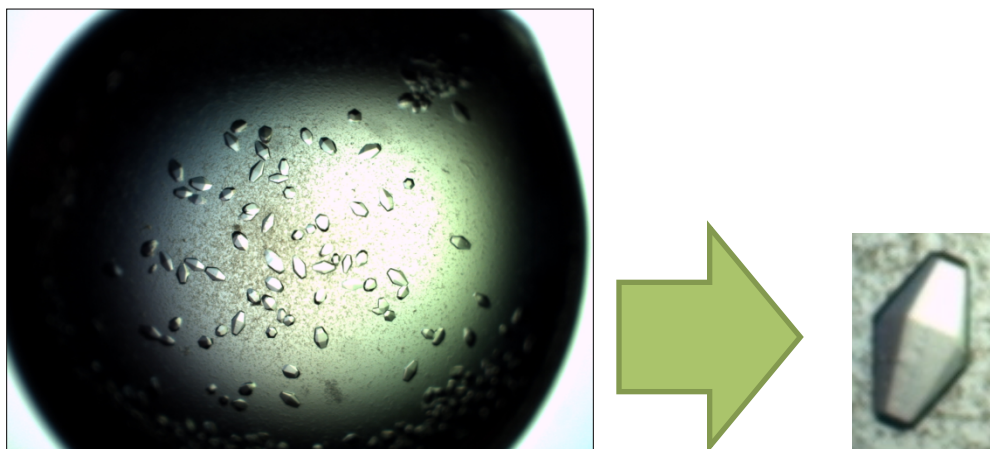


Figure 2.8: Crystals used for screening cryoprotectants and testing for x-ray diffraction. Crystals were formed in 10uL drops consisting of MbClassII-71 solution with 10mM Hexamine Cobalt(III) Chloride. SEM-dPGAM5 protein concentration was 6mg/ml. Drop was setup at a ratio of 1:1 and incubated at 18C.

2.9 Cryoprotectants and x-ray diffraction of SEM-dPGAM5

Freezing of crystals helps reduce crystal degradation caused by exposure to the x-ray beam. Frozen crystals also helps reduce background noise caused by random motion of the crystal. To freeze crystals, they are flash frozen in liquid nitrogen, however, simply freezing the crystal typically results in cracking of the crystal. Therefore, it is important to find an appropriate cryoprotectant that prevents cracking of the crystal upon freezing and does not interfere with diffraction. We tested four cryoprotectants but determined that they were not suitable cryoprotectants (Table 2.10). The cryoprotectants were not suitable for they either resulted in cracking of the crystal once submerged in the cryoprotectant or in a loss of diffraction signal as compared to non-frozen conditions, as discussed in section 2.8.

Table 2.9: Cryoprotectants tested with crystals

| Cryoprotectant | Notes |
|---------------------------------------|--|
| 35% PEG 4000 (w/v) | Solution 1 (35% PEG 4000) The crystals had some initial cracking. The well had dried up (probably bad sealing of the well). |
| 20% Glycerol (v/v) | Solution 2 (20% Glycerol) The crystals look good. There was no cracking of the crystal. No diffraction data was obtained after a 10 minute exposure (150 distance) on the R-axis. From the diffraction data, it appeared that there was ice ring formation. |
| 20% PEG 400 (v/v) | Solution 3 (20% PEG 400) The crystals appeared to have no cracking. The diffraction data obtained on the R-axis was poor. |
| 30% PEG 4000 (w/v), 20% PEG 400 (v/v) | Solution 4 (30% PEG 4000, 20% PEG 400) The crystals looked in good condition. There was a film that developed on the drop that made it difficult to remove crystals from the drop without contaminating the crystal with debris from the film. No diffraction data was obtained on the R-axis. |

Table 2.9: Cryoprotectants test with SEM-dPGAM5 crystals. Column 1 indicates the cryoprotectant tested. Column 2 describes the results obtained upon submerging crystals into the cryoprotectant and the ability of the crystal to diffract.

We also tested the JBScreen PE HTS, as this screen not only provides unique conditions for crystallization but also acts as a cryoprotectant. This allows one to transfer the crystals formed in the drop immediately into liquid nitrogen, bypassing any additional soaking in cryoprotectants. Two solutions gave crystals that would be worth optimizing (Figure 2.9). These crystals obtained from JBScreen would be candidates for optimization and to test for x-ray diffraction.

Figure 2.9: Crystallization of SEM-dPGAM5 using JBScreen

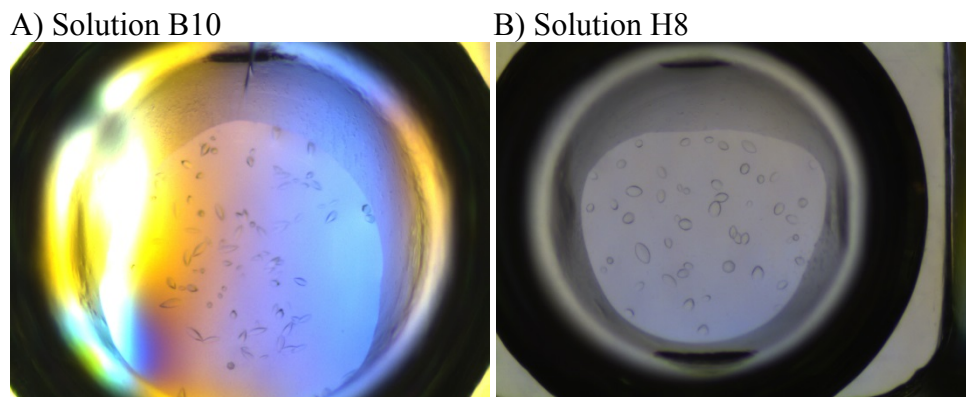


Figure 2.9: Crystallization of SEM-dPGAM5 using JBScreen. Drops were setup using 8mg/ml SEM-dPGAM5 in the JBScreen. (A) Crystals formed in solution B10 (25% w/v PEP 426, 100mM Tris pH 8.5,

50mM Magnesium chloride) using a 1:1 ratio. (B) Crystals formed in solution H8 (35%w/v PEE 797, 100mM Hepes pH 7.5, 200mM ammonium sulfate) using a 3:1 ratio.

2.10 X-ray diffraction of SEM-dPGAM5 crystals using the dry method

Since we had little success obtaining diffraction data (see notes in Table 2.10) from crystals screened after being incubated in cryoprotectants, we screened three crystals using a dry method. Briefly, crystals were picked from the drop and covered using a small capillary tube, which contains a small amount of the well solution (Figure 2.10). This method allows us to determine if our crystals will diffract. However, without the use of a suitable cryoprotectant, the crystals will quickly degrade after being exposed to the x-rays. This leads to rapid degradation of signal from diffracted x-rays, preventing us from collecting sufficient data to determine a structure for dPGAM5.

Figure 2.10: Diagram depicting dry method

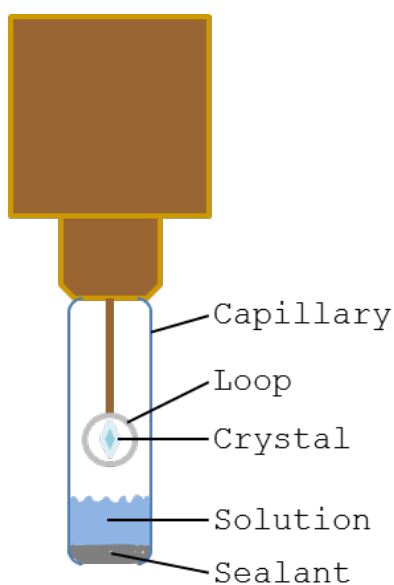


Figure 2.10: Diagram depicting dry method. Crystals are picked from the solution using a mounted cryoloop. A thin-walled capillary containing a small volume of well solution is placed around the crystal to form a closed environment. Sealant (silicon) was used to ensure closure of the system.

Using crystals generated from the conditions shown in figure 2.10, we collected diffraction data for 30min using the dry method. The dry method generated the best set of reflections, thus far, with various intensities and a resolution of about 4.7Å (Figure 2.11). This confirms that the crystals are capable of generating diffraction data. One issue of collecting diffraction data at room temperature is that the crystal will quickly degrade. Therefore, you cannot obtain adequate diffraction data to elucidate any structure. This approach simply confirms that crystals grown in these conditions can diffract and that it is necessary to find an optimal freezing condition in order to obtain higher resolution data.

Figure 2.11: Diffraction of SEM-dPGAM5 crystals using dry method

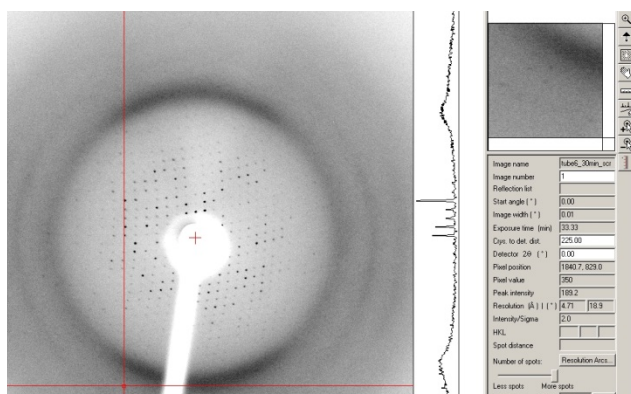


Figure 11: Diffraction of SEM-dPGAM5 crystals using the dry method. SEM-dPGAM5 crystals were mounted using the dry method (as described in figure 10). The crystals were exposed to the x-rays and data was collected for 30 minutes. The maximum resolution achieved was about 4.7Å.

2.11 Discussion

In this chapter, we tested three human PGAM5 proteins for phosphatase activity. Both the full-length and ΔN49-PGAM5 proteins were active phosphatases. ΔN89-PGAM5 consisted of amino acids 89-289 of PGAM5, which was inactive as a phosphatase. The protein used to determine the structure of PGAM5 consisted of amino

acids 98-289, which, from our studies, is inactive as a phosphatase (see chapter 3). The goal of these experiments was to obtain a structure for PGAM5 that was active as a phosphatase.

Our initial attempt to crystallize PGAM5 was with human PGAM5 proteins. While we were able to concentrate Δ N89-PGAM5 up to 5mg/ml, we did not pursue many trials with this protein because we knew it was an inactive phosphatase (Table 2.1). The Δ N49-PGAM5 protein was difficult to concentrate over 1mg/ml before it would begin falling out of solution. We set up several crystal trials using Δ N49-PGAM5 at 1mg/ml (Table 2.4), however, we did not find any conditions that would crystallize Δ N49-PGAM5.

Several strategies are used by crystallographers in attempt to improve the solubility and/or stability of proteins in solution, which hopefully allows the crystallographer to identify more conditions in which proteins will crystallize. Point mutations are used to change the charge or polarity of amino acids in order to help increase solubility and or stability of your protein in solution [136]. Purified proteins that are unstable in solution are sometimes stabilized through interactions with known binding partners and can therefore be crystallized as a complex [135]. It is often times the case that homologous proteins from other species conserve function and structure, therefore, using homologous proteins provides a means of using a protein with a different amino acid composition, which may help with stability and solubility [137].

We purified the *Drosophila* form of PGAM5, residues 30-289, and were able to concentrate dPGAM5 up 13mg/ml and confirmed it to be an active phosphatase (Table 2.1). We screened hundreds of unique conditions and narrowed down the conditions that

gave the most optimal crystals in term of shape and size. The current condition optimized for *Drosophila* PGAM5 (V30-TGA) is 0.1M Lithium Sulfate, 0.1M ADA pH 6.5, 12% (w/v) PEG 4000 with 10mM Hexamine Cobalt(III) Chloride. This condition produced crystals that were symmetrical and sharp-edged (Figure 2.8) and capable of diffraction up to 4.5 angstroms (Figure 2.11).

The next step is to determine optimal conditions for freezing dPGAM5 crystals to allow us to expose PGAM5 to x-ray sources for longer periods of time in order to collect more diffraction data for structure determination. The cryoprotectants we tested caused cracking of the crystals or degraded the quality of the diffraction data. When we tested diffraction of crystals using the dry method, we were able to collect data to 4.5 angstroms. However, in the presence of cryoprotectant, the diffraction data worsened or was completely lost. Crystals have been shown to grow well in glycerol and PEG 797, which are known cryoprotectants (Figure 2.6 and 2.9). These cryoprotectants would be a good start for determining freezing conditions.

In chapter 3, we show that PGAM5 forms a multimeric structure. Furthermore, we show that purified PGAM5 exists in at least three different complexes. As determined by size exclusion chromatography, PGAM5 elutes in three pools. One pool eluted in the void volume of the column. The second pool eluted as a dodecamer, while the third pool eluted as a dimer. The protein used for crystal trials was not purified by size exclusion, which means our trials were carried out using a complex mixture of PGAM5 proteins. We confirmed that the PGAM5 dodecamer was a stable complex and that it contained phosphatase activity. Therefore, future crystal trials should be carried out using the dodecamer to ensure a single population of PGAM5 is being used, which

may improve the overall quality of the crystals, allow diffraction data to be collected, and facilitate attempts to find a suitable cryoprotectant.

Chapter 3

Multimerization of PGAM5 is necessary for
PGAM5 phosphatase activity and
mitochondrial morphology

Mitochondria participate in several cellular events including generation of ATP, production of reactive oxygen species (ROS), and cell death [4, 5, 7, 8, 141]. Each of these events is associated with the ability of mitochondria to establish a membrane potential [142, 143]. During oxidative phosphorylation, electrons are transported along the electron transport chain, which is coupled to the pumping of protons from the mitochondrial matrix into the mitochondrial intermembrane space [5]. This results in a net negative charge in the matrix and a net positive charge in the intermembrane space. The protonophore carbonyl cyanide m-chlorophenyl hydrazine (CCCP) is well known for its ability to uncouple mitochondria by disrupting the proton gradient generated during oxidative phosphorylation [144]. In mammalian cells, CCCP has also been shown to induce mitochondrial fragmentation [145]. Several studies suggest that mitochondrial fragmentation upon loss of mitochondrial membrane potential (MMP) is induced by the differential proteolytic cleavage of the mitochondrial fission protein OPA1 by OMA1 protease [146-148].

Recently, the protein phosphoglycerate mutase 5 (PGAM5) was shown to be cleaved by the mitochondrial rhomboid protease PARL in response to loss of mitochondrial membrane potential (MMP) [128]. PGAM5 is a Ser/Thr phosphatase that is targeted to the mitochondria by an N-terminal mitochondrial localization signal (MTS) [120, 121]. In this study we characterized the phosphatase activity of PGAM5 and provide evidence that PGAM5 has a greater affinity for substrates that have negatively charged amino acids near the phosphorylation site. We discovered a multimerization domain in PGAM5 that is required for multimerization of PGAM5 and phosphatase activity. Furthermore, we show that PGAM5 exists in two distinct pools in cells; One

high molecular weight (MW) pool around 300KDa and one low MW pool around 60KDa. Upon CCCP treatment, PGAM5 undergoes proteolytic cleavage by PARL and exists solely in the low MW pool. Overexpression of PGAM5 harboring mutations in the multimerization domain results in fragmentation of mitochondria. Our data suggests a model in which PGAM5 exists in a high MW complex that behaves as an active phosphatase. During mitochondrial uncoupling, PGAM5 is cleaved by PARL, resulting in inactivation and dissociation of the PGAM5 complex. Inactivation of PGAM5 in turn results in mitochondrial fragmentation.

3.1 Characterization of PGAM5's phosphatase activity

The human phosphoglycerate mutase (PGAM) family consists of eleven members that are characterized by containing a PGAM motif that contains a highly conserved RHG sequence in which the Arg-His residues play critical roles in catalysis [116]. PGAM5 was previously characterized as a Ser/Thr phosphatase, but little is known about its substrate specificity [121]. To help characterize substrate specificity, we utilized eight model phosphopeptides and tested them as substrates for PGAM5 (Table 3.1). Our results confirm that PGAM5 is a Ser/Thr-phosphatase while lacking Tyr-phosphatase activity (Table 3.1). We found that PGAM5 was considerably more active against the phosphopeptide containing two negatively charged aspartic acid residues ($K_m = 71\mu M$) compared to the phosphopeptide containing two positively charged arginine residues ($K_m = 1953\mu M$). Our data would suggest that PGAM5 has a preferential binding and activity for substrates that contain negatively charged residues near the phosphorylation site.

Table 3.1: Kinetic parameters of PGAM5 phosphatase activity against model phosphopeptides

| Peptide ¹ | K _m (μM) ² | V _{max} (pmol/min/μg) ³ |
|----------------------|----------------------------------|---|
| END(T)INASL | 112.6 (3.9) | 2403.7 (38.8) |
| DDA(T)VA | 71.8 (2.0) | 2592.9 (28.6) |
| AAA(T)VA | 206.4 (7.4) | 2104.2 (42.8) |
| RRA(T)VA | 1953.5 (184.8) | 1212.3 (95.2) |
| RRA(S)VA | 1354.3 (203.8) | 1858 (183.8) |
| RRA(Y)VA | N.D. | N.D. |
| END(Y)INASL | N.D. | N.D. |
| DADE(Y)LIPQQG | N.D. | N.D. |

Table 3.1: Kinetic parameters of PGAM5 phosphatase activity against model phosphopeptides. Recombinant HIS-PGAM5 was expressed in bacterial cells. Bacterial lysates were subjected to affinity purification using a Ni-NTA column. HIS-PGAM5 was eluted and desalted to 150mM NaCl, 10mM Hepes, pH 7.2 and used in phosphatase assays. Briefly, HIS-PGAM5 was incubated with various concentrations of phosphorylated peptide. Reactions were quenched using HCl and free-phosphate was detected using a shift in malachite green absorbance at 620nm. Velocity curves were generated and fitted using KaleidaGraph software to determine Vmax and Km values against the phospho-peptides tested. Values were determined using the average value triplicate runs.

¹The peptide sequence analyzed indicating the phosphorylation site within parenthesis.

²The Michaelis constant Km determined for the respective peptide with the Km error indicated in parenthesis.

³The maximum velocity (Vmax) achieved by PGAM5 for the respective peptide. Presented in pmol of free-phosphate generated per minute per μg of PGAM5 used. Vmax error is indicated in parenthesis. N.D. = not determined due to insufficient phosphatase activity against respective peptide.

PGAM5 has previously been reported to interact with several proteins including ASK1 (MAP3K5, Gene ID: 4217), BCL-XL (BCL2L1, Gene ID: 598), DRP1 (DNM1L, Gene ID: 10059), and KEAP1 (KEAP1, Gene ID: 9817) [53, 117, 118, 120, 121]. To further analyze PGAM5 substrate specificity, we designed 13 phosphopeptides that correspond to known phosphorylation sites found within the candidate targets for PGAM5 phosphatase activity (Table 3.2) [53, 117, 120, 121].

Table 3.2 Kinetic parameters of PGAM5 phosphatase activity against candidate substrates

| Protein ¹ | phosphorylation Site ² | Peptide ³ | K _m (μM) ⁴ | V _{max} (pmol/min/μg) ⁵ |
|----------------------|-----------------------------------|----------------------|----------------------------------|---|
| ASK1 | Ser-83 | RGRGS(S)VGGGS | 656.4 (22.0) | 51.0 (0.9) |

| | | | | |
|-----------|----------|---------------|----------------|----------------|
| ASK1 | Thr-838 | NPCTE(T)FTGTL | 64.5 (4.5) | 2325.1 (63.4) |
| ASK1 | Ser-958 | ALSAG(S)NEYLR | 2749.0 (475.7) | 1304.7 (120.7) |
| ASK1 | Ser-966 | YLRSI(S)LPVPV | 237.1 (30.0) | 966.4 (72.4) |
| ASK1 | Ser-1029 | NFEDH(S)APPSP | 23.3 (2.3) | 2663.8 (78.9) |
| ASK1 | Ser-1033 | HSAPP(S)PEEKD | 26.4 (2.0) | 1712.4 (40.5) |
| Bcl-XL | Thr-47 | ESEME(T)PSAIN | 49.7 (6.8) | 769.1 (27.7) |
| Bcl-XL | Ser-62 | WHLAD(S)PAVNG | 28.5 (1.7) | 2053.9 (39.1) |
| Bcl-XL | Thr-115 | SQLHI(T)PGTAY | 480.4 (28.6) | 789.5 (14.9) |
| Bcl2 | Thr-69 | DPVAR(T)SPLQT | N.D. | N.D. |
| Bcl2 | Ser-70 | PVART(S)PLQTP | 98.4 (9.4) | 1283.8 (37.1) |
| Bcl2 | Ser-87 | AGPAL(S)PVPPV | 356.8 (12.6) | 2614.6 (40.0) |
| Cortactin | Ser-405 | QTPPV(S)PAPQP | 133.8 (13.2) | 528.7 (18.6) |
| Drp1 | Ser-548 | ASQEP(S)PAASA | 113.7 (32.5) | 1229.7 (163.0) |
| Drp1 | Ser-616 | PIMPA(S)PQKGH | N.D. | N.D. |
| Drp1 | Ser-637 | VARKL(S)AREQR | 409.2 (69.3) | 1722.4 (103.0) |
| Nrf2 | Ser-40 | EVFCF(S)QRRKE | N.D. | N.D. |
| Stathmin | Ser-25 | FELIL(S)PRSKE | 179.0 (99.0) | 46.2 (6.7) |
| Stathmin | Ser-38 | PEFPL(S)PPKKK | N.D. | N.D. |

Table 3.2. Kinetic parameters of PGAM5 phosphatase activity against candidate substrates. Recombinant HIS-PGAM5 was expressed in bacterial cells. Bacterial lysates were subjected to affinity purification using a Ni-NTA column. HIS-PGAM5 was eluted and dialyzed against 150mM NaCl, 10mM Hepes, pH 7.4 and used in phosphatase assays. Briefly, HIS-PGAM5 was incubated with various concentrations of phosphorylated peptide. Reactions were quenched using HCl and free-phosphate was detected using a shift in malachite green absorbance at 620nm. Velocity curves were generated and fitted using KaleidaGraph software to determine Vmax and Km values against the phospho-peptides tested. Values were determined using the average value triplicate runs.

1The name of the human protein from which the peptides were derived.

2The residue and amino acid position of the phosphorylation site found within the protein.

3The peptide sequence analyzed indicating the phosphorylation site within parenthesis.

4The Michaelis constant Km determined for the respective peptide. Km error indicated in parenthesis.

5The maximum velocity (Vmax) achieved by PGAM5 for the respective peptide. Vmax error indicated in parenthesis.

N.D. = not determined due to insufficient phosphatase activity against respective peptide.

PGAM5 displayed activity against 15 of the 19 tested phosphopeptides. Km values ranged from 23μM to greater than 600μM, the Vmax ranged from 51 to greater than 2,500 pmol free-phosphate/minute/μg of PGAM5. The top five peptides with the

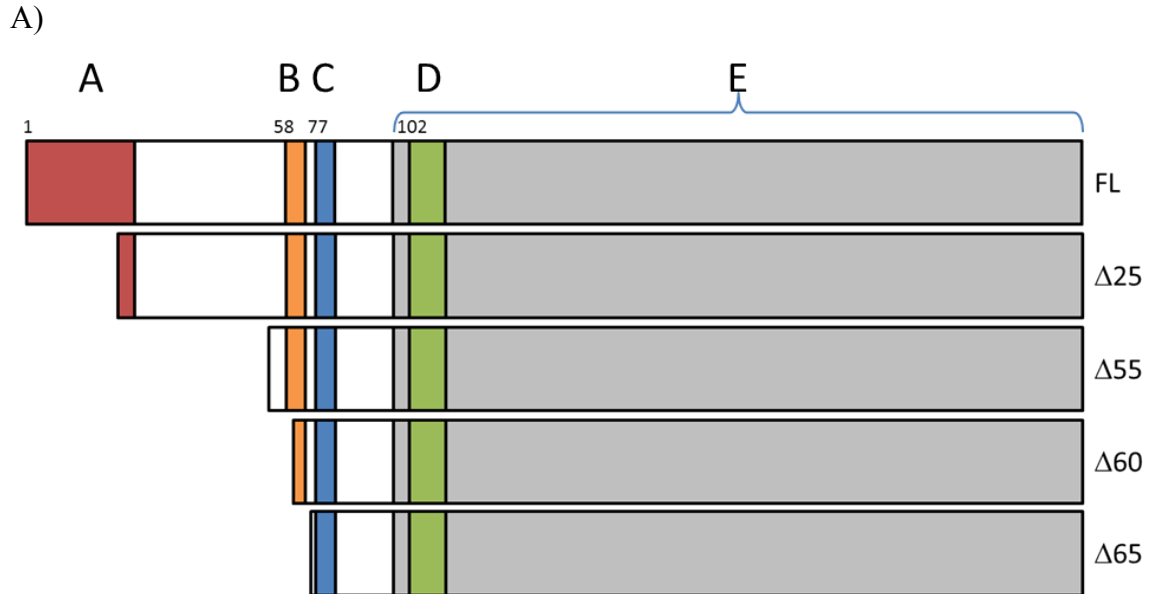
lowest K_m values contained one or more negatively charged residue. These data indicate that PGAM5 has a preference for negatively charged residues near the phosphorylation site of its substrate.

3.2 PGAM5's N-terminus is required for phosphatase activity

The catalytic domain of PGAM5 is believed to reside within the region of shared homology with other members of the PGAM family. This region starts at amino acid 98 in the human PGAM5 protein and continues through the remainder of the long form of PGAM5, which is 289 amino acids in length. This region contains several residues required for catalytic activity, including R104 and H105, which are both located in the signature motif that defines the PGAM family. However, the PGAM domain is not sufficient for activity of PGAM5 protein, as a truncated PGAM5 protein that starts at amino acid 89 was devoid of activity against several of the best peptide substrates tested in Table 1 (data not shown).

To define N-terminal residues that are required for PGAM5's enzymatic activity we generated a series of N-terminal truncated proteins (Figure 3.1). We assayed each protein for activity and found that removal of the first 55 amino acids of PGAM5 did not significantly affect the phosphatase activity of PGAM5. However, all truncations beyond amino acid 60 resulted in a complete loss of activity (Figure 3.2).

Figure 3.1: N-terminally truncated PGAM5 proteins



| Region | Amino Acids | Motif |
|-------------------------------------|-------------|------------|
| A) Mitochondrial Targeting Sequence | 1-28 | VLFSAVAV |
| B) Dimerization Domain (WD Motif) | 58-63 | WDPNWD |
| C) Keap1 Binding Region | 77-82 | NVESGE |
| D) PGAM Motif | 102-111 | LIRHSQYHVD |
| E) PGAM domain | 98-289 | |

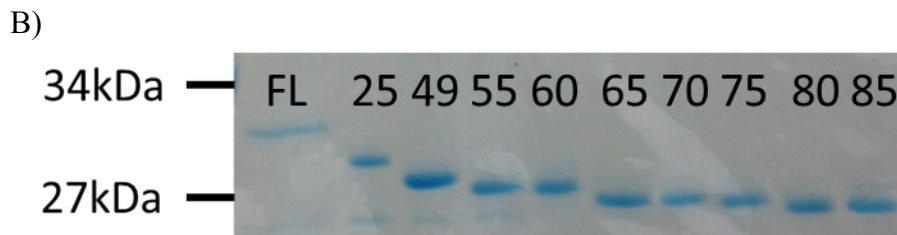


Figure 3.1: N-terminally truncated PGAM5 proteins. (A) Line diagrams depicting the N-terminal truncations of PGAM5 protein used for various assays. FL: full-length PGAM5 protein. Δ55, Δ60, Δ65: indicate a 55, 60, or 65 amino acid truncation, respectively, at the N-terminus of PGAM5. The table depicts regions of interest within PGAM5. (B) HIS-PGAM5 was expressed in bacterial cultures and purification from bacterial lysates was facilitated using a Ni-NTA column. Eluted proteins were exchanged into buffer containing 100mM NaCl and 20mM Hepes pH 7.2. Purified PGAM5 protein was resolved by SDS-PAGE and visualized by coomassie staining. Proteins from left to right: Full-length PGAM5, ΔN25-PGAM5, ΔN49-PGAM5, ΔN55-PGAM5, ΔN60-PGAM5, ΔN65-PGAM5, ΔN70-PGAM5, ΔN75-PGAM5, ΔN80-PGAM5, ΔN85-PGAM5.

Figure 3.2: Phosphatase activity of truncated PGAM5

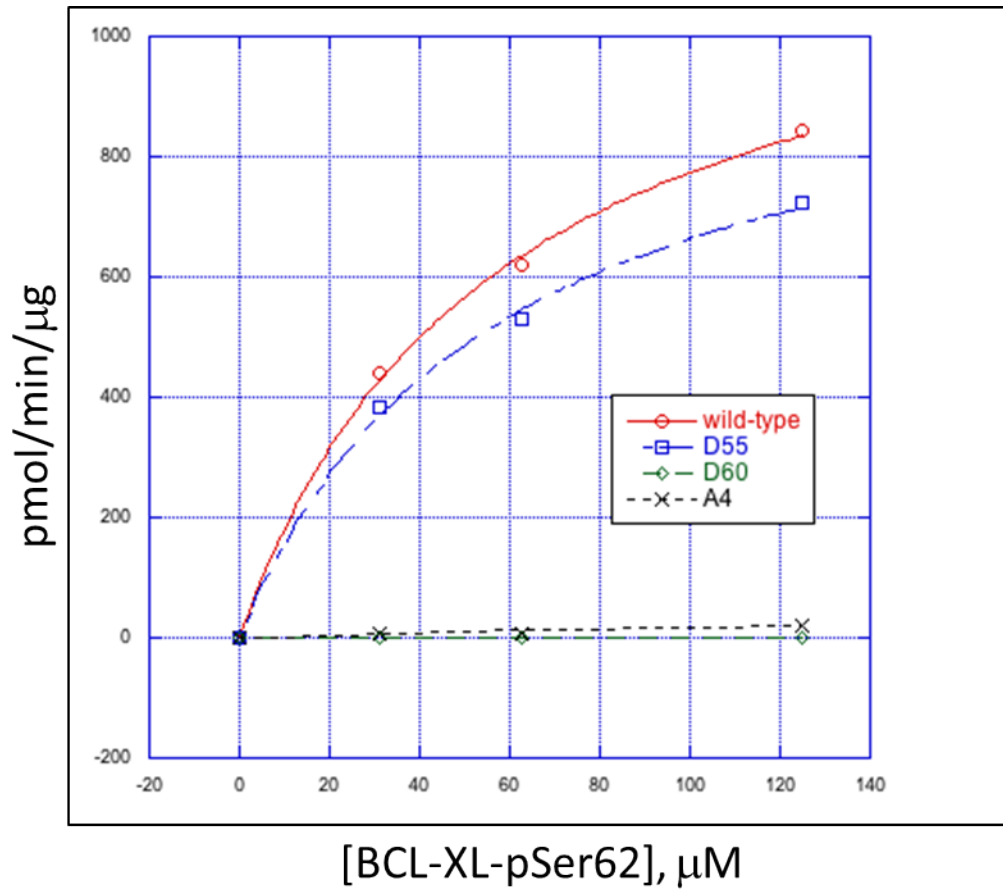


Figure 3.2: Phosphatase activity of truncated PGAM5. Full-length or truncated HIS-PGAM5 was incubated with various concentrations of the phosphopeptide BCL-XL-S62 (see Table 2). Reactions were quenched using HCl and free-phosphate was detected using a shift in malachite green absorbance at 620nm. Velocity curves were generated and fitted using KaleidaGraph software.

To confirm if these results were consistent in vivo we determined the ability of full-length PGAM5, $\Delta\text{N}55$ -, or $\Delta\text{N}60$ - PGAM5 to dephosphorylate BCL-XL at Ser-62 in cells. We co-transfected COS1 cells with expression vectors containing PGAM5 and BCL-XL. We used a phospho-specific antibody to detect the phosphorylation status of BCL-XL at residue Ser-62 by western blot (Figure 3.3). Expression of BCL-XL alone increased the phosphorylation signal compared to the mock (empty vector). To test the specificity of the antibody we expressed mutant BCL-XL-Ser62Ala alone and saw no increase in the phosphorylation signal by western blot. To measure activity of PGAM5

against BCL-XL, we titrated the amount of PGAM5 vector used in each transfection while keeping the amount of BCL-XL consistent. Both full-length PGAM5 and Δ N55-PGAM5 dephosphorylated BCL-XL with comparable activity. Δ N60 PGAM5, however, showed no activity against BCL-XL.

Figure 3.3: Phosphatase activity of PGAM5 against BCL-XL in cells

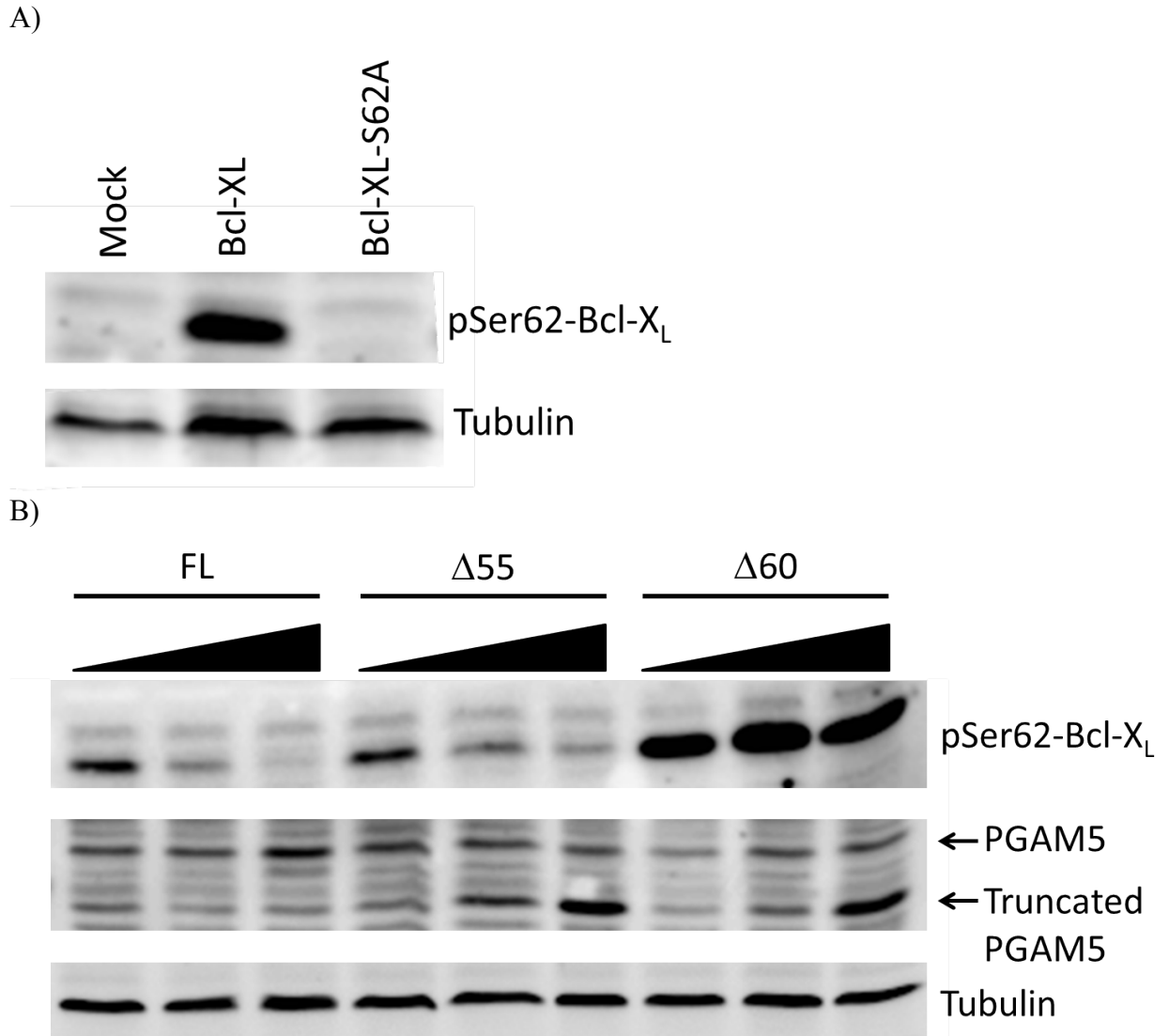
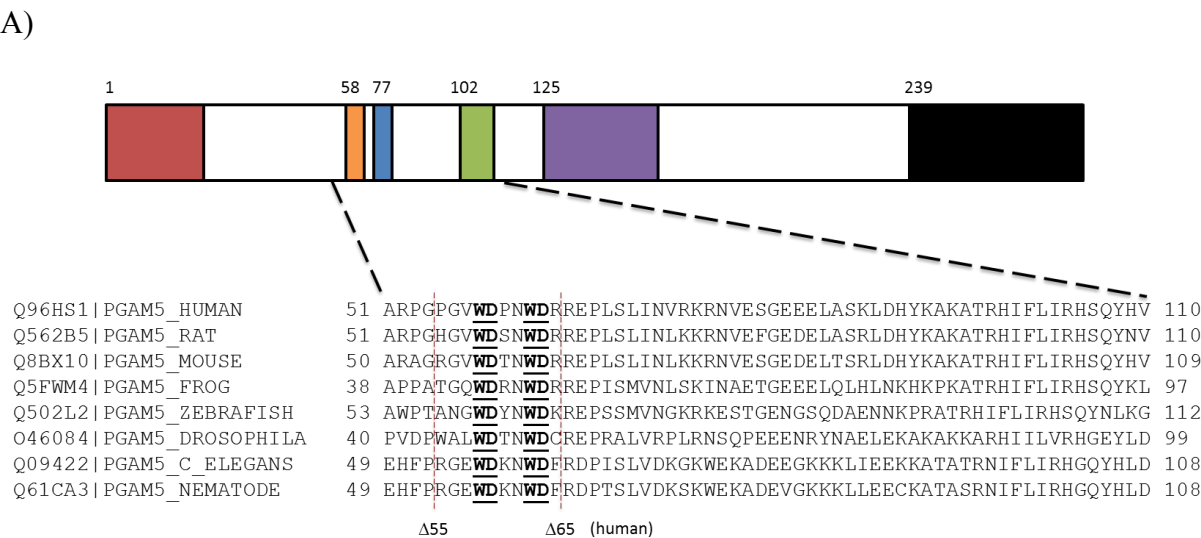


Figure 3.3: Phosphatase activity of PGAM5 against BCL-XL in cells. COS1 cells were transfected with expression vectors containing empty vector (mock), BCL-XL, BCL-XL-S62A, full-length PGAM5, Δ N55-PGAM5, or Δ N60-PGAM5. (A) Controls lanes transfected with a single vector as indicated. (B) Each lane was transfected with equivalent amounts of BCL-XL vector and was titrated with 0.01, 0.1, or 1 μ g of PGAM5 vector with the indicated construct. Phosphorylation of BCL-XL at Ser-62 was detected using a phospho-specific antibody (Santa Cruz). PGAM5 was detected using an affinity purified antibody. Tubulin antibody was purchased from Sigma.

3.3 The conserved WDxNWD motif is required for PGAM5's phosphatase activity

Analysis of PGAM5's amino acid sequence revealed the motif WDxNWD, which was conserved across all species of PGAM5 (Figure 3.4A). Since this motif was present in ΔN55-PGAM5 and partially deleted in ΔN60-PGAM5, we wanted to determine if this motif was critical for PGAM5's phosphatase activity. We generated three mutants of PGAM5 substituting each WD group individually or both together with alanine residues (Figure 3.4B). Each WD mutant was inactive as a phosphatase, supporting the notion that the WDxNWD motif is critical for PGAM5 phosphatase activity (Figure 3.4B).

Figure 3.4: Alignment of PGAM5 WDxNWD motif across various species



B)

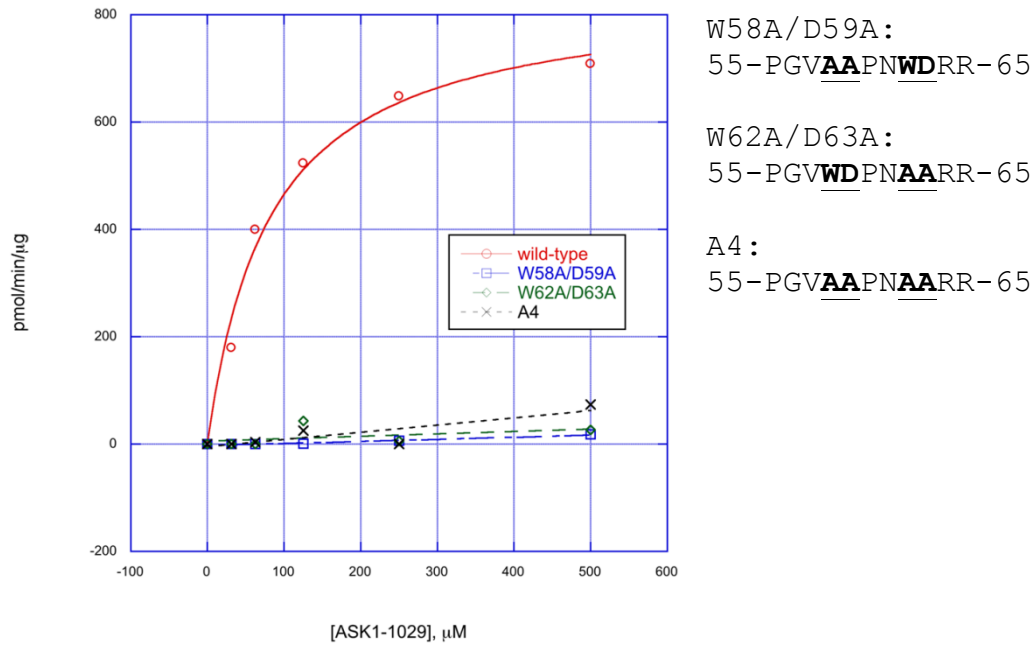


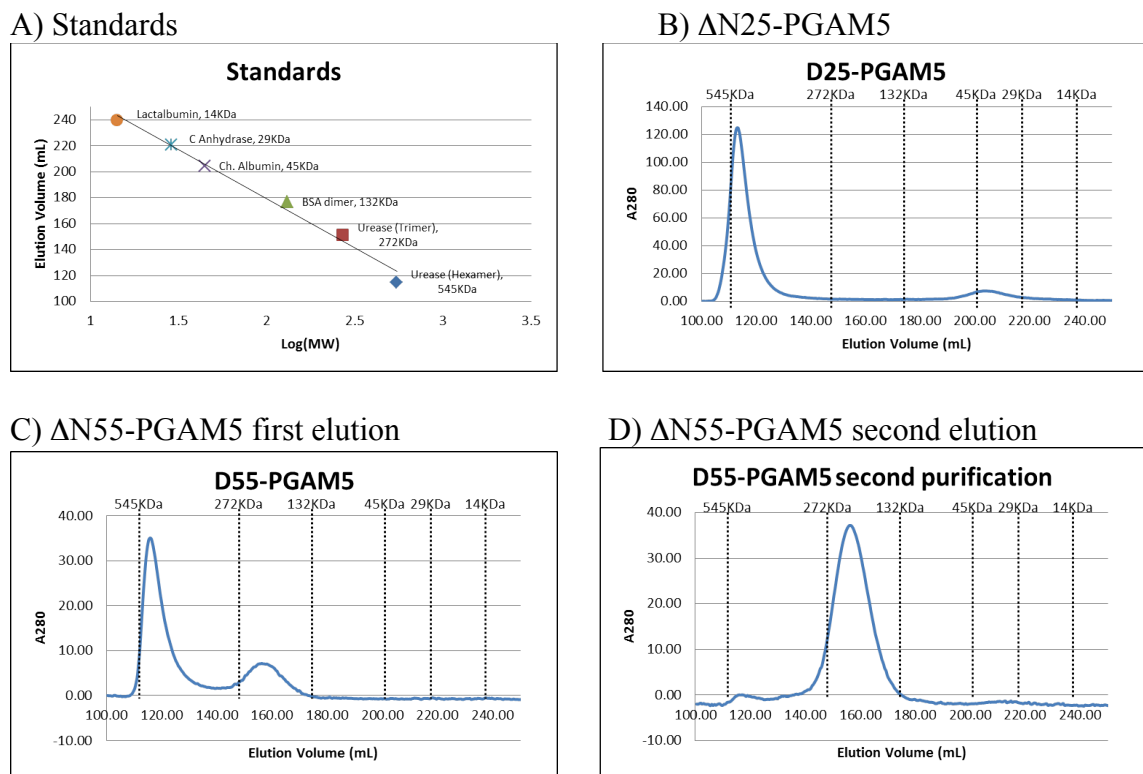
Figure 3.4: Alignment of PGAM5 WDxNWD motif across various species. (A) Top, line diagram depicting the region of the human PGAM5 protein used for sequence alignment with PGAM5 proteins from other species. Bottom, amino acid sequence alignment of PGAM5 from various species. Alignment was generated using ClustalW. (B) Phosphatase assay of WD-mutant PGAM5 proteins. To the right of the graph is the amino acid sequence of PGAM5 from 55 to 65 showing the various mutations generated.

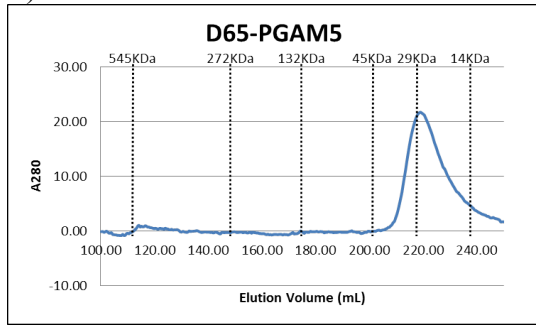
3.4 PGAM5 multimerization requires the WDxNWD motif

Within the human PGAM family, the protein STS-1 shares the greatest sequence homology with PGAM5. The crystal structure for PGAM5's and STS-1's PGAM domain was solved and showed that both proteins existed as dimers [134, 149]. To verify that PGAM5 existed as a dimer in solution we analyzed purified protein of both active and inactive PGAM5 proteins by size exclusion chromatography (SEC) (Figure 3.5). To our surprise, active PGAM5 predominately eluted in the void volume while about 25% of the protein eluted with an apparent MW of about 250,000Da (Figure 3.5 B and C). We isolated the 250KDa peak of ΔN55-PGAM5 and passed it over the column a second time to check the stability of the peak. We determined that the peak remained as a single

peak, rather than dissociating back into two peaks, indicating that the 250KDa peak of Δ N55-PGAM5 is stable. Interestingly, inactive PGAM5 eluted with an apparent molecular weight of about 30,000-45,000Da (Figure 3.5 E and F). We analyzed these proteins by light scattering in order to determine a more precise mass for these proteins. Analysis of these proteins by light scattering determined that Δ N55-PGAM5 and WD58/59AA-WD62/63AA-PGAM5 (A4-PGAM5) proteins have a MW of 334KDa and 66KDa, respectively (Figure 3.6). This is consistent with Δ N55-PGAM5 being a dodecamer and A4-PGAM5 being a dimer.

Figure 3.5: PGAM5 exists as a multimeric complex



E) Δ N65-PGAM5

F) A4-PGAM5

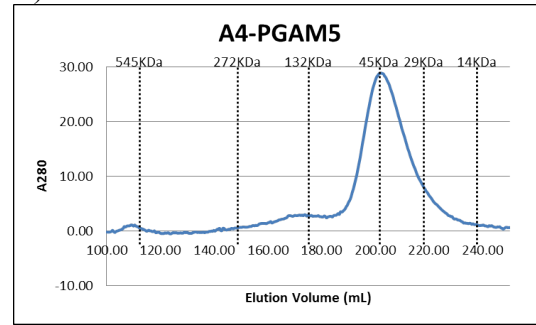


Figure 3.5: PGAM5 exists as a multimeric complex. Size exclusion chromatography of PGAM5 on HiLoad 26/60 Superdex 200 pg column. Each PGAM5 protein was purified on Ni-NTA columns and dialyzed to the same conditions of the running buffer prior to SEC. Proteins were detected using absorbance at 280nm. (B-F) apparent MW is indicated at top of trace as determined by the standard curve. (A) Standard curve using MW standards (Sigma). The protein and MW of each protein is indicated on the graph. (B) SEC of wild-type D25-PGAM5. (C) SEC of D55-PGAM5. The slower migrating peak (approximately at 160mL) was isolated and passed over the column for a second run (D). (E) SEC of D65-PGAM5. (F) SEC of D25-A4-PGAM5.

Figure 3.6: Molar mass determination of PGAM5 complexes

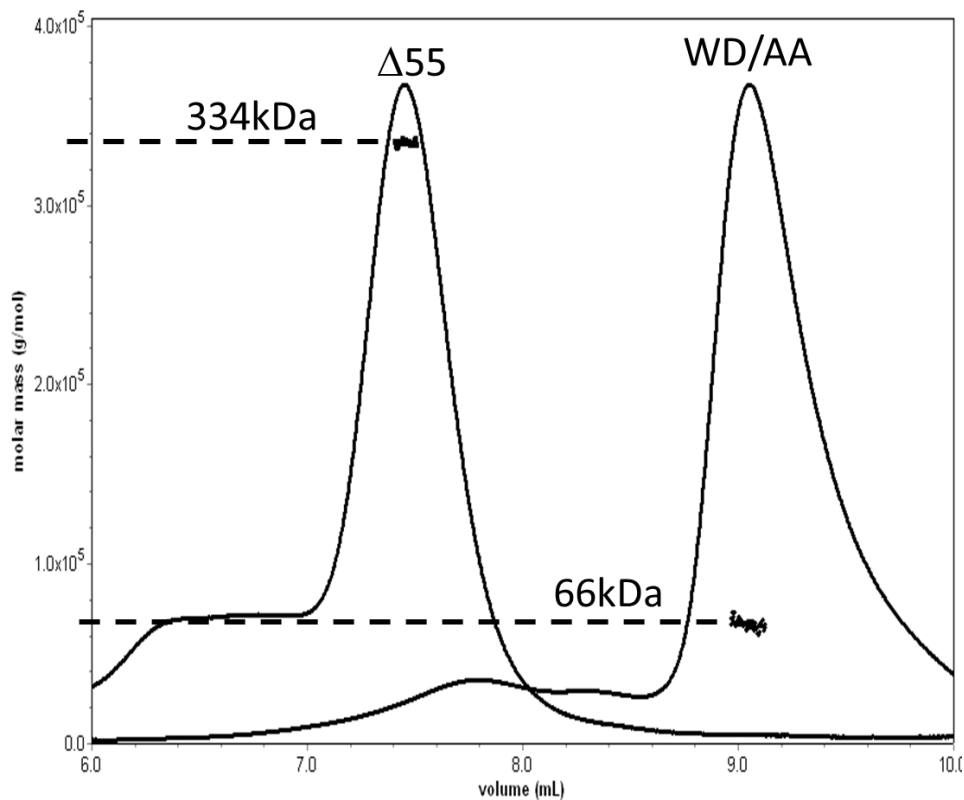


Figure 3.6: Molar mass determination of PGAM5 complexes. Purified PGAM5 protein eluted from the Ni-NTA column was desalted to 150mM NaCl, 10mM Hepes, pH 7.2. Desalted PGAM5 was subjected to size exclusion chromatography. Protein concentration was monitored by refractive index and the molar mass was determined by light scatter.

3.5 Two populations of PGAM5 exists in MEFs

We subjected MEF lysates to SEC to determine if PGAM5 existed as a higher ordered complex in cells. We stably expressed PGAM5 with a c-terminal FLAG-tag (PGAM5-FLAG) in PGAM5-deficient MEFs (see chapter 4). Since PGAM5 contains an N-terminal MTS, we used a C-terminal tag to ensures proper localization to mitochondria. MEF lysates were collected and separated by SEC (Figure 3.7A). We collected 10mL fractions and performed a trichloroacetic acid (TCA) precipitation. TCA precipitated proteins were resuspended in sample buffer and analyzed by western blot (Figure 3.7B). We found that PGAM5-FLAG existed in two separate pools. One pool had an average apparent size of approximately 300KDa, while the second pool was approximately 60KDa in size.

We noticed by western blotting in untreated conditions that the upper band of PGAM5-FLAG was more prominent in the high MW pool, while the lower band of PGAM5-FLAG was more prominent in the lower MW pool. Recently, PGAM5 was shown to be cleaved by PARL after carbonyl cyanide 3-chlorophenylhydrazone (CCCP) treatment, which gives rise to the lower band of PGAM5 as seen by western blot analysis [128]. Therefore, we hypothesized that CCCP treatment would cause cleavage of PGAM5-FLAG and shift the pools of PGAM5-FLAG in cells predominately to the lower MW pool. Indeed, after CCCP treatment, all of PGAM5-FLAG was found strictly in the low MW pool (Figure 3.7B). This suggests that multimerization of PGAM5, in part, is dependent on mitochondrial membrane potential.

Figure 3.7: PGAM5 exists in two distinct pools in MEFs

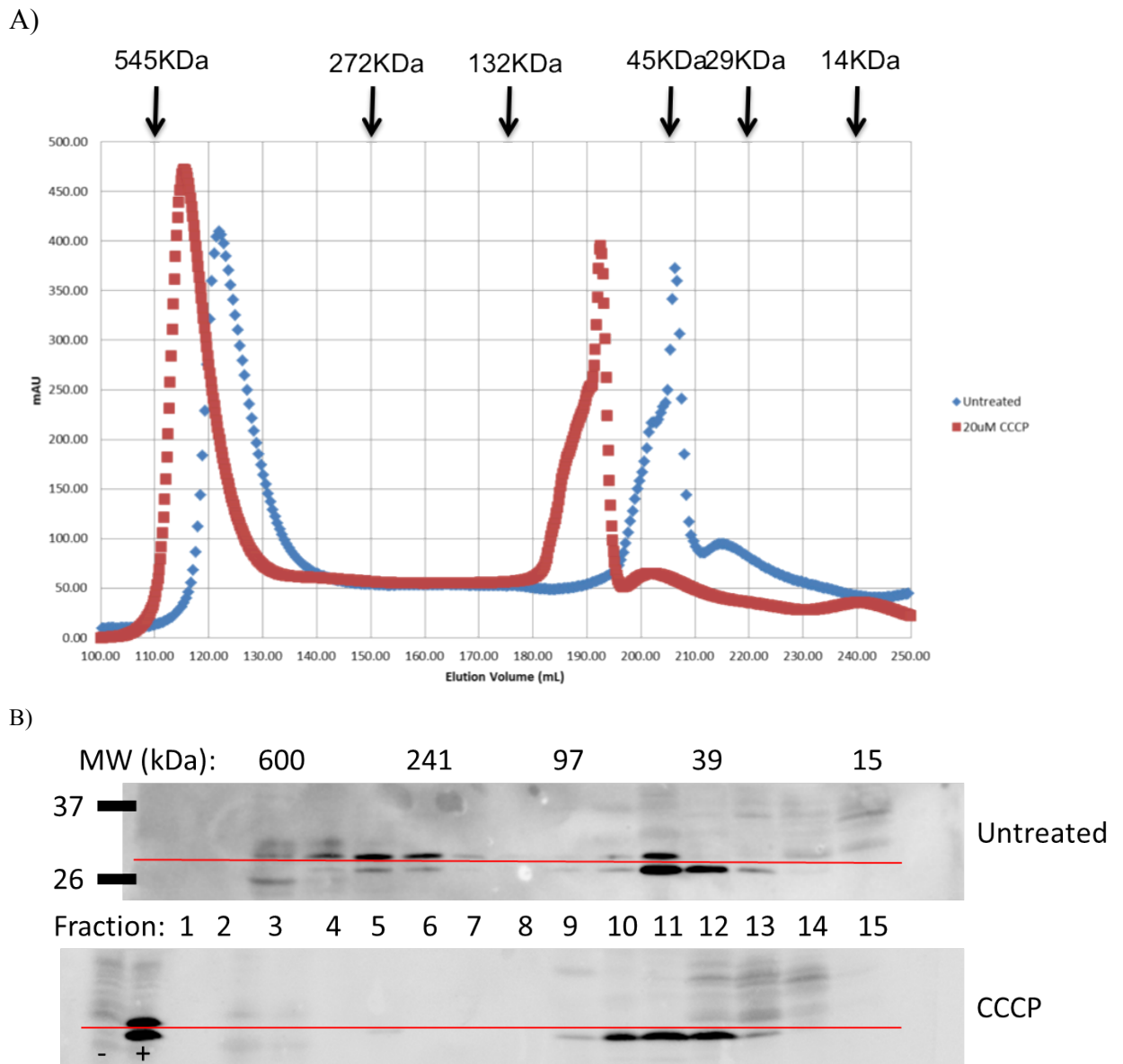


Figure 3.7: PGAM5 exists in two distinct pools in MEFs. (A) MEFs stably expressing PGAM5-FLAG were left untreated or treated with 20uM CCCP for 16 hours. Lysates were collected and separated by SEC. 10mL fractions were collected and TCA precipitated. Precipitated protein was resuspended in sample buffer and analyzed by western blot (B). Untreated negative (no PGAM5-FLAG) and positive (PGAM5-FLAG) controls were included on the western blot containing CCCP treated MEFs to easily distinguish the upper and lower bands of PGAM5. Each fraction number represents 10mL eluted volume. Approximate MW of the fractions is indicated above the western blot. PGAM5-FLAG was detected using FLAG antibody (Sigma).

3.6 A4-PGAM5 causes mitochondrial fragmentation

We wanted to determine if the multimeric state of PGAM5 affected normal mitochondrial dynamics in cells. We used standard immunofluorescent techniques to visualize mitochondria and PGAM5 in both MEF and COS1 cells. We stably expressed PGAM5-FLAG in PGAM5-deficient MEFs and determined the effects that CCCP treatment had on mitochondria and PGAM5 in MEFs. Under normal conditions, mitochondria were spread out in a tubular network and PGAM5-FLAG was evenly distributed across mitochondria (Figure 3.8A). When treated with CCCP, mitochondria became fragmented and PGAM5-FLAG redistributed to distinct punctate spots on the mitochondria (Figure 3.8B). Interestingly, many of the punctate spots were located at the terminals of mitochondria where sites of fission were likely to have occurred.

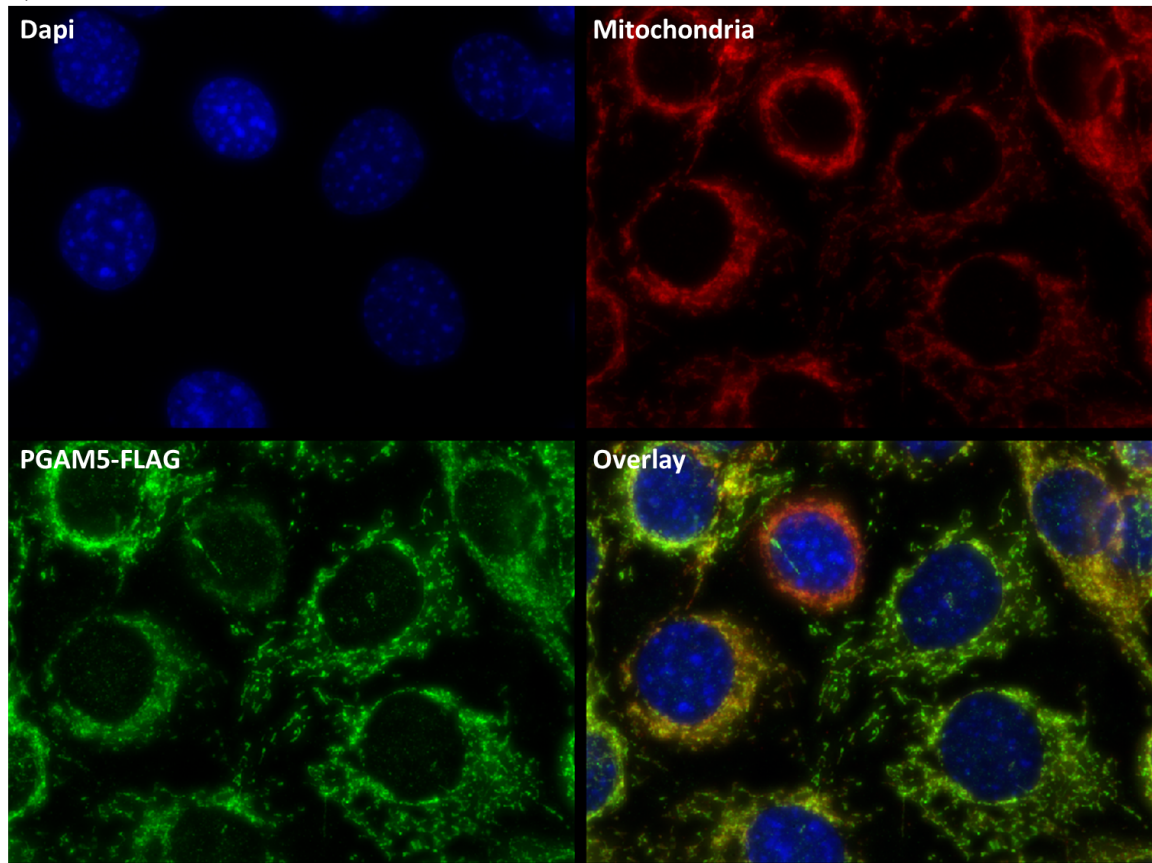
To examine if multimerization of PGAM5 affected mitochondrial dynamics in cells, we overexpressed A4-PGAM5-FLAG in COS1 cells (Figure 3.8C). In COS1 cells, mitochondria form a tubular network. As seen in the overlay of Figure 3.8C, COS1 cells not expressing A4-PGAM5-FLAG have tubular mitochondria. The mitochondria in COS1 cells expressing A4-PGAM5-FLAG, however, are fragmented with a distinct punctate pattern of A4-PGAM5-FLAG staining, which was strikingly similar to that of MEF cells treated with CCCP.

As determined by SEC in MEFs, CCCP treatment causes destabilization of PGAM5 into its dimeric form (Figure 3.7). We also showed that A4-PGAM5 elutes as a dimer (Figure 3.6). Furthermore, expression of A4-PGAM5-FLAG has a similar phenotype seen in MEFs that are treated with CCCP. Therefore, it is plausible to

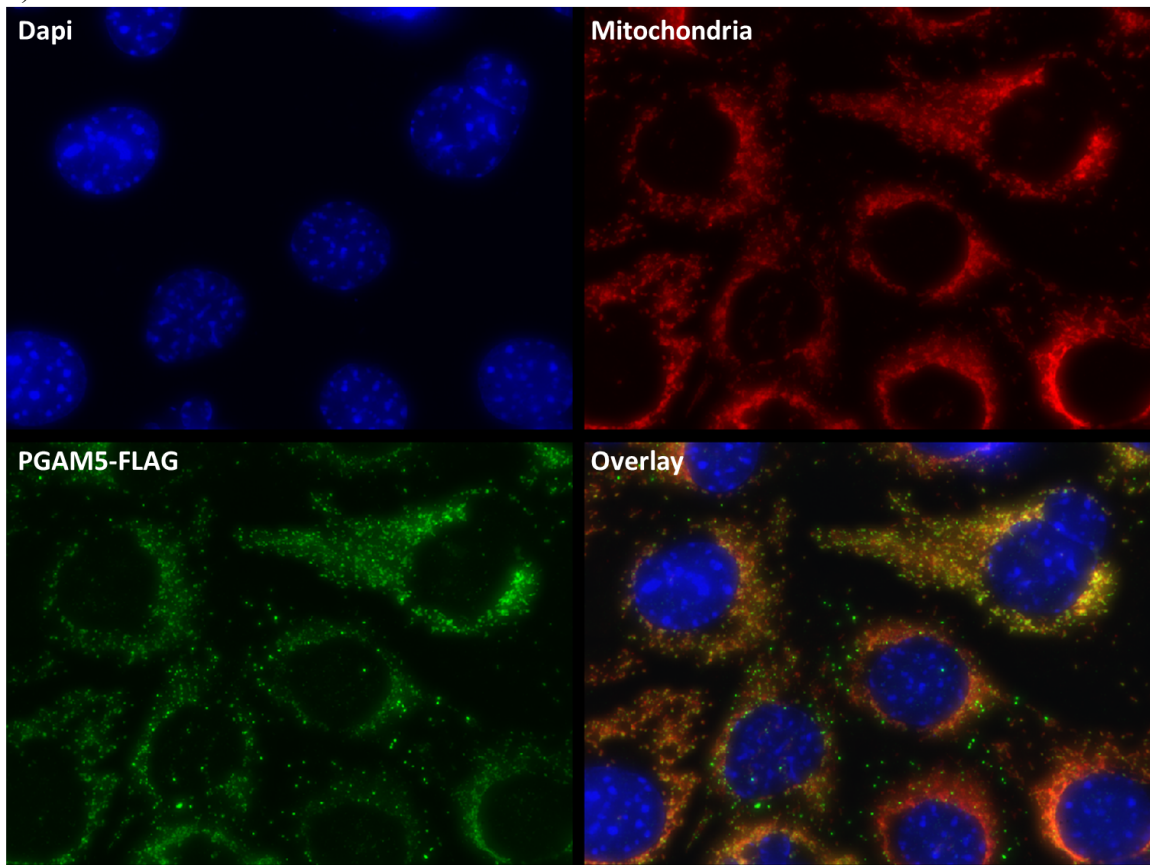
consider that loss of MMP disrupts PGAM5 multimerization, which in turn affects mitochondrial morphology.

Figure 3.8: PGAM5 multimerization is required for proper mitochondrial morphology

A) MEFs - Untreated



B) MEFs – CCCP



C) COS1 – A4-PGAM5 - Untreated

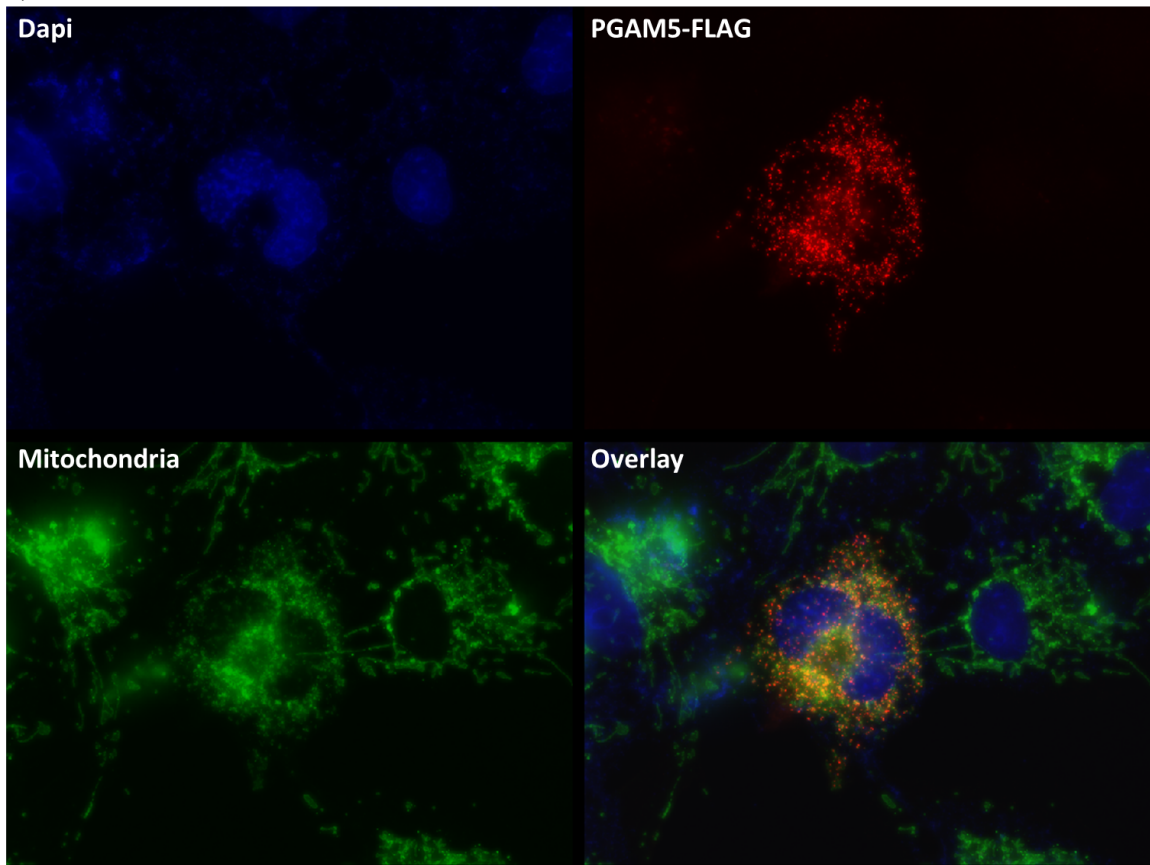


Figure 3.8: PGAM5 multimerization is required for proper mitochondrial morphology. Cells were either untreated or treated with 20 μ M CCCP for 16 hours. All cells were fixed and mitochondria and PGAM5-FLAG were visualized using standard indirect immunofluorescent techniques. Mitochondria were detected using the TOM20 antibody (Santa Cruz) and PGAM5-FLAG was detected using the FLAG antibody (Sigma). (A) Untreated MEFs. (B) CCCP treated MEFs. (C) COS1 cells transfected with A4-PGAM5-FLAG.

3.7 Discussion

Mitochondria are dynamic organelles that undergo cycles of fission and fusion and are continually transported throughout the cell [70, 146]. Mitochondria are also major producers of ROS and play critical roles in metabolism and cell death [4, 5]. Mitochondrial dysfunction has been implicated in cardiovascular disease, aging, and neurodegeneration including Alzheimer's disease and Parkinson's disease [1, 3, 129]. We present evidence that the mitochondrial localized protein PGAM5 is a sequence

specific phosphatase and that PGAM5's phosphatase activity is dependent on the multimeric state of PGAM5. Our data suggests that multimerization of PGAM5 may be dependent on MMP. Furthermore, the multimeric state of PGAM5 may affect mitochondrial morphology. Therefore, a better understanding of PGAM5 function and the mechanisms that regulate mitochondrial morphology may provide novel methods for treating mitochondrial dysfunction and related diseases.

We discovered an N-terminal motif, WDxNWD, that is conserved across all species of PGAM5 and is crucial for both multimerization and phosphatase activity of PGAM5. Mutation of the WDxNWD motif results in inactivation of PGAM5's phosphatase activity. Light scattering revealed that PGAM5 forms a stable dodecamer that is dependent on the presence of the WD motif. Deletion or mutation of the motif prevented PGAM5 from forming a multimeric complex. Furthermore, we demonstrated that PGAM5 exists as both high and low MW complexes in cells and that these two pools of PGAM5 are, in part, dependent on mitochondrial membrane potential.

Uncoupling of mitochondria with CCCP causes fragmentation of mitochondria and results in the degradation of mitochondria mediated through the PINK1/PARKIN pathway [61, 67]. Under normal conditions, the rhomboid protease PARL cleaves PINK1, which results in PINK1 degradation. Uncoupling of mitochondria stabilizes PINK1 and results in PARL-mediated cleavage of PGAM5 [128]. Our results suggest that uncoupling of mitochondria with CCCP not only results in the cleavage of PGAM5, but also in the destabilization of the multimeric form of PGAM5 to the dimeric form. From our SEC data and phosphatase studies, PGAM5 is inactive as a dimer. This would suggest that mitochondrial uncoupling results in inactivation of PGAM5. Inactivation of

PGAM5 may help facilitate PINK1/PARKIN degradation of damaged mitochondria or prevent PGAM5 from dephosphorylating proteins, which may help increase the activity of proteins that help maintain mitochondrial homeostasis.

In these studies we provide evidence that PGAM5 is a sequence specific phosphatase with a preference toward substrates that contain negatively charged residues near the phosphorylation site. We tested 19 phosphopeptides derived from substrate candidates and found that the best substrates were derived from the proteins ASK1 and BCL-XL. PGAM5 was previously identified as an interacting partner with both ASK1 and BCL-XL [117, 121]. ASK1 plays a role in stress-induced apoptosis [122], while BCL-XL is a pro-survival factor preventing apoptosis.

PGAM5 has been proposed to dephosphorylate and activate ASK1 [121]. While the exact site of dephosphorylation in ASK1 by PGAM5 was not determined, our data suggests that the preferred site of dephosphorylation within ASK1 is either Thr-838, Ser-1029, or Ser-1033. Phosphorylation of Ser-1033 is known to inactivate ASK1 [150], which would make this an ideal site for PGAM5 dephosphorylation and activation of ASK1. However, ASK1 is activated by cell stress, such as oxidative stress, and since mitochondria are major producers of ROS, and our data suggest that mitochondrial stress results in inactivation of PGAM5, Ser-1033 may not be the preferred site of dephosphorylation by PGAM5.

One attractive possibility is ASK1-Thr-838. Under normal conditions, ASK1-Thr-838 remains dephosphorylated rendering ASK1 inactive. During increased oxidative stress, ASK1-Thr-838 becomes phosphorylated and active [151]. This would fit a model in which during normal conditions, PGAM5 is active and dephosphorylates ASK1-Thr-

838 and inactivates ASK1. During increased oxidative stress, PGAM5 is inactive, allowing for accumulation of Thr-838 phosphorylation and activation of ASK1, which in turn, may trigger cell death.

Two sites of interest in BCL-XL were Thr-47 and Ser-62. Phosphorylation of BCL-XL -Thr-47 and -Ser-62 have been implicated in preventing progression through the cell cycle and decreasing the pro-survival activity of BCL-XL [152-154]. Both of these sites are attractive candidates for PGAM5's phosphatase activity as dephosphorylation of Thr-47 and Ser-62 would increase survival and help progression through cell cycle checkpoints, while increased mitochondrial stress would inactivate both PGAM5 and BCL-XL, resulting in cell death.

Our data may suggest a new level of regulation for PGAM5. It may be that in healthy cells, PGAM5 exists in equilibrium between a dimer and a higher order complex. It may be that the higher order complex promotes fusion, while depolarization of mitochondria may inactivate PGAM5, promoting fission. When normal mitochondrial function is perturbed with CCCP, the PGAM5 complex is destabilized into its dimeric form. Furthermore, disruption of the PGAM5 complex inactivates PGAM5 as a phosphatase. It is possible that PGAM5 forms a multimeric structure that is capable of binding to its substrates and dephosphorylating them while mitochondria are healthy. Depolarization of mitochondria results in the destabilization of the PGAM5 multimer, which inactivates PGAM5's phosphatase activity and ability to interact with its substrates. Further investigation of the mechanisms that regulate PGAM5 function and complex formation are required and may provide novel insight into mitochondrial regulation and cell death.

Chapter 4

PGAM5 Gene-trap mice: Microarray analysis and characterization

PGAM5 was originally identified as an interacting partner of BCL-XL [117], and subsequently as a substrate for the KEAP1-CUL3-ubiquitin ligase complex, which targets PGAM5 for degradation by the proteasome [118]. Our lab demonstrated that PGAM5 facilitates the formation of a ternary complex on mitochondria that includes the proteins NRF2 and KEAP1 [120]. PGAM5 is targeted to the mitochondria by an N-terminal mitochondrial localization signal and overexpression of PGAM5 profoundly alters the morphology of mitochondria [120].

Subsequent work from other laboratories has provided additional information on the biological and biochemical properties of PGAM5. In one study, PGAM5 was shown to have a Ser/Thr-specific phosphatase activity capable of dephosphorylating two Ser residues in ASK1, leading to activation of ASK1's kinase activity [121]. PGAM5 has also been identified as an interacting partner for PINK1 [127], in a report that demonstrated that loss of PGAM5 alleviated the deleterious consequences of loss-of-function PINK1 mutations in *Drosophila* [127]. Other studies have implicated PGAM5 in both necrotic and apoptotic cell death, acting through RIPK1/3 pathway or KEAP1/BCL-XL, respectively [53, 124]. Despite these intriguing findings on the biological role(s) of PGAM5, the function of PGAM5 in mammalian cells remains poorly understood.

In this chapter, the results of a series of experiments using mice and cells that contain a disrupted PGAM5 gene are reported. This chapter is divided into three sections. First, the generation and characterization of a mouse line that contains a gene-trap disruption of the PGAM5 locus is described. Mice that do not contain at least one functional PGAM5 allele are not viable, with the absence of PGAM5 causing early embryonic lethality. Second, the generation and characterization of a line of mouse

embryo fibroblasts that do not express PGAM5 is described. Cells that do not express PGAM5 display increased sensitivity to staurosporine-induced apoptosis and the re-introduction of PGAM5 into PGAM5-deficient cells restores resistance to staurosporine-induced cell death. Finally, a microarray analysis was carried out using the PGAM5-deficient mouse embryo fibroblasts, in an attempt to identify genes that are differentially expressed between wild-type and PGAM5-deficient cells. The differentially expressed genes were mapped onto KEGG pathways using DAVID, a web-based bioinformatics tool. Analysis of the microarray data by DAVID/KEGG would suggest that PGAM5 may have a critical role in regulation of primary metabolism, particularly relating to purine and pyrimidine biosynthesis. Taken together, these results provide novel insights into the biological functions of PGAM5.

4.1 Generation and characterization of a mouse containing a gene-trap disruption in the PGAM5 locus

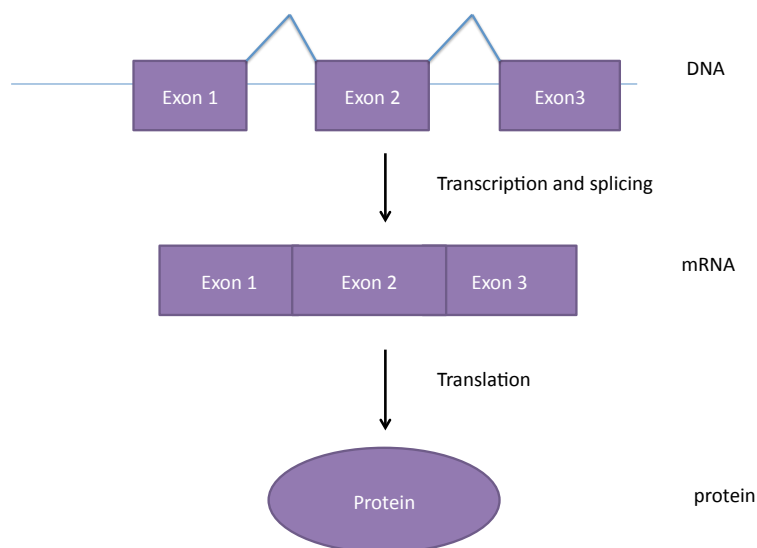
4.1.1 Gene trap vectors are tools for generation of loss of function mutations

Mice are widely used as models for studying the genetic pathways that give rise to human disease. A standard genetic approach in mice is to generate loss-of-function mutations in specific genes and to characterize the phenotypic effects of these mutations. One approach for the generation of loss-of-function mutations in mice is gene targeting, in which homologous recombination in embryonic stem cells is used to introduce specific mutations at a specific locus. Although this technique is widely used, it requires the construction of a targeting vector and is dependent on DNA transfection into embryonic stem cells followed by homologous recombination to insert a specific DNA sequence at the locus of interest. This approach can be costly and time-consuming.

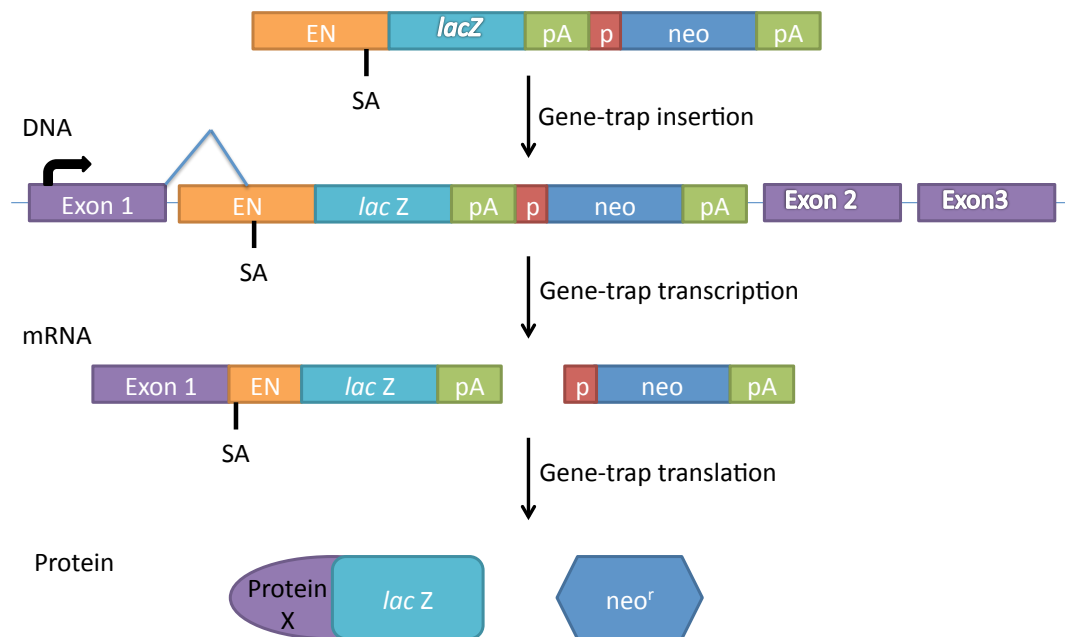
An alternative approach is the use of gene trap vectors. This approach uses a retroviral vector to introduce into embryonic stem cells a DNA sequence that contains a splice acceptor site. The introduced DNA sequence integrates randomly across the genome and, at an appropriately low multiplicity of infection, only one insertion will occur per infected cell. This technique efficiently generates a large number of clonal ES cell lines, each with a different insertion site. Sequencing of cDNA isolated from clonal ES cell lines containing the gene trap will reveal the insertion locus. Since the introduced DNA sequence contains a splice acceptor site, normal splicing at that locus is disrupted, often resulting in a loss-of-function phenotype. Typically, the abnormally spliced RNA is rapidly degraded, although it is possible that a novel fusion protein will result from a gene-trap event (Figure 4.1) [155].

Figure 4.1: Gene disruption by gene-trap

A. Transcription, splicing and translation of a typical gene.



B. Disruption of gene expression by a gene-trap vector.



Legend to Figure 4.1. (A) A diagram summarizing normal transcription, splicing and translation of a gene. (B) A diagram summarizing how a gene-trap cassette, containing a splice acceptor from the Engrailed gene, disrupts splicing when inserted into a genomic locus.

4.1.2 Characterization of a gene-trap insertion into the mPGAM5 locus

The murine PGAM5 locus is located on chromosome 5 (locus NC_000071). An embryonic stem cell line, RRZ048, was obtained from BayGenomics. As reported by BayGenomics on their website, sequence analysis of cDNA from this cell line indicated that the gene-trap insertion occurred between exons 5 and 6 at the PGAM5 locus. Using the services of the MU Transgenic Core, three male chimeric mice were generated and screened for germ line transmission by breeding to C57Bl6 females. The offspring from two of the male chimeras were positive for the gene-trap insertion. These offspring were used to establish a colony of mice in the LSC vivarium. As the ES cell line was derived from 129 mice and the chimeras were mated with C57Bl6, the offspring were a mixture

of 129 and C57Bl6 (Table 4.1). In a subsequent set of experiments, three additional male mice were derived by the Transgenic Core and were bred with 129Sv females to generate a colony on an inbred 129 background (Table 4.2). No significant differences in the distribution of genotypes at the PGAM5 locus were observed between these two genetic backgrounds.

Disruption of the mouse PGAM5 (mPGAM5) gene occurred between exons 5 and 6 at nucleotide position 9044 (Figure 4.2). We used a series of primers to map the insertion of the gene trap by PCR (Table 4.1). These primers were also used to genotype the wild-type and gene-trap alleles, using DNA isolated from tail clips, followed by PCR and agarose gel electrophoresis (see Figure 4.3 for an example of the genotyping analysis). We sequenced the PCR products to confirm we had the correct products.

A DNA fragment of 1054 base pairs was amplified from the wild-type PGAM5 allele, using primer set #1 (Table 4.1). The primers used for the wild-type allele spanned the site at which the gene trap was inserted into the genome. Furthermore, sequence analysis of PCR products revealed that the gene trap allele also had a deletion of more than 2300 base pairs located just 5' of the insertion site. The 5' primer used for PCR analysis of the wild-type PGAM5 allele was derived from within this deleted region.

Two different pairs of primers were used to identify the gene trap allele. Primer set #2 was located in the *neo* gene of the gene trap insert and yielded a PCR product of 385 base pairs. Primer set #3 spanned both the deletion and the insertion site of the gene trap insert, with the 5' primer being located 5' to the deletion and the 3' primer being located within the Engrailed sequence. Primer set #3 yielded a PCR product of 640 base pairs.

Figure 4.2: The mPGAM5 locus

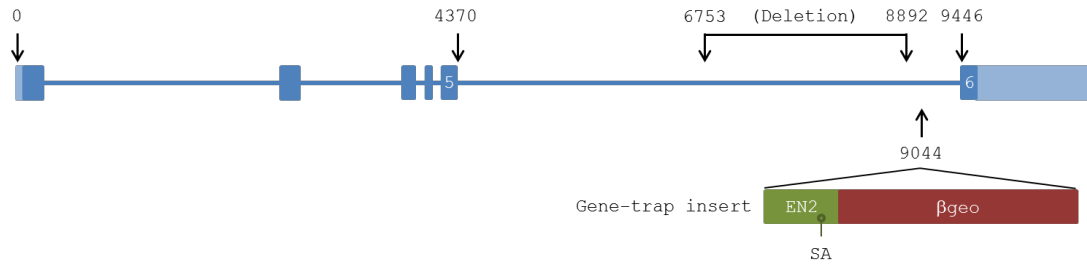


Figure 4.2 Legend: A map of the PGAM5 locus and the location of the gene trap insertion in the RRZ048 ES cell line. Insertion of the gene-trap cassette occurred between exons 5 and 6 at nucleotide position 9044. A deletion from nucleotides 6753-8892 occurred upstream of the gene-trap insertion site.

Table 4.1: Primer sets used to genotype PGAM5 gene-trap mice.

| Primer set ¹ | Identity ² | Sequence (5'-->3') ³ | Region ⁴ | Product size (bp) ⁵ |
|-------------------------|-----------------------|-----------------------------------|---------------------|--------------------------------|
| 1 | WT allele | cag gaa atg tca cgt gtt gg | Intron 5-6 | 1054 |
| | | gga cag cgt gca gtc tga ta | Exon 6 | |
| 2 | Gene-trap | tta tcg atg agc gtg gtg gtt atg c | Bgeo | 385 |
| | | gcg cgt aca tcg ggc aaa taa tat c | Bgeo | |
| 3 | Gene-trap | ctt tgc atg acc cct tca gt | Intron 5-6 | 640 |
| | | gtaccagactctcccatccactac | Engrailed 2 | |

Table 4.1: Primers used to genotype mice by PCR.

¹Primer set number. Primer set 1 was used to identify WT alleles, while primer sets 2 and 3 were used to confirm insertion of the gene-trap cassette.

²Indicates the product generated by the primer set

³Sequence of primer set

⁴Regions that the primers recognize

⁵Product size obtained by PCR.

4.1.3 An intact PGAM5 locus is required for embryonic development in the mouse

Tail clip DNA was isolated and used to genotype 187 mice from the C57Bl6/129 mixed background and 34 mice from the inbred 129 background (Tables 4.2 and 4.3). In the C57Bl6/129 mixed background, 122 (65%) were heterozygous for both the wild-type PGAM5 allele and the gene trap allele (Table 4.2). The remaining 65 mice (35%) had the wild type allele but did not have the gene trap allele and were thus considered to be homozygous for the wild-type allele. Similar numbers were observed with mice from the inbred 129 background, in which 20 out of 34 mice (59%) were heterozygous and 14 out

of 34 (41%) were wild-type (Table 4.3). No mice were observed that did not have at least one copy of the wild-type PGAM5 locus.

Table 4.2: Genotype results in a mixed C57/129 background

| Parents | # pups | Homo -/- | HET +/- | WT +/+ |
|-----------|--------|----------|---------|--------|
| 314 x 315 | 9 | 0 | 0 | 9 |
| | 7 | 0 | 2 | 5 |
| 323 x 315 | 9 | 0 | 3 | 6 |
| 344 x 349 | 2 | 0 | 1 | 1 |
| 362 x 349 | 5 | 0 | 3 | 2 |
| | 8 | 0 | 6 | 2 |
| 345 x 319 | 4 | 0 | 3 | 1 |
| 346 x 319 | 6 | 0 | 5 | 1 |
| 413 x 390 | 5 | 0 | 4 | 1 |
| | 6 | 0 | 3 | 3 |
| | 12 | 0 | 11 | 1 |
| | 7 | 0 | 5 | 2 |
| | 8 | 0 | 4 | 4 |
| | 4 | 0 | 4 | 0 |
| | 3 | 0 | 3 | 0 |
| | 5 | 0 | 4 | 1 |
| 455 x 444 | 9 | 0 | 3 | 6 |
| | 6 | 0 | 5 | 1 |
| | 7 | 0 | 6 | 1 |
| | 8 | 0 | 4 | 0 |
| | 4 | 0 | 4 | |
| | 8 | 0 | 5 | 3 |
| | 5 | 0 | 5 | 0 |
| 419 x 416 | 3 | 0 | 3 | 0 |
| | 6 | 0 | 5 | 1 |
| | 6 | 0 | 6 | 0 |
| | 2 | 0 | 2 | 0 |

| | | | | |
|-----------|-----|---|-----|----|
| | 3 | 0 | 3 | 0 |
| 520 x 521 | 2 | 0 | 2 | 0 |
| 527 x 526 | 4 | 0 | 4 | 0 |
| 530 x 521 | 4 | 0 | 4 | 0 |
| Total: | 187 | 0 | 122 | 65 |

Table 4.3: Genotype results in a 129 background

| Parents | # pups | Homo -/- | HET +/- | WT +/+ |
|-----------|--------|----------|---------|--------|
| 701 x 662 | 4 | 0 | 4 | 0 |
| | 4 | 0 | 3 | 1 |
| | 8 | 0 | 6 | 2 |
| | 2 | 0 | 2 | 0 |
| 694 x 696 | 5 | 0 | 2 | 3 |
| | 2 | 0 | 1 | 1 |
| | 5 | 0 | 1 | 4 |
| | 4 | 0 | 1 | 3 |
| Total: | 34 | 0 | 20 | 14 |

4.1.4 Genotype analysis of embryos

The outcome of these breeding experiments suggested that disruption of the PGAM5 locus is not compatible with embryonic development. To determine at what stage during embryonic development PGAM5 might be required, embryos were obtained from heterozygous females that had been bred to heterozygous males. These experiments were performed with mice from the C57Bl6/129 mixed background. Embryos were staged according to standard criteria and genotyped using primers for both the wild type PGAM5 locus and the gene trap allele. Out of 73 embryos, ranging from E9.5 to 14.5, 54

(74%) were heterozygous for the wild type PGAM5 and gene trap alleles, which the remaining 19 (26%) were homozygous for the wild-type PGAM5 allele. No embryos were observed that were homozygous for the gene-trap allele, although 8 resorbed embryos, which could not be genotyped, were observed.

Table 4.4: Genotyping results of embryos derived from het x het matings

| Parents | E stage | # resorbed | # viable | HET | WT | Homozyg. |
|-----------|-----------|---------------|----------|-----|----|----------|
| 542 x 539 | 9.5 | 0 | 12 | 7 | 5 | 0 |
| 543 x 540 | 9.5 | 0 | 11 | 10 | 1 | 0 |
| 541 x 538 | 11.5 | 0 | 5 | 4 | 1 | 0 |
| 544 x 548 | 11.5 | 0 | 6 | 5 | 1 | 0 |
| 675 x 665 | 14.5 | 6 | 4 | 4 | 0 | 0 |
| 672 x 666 | 14.5 | 0 | 10 | 6 | 4 | 0 |
| 673 x 667 | 14.5 | 2 | 8 | 5 | 3 | 0 |
| 671 x 669 | 15.5 | 0 | 9 | 6 | 3 | 0 |
| 674 x 670 | 14.5 | 0 | 8 | 7 | 1 | 0 |
| total: | 9 litters | 8 | 73 | 54* | 19 | 0 |

* 9 of the het embryos were delayed by one day relative to their siblings

4.2 Generation and characterization of a PGAM5-deficient mouse embryo fibroblast cell line

4.2.1 Identification of a PGAM5-deficient mouse embryo fibroblast cell line

The embryos from one of these females, #666, were used to generate mouse embryonic fibroblasts (MEFs). Embryos were harvested at embryonic development day 14.5. Mouse embryo bodies were separated from the central nervous system (CNS), rinsed, and trypsinized to dissociate the tissue. Primary MEFs were transferred to a clean dish and allowed to settle (passage 0). DNA from primary MEFs was used to genotype

each of the cell lines that were generated (MEFs 666 A through J) (Figure 4.3). We determined that four of the MEFs 666 (B, G, H, and J) were homozygous for the wild-type PGAM5 allele, while the remaining MEFs 666 (A, C, D, E, F, and I) were heterozygous for the wild-type and gene trap alleles. To overcome the tendency of mouse embryonic fibroblasts to enter crisis and stop proliferating, each MEF cell line was subsequently infected with a retroviral vector encoding SV40 T antigen and a puromycin selectable marker. Expression of T antigen was confirmed by immunoblot analysis (data not shown). These T-antigen positive MEF cell lines were capable of sustained proliferation in culture.

Figure 4.3: Genotyping results of MEF cell lines.

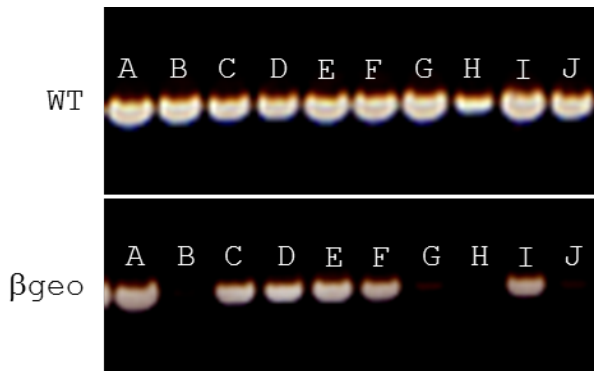


Figure 4.3 Legend: DNA was extracted from MEFs 666 A-J and primer sets 1 and 3 (Table 1) were used for genotyping the MEFs. Primer set 1 (WT) was used to detect the WT allele. Primer set 2 (*Bgeo*) was used to detect the gene trap allele.

PGAM5 protein abundance in the ten MEF cell lines was determined by western blot (Figure 4.4). The four wild-type MEF cell lines (B, G, H, and J) had higher levels of PGAM5 protein compared to MEF cell lines that were heterozygous at the PGAM5 locus (A, C, D, E, F, and I). Of particular interest was the MEF A cell line, because it had no detectable levels of PGAM5.

Figure 4.4: PGAM5 protein levels in MEF cell lines

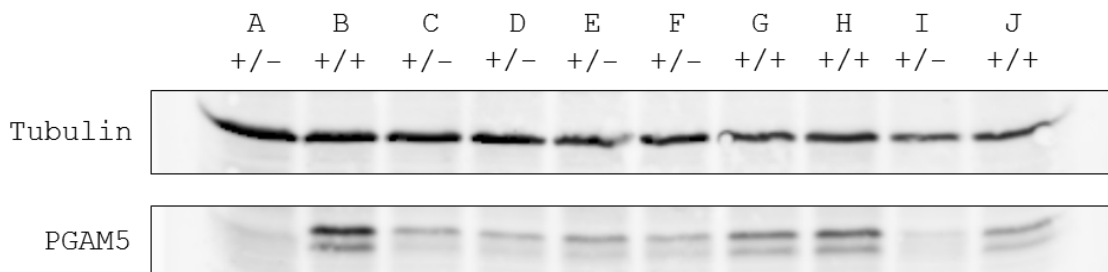


Figure 4.4 Legend: Primary MEFs 666 were harvested in sample buffer and analyzed by SDS-PAGE. Affinity purified PGAM5 antibody was used to detect levels of PGAM5 in the primary MEFs. Tubulin (Sigma) was used as a loading control.

To further confirm the absence of PGAM5 in the MEF 666A cell line, we analyzed PGAM5 mRNA transcript levels in cell lines 666A, 666B, and 666C by RT-PCR (Figure 4.5). Total RNA was extracted and used for reverse transcription followed by PCR to detect PGAM5 transcript levels. The MEF 666A cell line did not express detectable levels of PGAM5 mRNA (Figure 4.5).

Figure 4.5: MEF A cells do not express detectable levels of the wild-type PGAM5 transcript

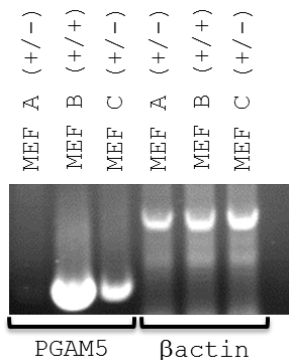


Figure 4.5 Legend: Total RNA was extracted from primary MEFs 666 A, B, and C. Equivalent amounts of total RNA were used for reverse transcription and transcript levels of PGAM5 were detected by PCR. Levels of βactin were used as a loading control.

4.2.2 Reconstitution of PGAM5 expression into the MEF 666A cell line

Each primary cell line was immortalized through infection with the retroviral vector pBABE-puro containing SV40. To reconstitute PGAM5 in the PGAM5-deficient MEF 666 A line, we used the retroviral vector pWZL-hygro to generate an empty vector

(EV) or vector containing PGAM5 (Figure 4.6). Infected cell lines were treated with 200ug/mL hygromycin to select for cells stably expressing the pWZL constructs. Both MEF 666 B-EV and MEF 666 A-EV displayed no apparent differences when compared to the MEF cell lines from which they were derived (data not shown). MEF 666 A stably expressing PGAM5 showed an increase in PGAM5 expression compared to MEF 666 B and A –EV cell lines (Figure 4.6).

Figure 4.6: Reconstitution of PGAM5 expression

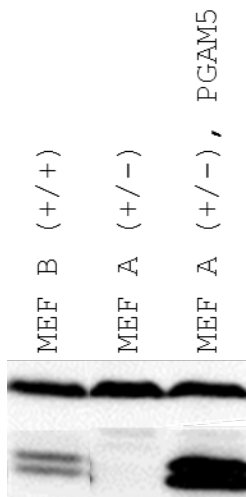


Figure 4.6 Legend: To reconstitute PGAM5, T antigen-immortalized MEFs were infected with an expression vector containing either an empty vector (lanes 1 and 2) or a vector containing PGAM5 (lane 3). Immortalized MEFs reconstituted with EV or PGAM5 were subjected to hygromycin selection.

4.2.3 PGAM5-deficient cells have increased sensitivity to staurosporine-induced apoptosis

Given that PGAM5 is known to associate with several proteins implicated in apoptosis, including BCL-XL and ASK1, we screened the MEF 666 A and MEF 666 B cell lines for differential sensitivity to the general kinase inhibitor staurosporine. Staurosporine is a potent inducer of apoptosis in cells that have a functioning intrinsic apoptotic pathway. Cell survival was monitored using the XTT cell viability assay

(Biotium) (Figure 4.7). The PGAM5-deficient MEF 666 A cell line was found to have increased sensitivity to staurosporine-induced apoptosis (Figure 4.7A) and reconstitution of PGAM5 expression into the MEF 666 A cell line decreased their sensitivity to staurosporine-induced cell death.

Figure 4.7: Cell death assay

A. MEF 666A cells display increased sensitivity to staurosporine-induced cell death.

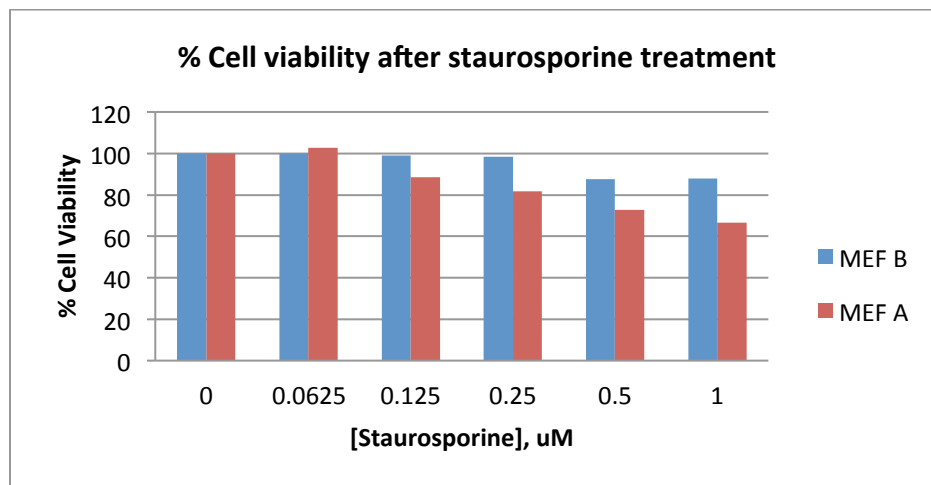


Figure 4.7A Legend: 5000 MEFs were plated in a 96-well plate and allowed to grow overnight. (A and B). MEFs were treated with various concentrations of staurosporine for 20 hours and cell viability was measured using the XTT assay (Biotium).

B. Introduction of PGAM5 increases resistance of MEF 666A to staurosporine-induced cell death.

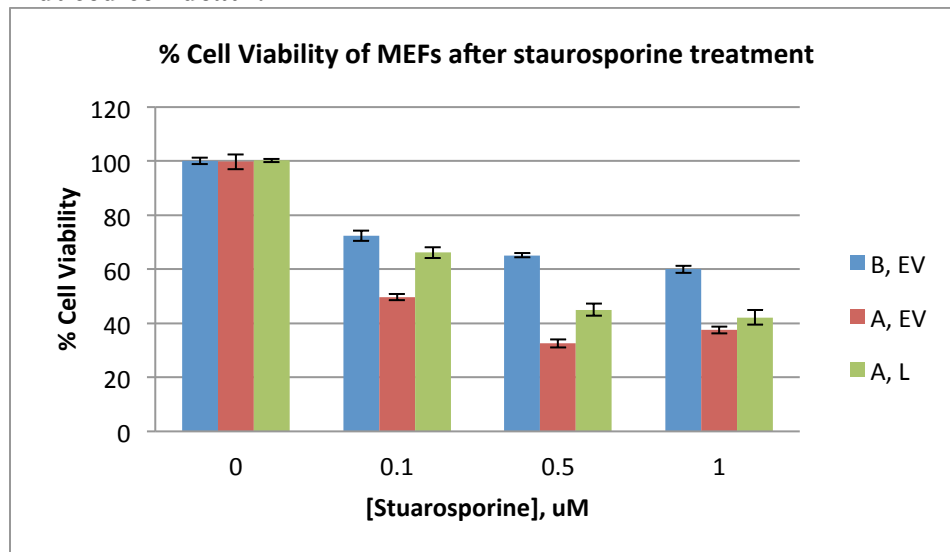


Figure 4.7B legend: 5000 cells were plated in 96 well plates and allowed to grow overnight. Staurosporine was added at the designated concentrations for 20 hours. Cells were rinsed and viability of the MEFs was measured using the XTT assay (Biotium). Samples are: (B, EV): MEF 666B cells transduced with the pWZL empty vector; (A, EV) MEF 666A cells transduced with the pWZL empty vector; (A, L) MEF 666A cells transduced with the pWZL PGAM5 expression vector.

Staurosporine is known to induce apoptosis through caspase-3 activation, though the exact mechanism is not fully understood. Normally, caspase-3 is maintained in an inactive state. Cell death stimuli lead to a series of event that result in cleavage of caspase-3 and its activation. Active caspase-3 commits the cell to apoptosis [30]. To determine if staurosporine-mediated cell death in the MEFs resulted in increased caspase-3/7 activation, we treated MEFs with staurosporine and assayed the MEFs for caspase-3/7 activation (Promega). We found that increased staurosporine-induced cell death in PGAM5-deficient MEFs correlated to an increase of caspase-3/7 activity (Figure 4.8).

Figure 4.8: Caspase 3/7 activity during staurosporine-induced cell death.

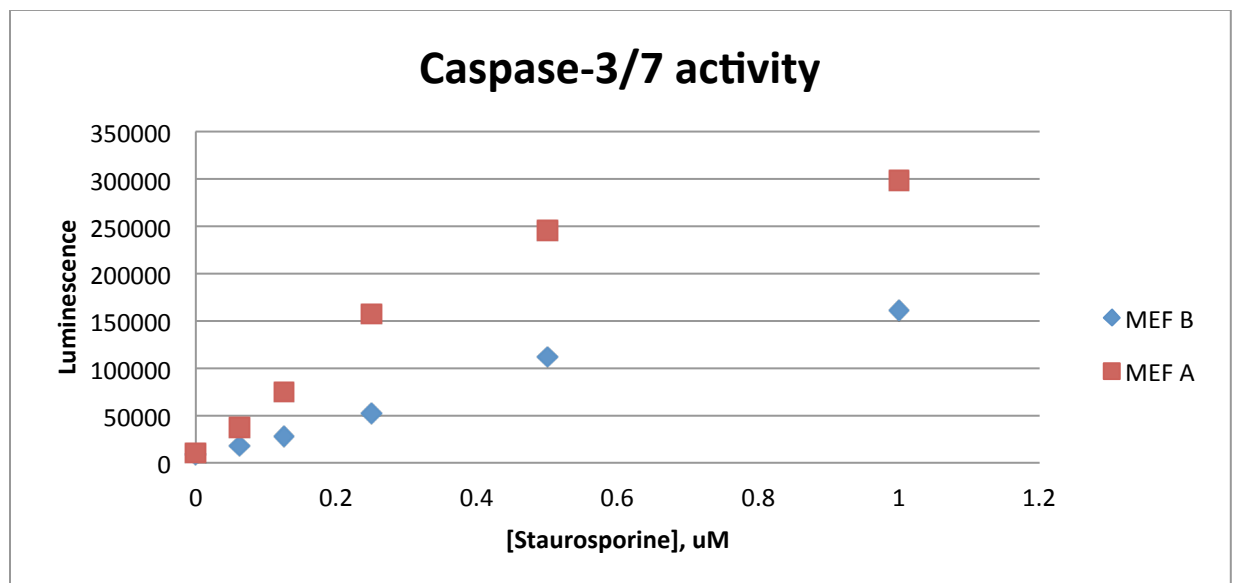


Figure 4.8 Legend: Cells were treated with staurosporine and caspase 3/7 activity was measured using a luminescent substrate.

4.3 Identification of genes and pathways that are differentially regulated in PGAM5-deficient mouse embryo fibroblasts

4.3.1 Microarray analysis to identify genes that are differentially expressed in PGAM5-deficient mouse embryo fibroblasts

The availability of a viable yet PGAM5-deficient MEF line provided us with a unique reagent to investigate the function of PGAM5 on a cellular level. One approach we took was to determine if the absence of PGAM5 resulted in any changes in gene expression. To this end, mRNA from the MEF 666 A and from the MEF 666 B cell lines were isolated, converted to cDNA and analyzed using the Illumina microarray technology to quantify levels of global gene expression.

4.3.2 Identification of genes that are differentially expressed between the MEF 666 A and MEF 666 B cell lines

As a visual depiction of genes that are differentially expressed between two conditions, scatter plots were generated comparing the MEF 666 A (or treated) to MEF 666 B (or untreated) samples. A scatter plot for the MEF 666 A vs MEF 666 B comparison is shown in Figure 6. In this figure, the average signal intensity for any given gene under the two conditions is displayed as a single dot. As can be seen from the figure, the average signal intensity of the vast majority of the genes analyzed was less than 2-fold different between the two cell lines. Nevertheless, a substantial number of genes, particularly those at low signal intensity, were outside of the arbitrary two-fold cut-off.

Figure 4.9: Scatter plot of genes differentially expressed in MEF 666A vs MEF 666B cells

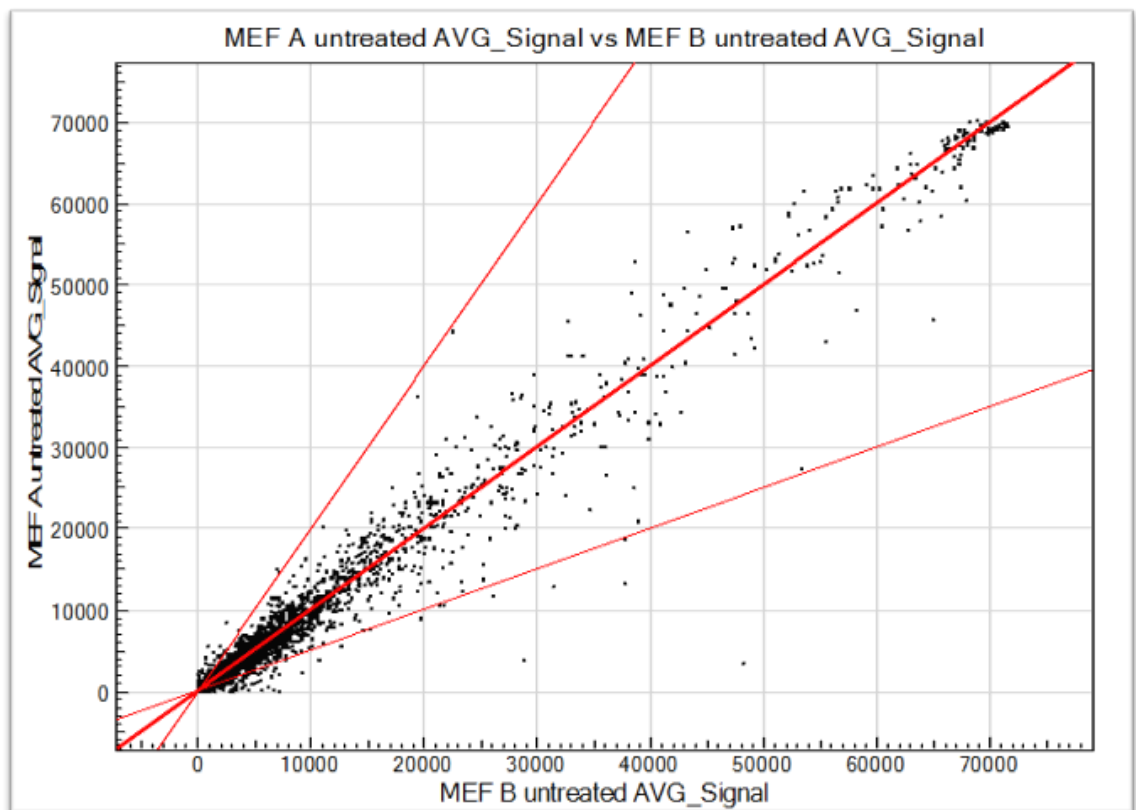


Figure 4.9 Legend. Differential expression plots of MEFs B and A. The reference cell line was plotted on the x-axis while the sample group was plotted on the y-axis using Illumina BeadStudio software. The red lines indicate the 2-fold cutoff point for differentially expressed genes.

Illumina's Bead Studio software was used to analyze the data generated from the microarray analysis. This software provides several important statistical tests to help investigators determine if expression of any given gene is statistically significant and if any given gene is differentially expressed in two different samples. One test is the probability that the gene is actually expressed, i.e., that a given mRNA is present in the original sample. This parameter is the detection p-value. In our analysis, a detection p-value of 0.05 was used. That is, any given gene was considered as "not present" and not included in any subsequent analyses when its p-value was more than 0.05.

A second test is the differential expression p-value, which is used to determine the probability that any given gene is differentially expressed between two different samples. In our analysis, a differential expression p-value of 0.05 was used. That is, any given gene was considered as not differentially expressed and not considered in any subsequent analysis if the differential expression p-value was more than 0.05. This cut-off value was less stringent than the often-used two-fold difference in average signal intensity, as a careful examination of genes that had a differential p-value at or near 0.05 revealed differences in average signal intensity of approximately 20%. Together, the detection p-value and the differential expression p-value were used to exclude genes that were either not expressed in at least one of the samples or were not statistically different in their level of expression.

After applying the two p-value cutoffs, the resultant gene lists were still quite large. There were approximately 2800 genes that were differentially expressed between the MEF 666A and the MEF 666B samples using 0.05 as the cut-off value for both the detection p-value and the differential expression p-value. Of these, expression of some 1600 genes was increased in the MEF 666A cells as compared to the MEF 666B cells, while expression of some 1200 genes decreased.

The Illumina software also calculates a differential score, which is an estimate of the magnitude of the difference in expression of any given gene between two samples and provides a way to rank-order a list of genes in terms of the magnitude of their differential expression between two samples. For any given gene and comparing two samples, the differential score value will range from -350 and +350. Genes with a differential score of -350 are the top-ranked genes whose expression is decreased in one sample relative to the

other sample, while genes with a differential score of +350 are the top-ranked genes whose expression is increased the most in one sample relative to the other sample. In our analysis, the rank-ordered lists, based on differential score, were used to select genes to be analyzed using DAVID.

4.3.3 Analysis of differential gene expression using DAVID

DAVID is a web-based bioinformatics software package that helps investigators make biological sense out of long lists of differentially expressed genes [156, 157]. Given a list of genes, DAVID has several text-mining and pathway-mining tools that will carry out several different analyses, including gene functional classification, clustering and functional annotation. For our purposes, the ability of DAVID to map a gene list onto known pathways, such as the KEGG pathway, provides valuable insight into pathways that are likely to be differentially regulated by the absence of PGAM5.

Two rank-ordered lists of differentially expressed genes were analyzed using DAVID. The two lists contained, respectively, (A) genes that are up regulated in MEF 666A as compared to MEF 666B and (B) genes that are down regulated in MEF 666A as compared to MEF 666B. The outcome of the DAVID analysis, in which the top 200 rank-ordered genes in each list were mapped onto KEGG pathways, is provided.

A. KEGG pathway analysis of genes that are up regulated in MEF 666A vs MEF 666B

Table 4.5: Up regulated pathways in MEF 666 A

| <u>KEGG Pathway</u> | <u>Number of genes in pathway</u> | <u>P-Value</u> |
|------------------------------|-----------------------------------|----------------|
| <u>Purine metabolism</u> | 5 | 0.036 |
| <u>Pyrimidine metabolism</u> | 4 | 0.041 |

Figure 4.10: Purine metabolism

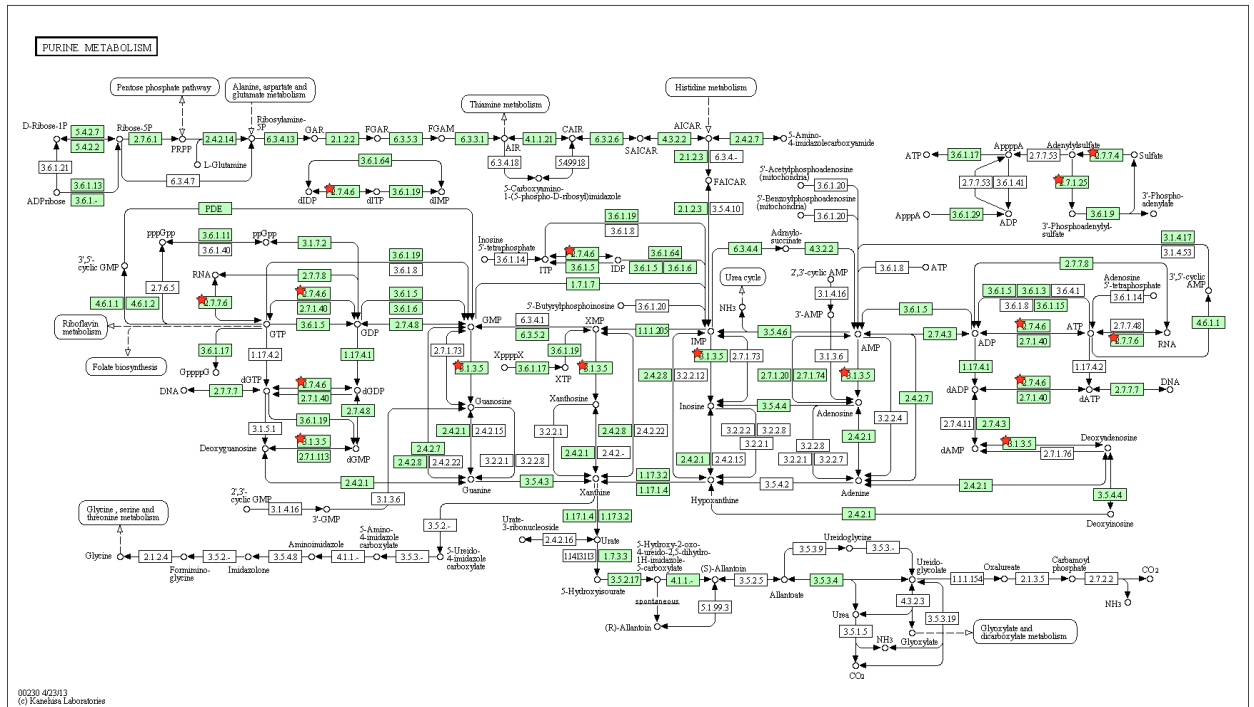


Table 4.6: Up regulated genes involved in purine metabolism

| ENTREZ GENE ID | GENE NAME |
|----------------|---|
| 23971 | 3'-phosphoadenosine 5'-phosphosulfate synthase 1 |
| 107569 | 5'-nucleotidase, cytosolic III |
| 66420 | polymerase (RNA) II (DNA directed) polypeptide E |
| 69833 | polymerase (RNA) II (DNA directed) polypeptide F |
| 100046163 | similar to Nme6 protein; non-metastatic cells 6, protein expressed in (nucleoside-diphosphate kinase) |

B. KEGG pathway analysis of genes that are down regulated in MEF 666A vs MEF 666B.

Table 4.7: Down regulated genes in MEF 666A

| KEGG Pathway | Number of genes in pathway | P-Value |
|----------------|----------------------------|---------|
| Focal adhesion | 7 | 0.0064 |
| Ribosome | 4 | 0.04 |

Figure 4.11: Focal adhesion pathway

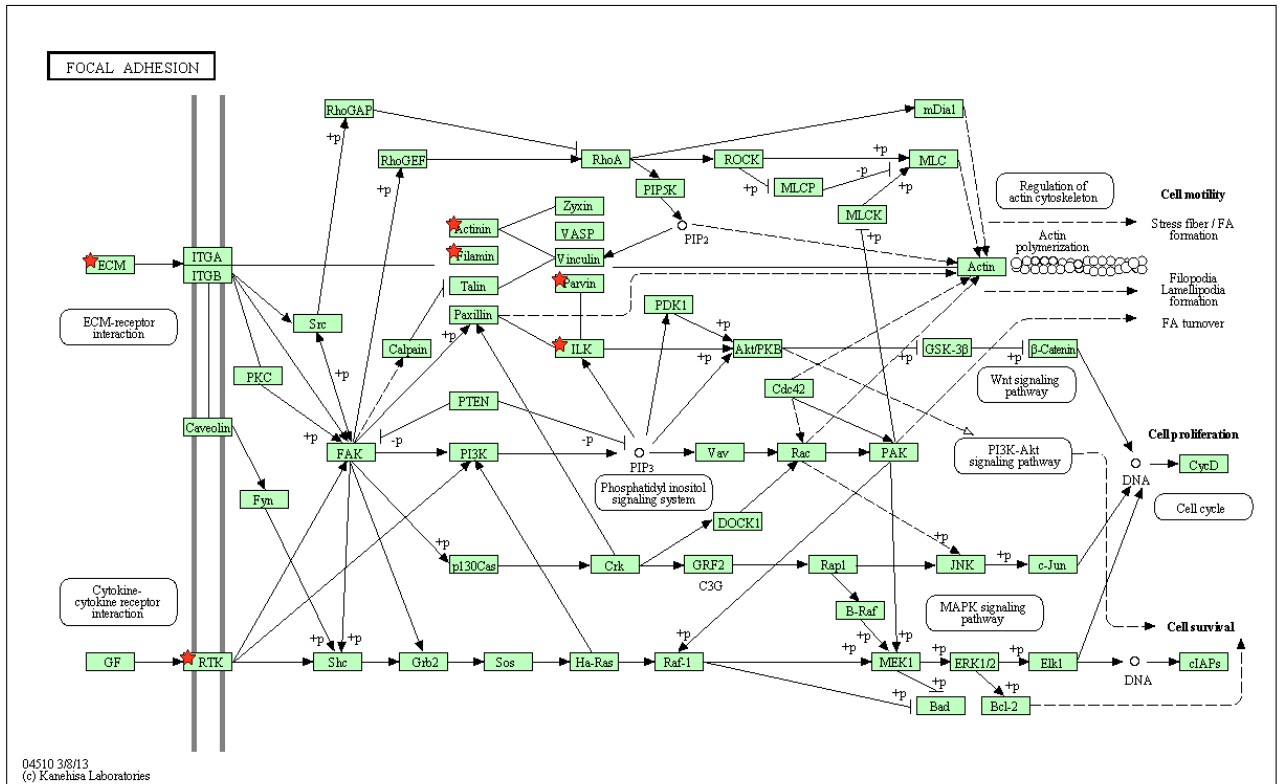


Table 4.8: Down regulated genes in focal adhesion pathway

Differentially expressed genes found in focal adhesion pathway (indicated by red star)

| ENTREZ_GENE_ID | GENE NAME |
|----------------|---|
| 109711 | <u>actinin, alpha 1</u> |
| 12825 | <u>collagen, type III, alpha 1</u> |
| 286940 | <u>filamin, beta</u> |
| 16202, 621824 | <u>integrin linked kinase; predicted gene 6263</u> |
| 226519 | <u>laminin, gamma 1</u> |
| 57342 | <u>parvin, alpha</u> |
| 18595 | <u>platelet derived growth factor receptor, alpha polypeptide</u> |

4.4 Discussion

The results presented in this chapter provide important insights into the biological function of PGAM5. The most striking finding is that a gene trap disruption of the PGAM5 gene is embryonic lethal in mice. More than 200 live offspring from heterozygous matings were genotyped, with 36% percent homozygous for the wild type allele and 64% heterozygous for both the wild type and gene trap allele. This is very close to the expected mendelian frequency of 2:1 when one of the alleles is embryonic lethal. Out of more than 70 embryos that were genotyped, none were homozygous for the gene trap allele. The embryos we analyzed were in mid-gestation developmental state, from E9.5 to E14.5. Taken together, the genotyping data indicate that disruption of the PGAM5 locus results in relatively early embryonic lethality. It is possible that PGAM5 may be required for implantation. One experiment that should be done is to genotype embryos that are flushed from female mice prior to implantation. If embryos that are homozygous for the gene trap allele are observed prior to implantation, this result would support the notion that PGAM5 is required during early embryonic development, perhaps at the implantation stage.

In our experiments, we characterized a gene trap disruption of the PGAM5 locus, not a targeted disruption. Our analysis of the gene trap locus revealed the presence of a 2000 bp deletion immediately upstream of the insertion site of the gene trap. It is possible that this deletion removes another genetic element, perhaps a microRNA gene, which has an independent function. To further understand the role of PGAM5 in development, and to conclusively determine that disruption of PGAM5 is embryonic lethal, it will be

necessary to construct and characterize a mouse containing an inducible PGAM5 allele, using Cre-lox technology.

A second surprising finding of our results is the identification of a PGAM5-deficient MEF line, MEF 666A. This cell line is heterozygous at the genetic level, having both the wild type and gene trap alleles. However, neither PGAM5 mRNA nor PGAM5 protein were detected. It is likely that the wild type allele has undergone epigenetic silencing, through DNA methylation and/or histone modifications of the PGAM5 promoter. These PGAM5-deficient cells appear to proliferate normally and, when immortalized by SV40 T antigen, are capable of sustained proliferation in culture. Thus, although PGAM5 appears to be required for embryonic development, it is not required for cell proliferation in culture. However, the MEF 666A cells were more sensitive to staurosporine-induced apoptosis. It is possible that loss of PGAM5 disrupts the homeostatic balance between cell survival and cell death, thus causing embryonic lethality that was observed in PGAM5-deficient embryos.

MEFs lacking PGAM5 were more sensitive to staurosporine-induced apoptosis. PGAM5-deficient MEFs had a 2-fold increase in caspase-3/7 activity compared to that of wild-type MEFs when treated with staurosporine. Furthermore, reconstitution of PGAM5 in PGAM5-deficient MEFs provided resistance to staurosporine-induced apoptosis. These results suggest that PGAM5 is protecting cells from apoptosis. As described in the previous chapter, overexpression of a mutant PGAM5 protein containing mutations in its multimerization motif caused mitochondria to become fragmented in COS1 cells. Since fragmentation often times precedes apoptosis, it may be that PGAM5 helps maintain proper mitochondrial morphology and, therefore, prevent cell death.

The availability of a PGAM5-deficient MEF cell line provided a unique opportunity to identify genes that might be regulated by signal transduction pathways that PGAM5 participates in. We used microarray analysis to identify genes that are differentially expressed between the PGAM5-deficient MEF 666A cell line and the MEF 666B cell line that was homozygous for the wild type allele. A surprisingly large number of genes, more than 2000, were differentially expressed between these two cell lines. Several explanations can be proposed to account for this finding. One possibility is that the large number of differentially expressed genes may reflect differences in one or more epigenetic regulatory systems between the two cell lines. Perturbation of one or more global epigenetic systems could account for repression of the wild type PGAM5 gene in the MEF 666A cells. Alternatively, it is possible that PGAM5 is a key regulatory participant in multiple signaling pathways, such that the absence of a functional PGAM5 protein perturbs the expression of a large number of genes. Reconstitution of PGAM5 expression in the MEF 666A cell line does increase cell survival in response to staurosporine-induced apoptosis. Thus, one way to distinguish between these two alternatives would be to repeat the array analysis (or use RNA-seq) on the MEF 666A-derived cell line in which PGAM5 expression has been restored through the use of a retroviral vector.

We used the DAVID bioinformatics tool to provide further insight into the genes that were differentially expressed between the MEF 666A and MEF 666B cell lines [156, 158, 159]. This analysis suggests that PGAM5 might play a role in both purine/pyrimidine metabolism and in regulation of focal adhesion signaling. At the moment, it is not clear if PGAM5 has a direct role in regulation of these pathways, or if

these pathway changes reflect global differences in gene expression between the MEF 666A and MEF 666B cell lines. If, after analyzing gene expression patterns in the MEF 666A cells in which PGAM5 expression has been restored, we find that these pathways are directly regulated by PGAM5, we will further investigate the biochemical connections between PGAM5 and both of these pathways.

Finally, the availability of this mouse strain containing a non-functional PGAM5 allele will be a useful tool for subsequent genetic experiments to further define the genetic role of PGAM5. For example, lethality resulting from gene disruption of one gene can sometimes be compensated by up- or down- regulating the expression of other genes. It is possible that the embryonic lethality resulting from homozygous gene trap disruption of PGAM5 is compensated by up- or down- regulating one or more proteins that act in the same signaling pathway. There are a number of candidate genes for this analysis, including proteins that are known or suspected to interact with PGAM5, including RIPK3, PINK1, ASK1, BCL-XL and DRP1. This proposed genetic analysis would complement the biochemical characterization of PGAM5-interacting partners and provide new insight into the biological functions of PGAM5.

Chapter 5

Discussion

5.1 Summary of the key findings of this dissertation

In the work reported in this dissertation, we provide new insight about the function and regulation of the phosphoglycerate mutase family member, PGAM5. These studies have addressed the function of PGAM5 on multiple levels, including organismal, cell biological, biochemical and structural. These findings, which represent a substantial contribution to our understanding of the PGAM5 protein, are summarized below. A more extensive discussion of the potential involvement of PGAM5 in different forms of cell death follows, along with some ideas for future research directions.

Embryonic stem cells containing a gene-trap insertion in the PGAM5 locus were used to derive heterozygous mice containing one copy of the disrupted PGAM5 allele. These heterozygous mice were viable and fertile, with no apparent differences between the heterozygous and wild-type siblings. Mice that were heterozygous at the PGAM5 locus were bred, in an attempt to generate PGAM5-deficient mice. However, no mice that were homozygous for the disrupted PGAM5 allele were observed in more than 200 live births to heterozygous parents. To determine when PGAM5 is required for embryonic development, more than 70 embryos were genotyped at mid gestation, ranging from E9.5 to 14.5. No embryos that were homozygous for the gene-trap insertion at the PGAM5 locus were observed. Taken together, these results demonstrate that PGAM5 plays a critical role(s) during early embryonic development.

To develop a cell culture model to analyze the function of PGAM5, mouse embryo fibroblasts (MEF) lines were individually derived from ten embryos from one heterozygous female following mating with a heterozygous male. Six of the ten embryos were heterozygous for the gene-trap allele, while four of the ten were wild type at the

PGAM5 locus. Surprisingly, one of the MEF lines did not express any PGAM5 mRNA or protein, presumably due to epigenetic repression of the wild type allele. These PGAM5-deficient MEFs were found to be more sensitive to staurosporine-induced apoptosis when compared to wild-type MEFs. Increased staurosporine sensitivity in PGAM5-deficient MEFs was accompanied by a 2-fold increase caspase activity when compared to wild-type MEFs. Furthermore, reconstitution of PGAM5 in PGAM5-deficient MEFs increased their resistance to staurosporine-induced apoptosis. These results suggest that PGAM5 plays a crucial role in cell survival and that PGAM5 is contributing to the regulation of apoptosis. A role for PGAM5 regulation in cell survival may suggest why homozygous gene disruption of PGAM5 is embryonic lethal.

To provide further insight into PGAM5's role(s) in cell physiology, microarray analysis was performed to identify genes that are differentially expressed in the wild type and PGAM5-deficient MEFs. This analysis revealed that more than 2000 genes are differentially expressed in PGAM5-deficient MEFs as compared to wild-type MEFs. Mapping the top-ranked differentially expressed genes onto KEGG pathways revealed that genes involved in the purine and pyrimidine metabolic pathways are up regulated in PGAM5-deficient MEFs, while expression of genes involved in the focal adhesion pathway are down regulated. The putative involvement of PGAM5 in these pathways is a very surprising result. These changes in gene expression may reflect the presence of a PGAM5-dependent signaling pathway(s) that regulate genes involved in nucleotide biosynthesis and focal adhesion. Alternatively, these changes in gene expression could reflect compensatory mechanisms that enable the MEF's used in these experiments to survive in the absence of PGAM5. It will be of considerable interest to define the

relationship between these metabolic and signaling pathways and the other aspects of PGAM5's function reported in this dissertation, particularly PGAM5's role in cell and organismal survival.

Our results provide evidence that PGAM5 is a sequence specific Ser/Thr phosphatase that has a preference for one or more negatively charged amino acid near the site of phosphorylation. We show that PGAM5 forms a higher order complex that is necessary for PGAM5's phosphatase activity. Multimerization of PGAM5 is dependent on a phylogenetically conserved WDxNWD motif that is located N-terminal to the core catalytic domain of PGAM5. Deletion of, or alanine substitutions within, the WDxNWD motif disrupts PGAM5 multimerization, resulting in the formation of a dimeric complex and rendering PGAM5 inactive as a phosphatase. Furthermore, overexpression of A4-PGAM5 in cells causes fragmentation of mitochondria, implicating PGAM5 in the regulation of fission, fusion, and/or movement of mitochondria. Given the central importance of mitochondria in regulation of cell death, it is likely that the ability of PGAM5 to regulate the morphology of mitochondria contributes to the enhanced sensitivity of PGAM5-deficient MEFs to staurosporine-induced apoptosis.

At the structural level, a structure of the catalytic domain of PGAM5, residues 98-289, has been reported [134]. This structure revealed that the isolated catalytic domain of PGAM5 forms an inactive dimer, with multiple subunit contacts located through the PGAM domain. As our biochemical experiments revealed that multimerization through the WDxNWD is required for catalytic activity, we sought out to determine the structure for the active form of PGAM5 using x-ray crystallography. These studies on the human PGAM5 protein were limited by the pronounced tendency of the active protein to form

aggregates and precipitate out of solution at concentrations greater than 1mg/ml. We were not able to identify suitable conditions for crystallization of several human PGAM5 proteins, containing different lengths of N-terminal amino acids. Therefore, we sought other means to improve PGAM5 solubility. We found that an N-terminal truncated *Drosophila* PGAM5 (dPGAM5) protein, in which the hydrophobic mitochondrial targeting sequence was removed, could be concentrated up to 13mg/ml. We have defined one set of conditions that can reproducibly generate crystals that are sharp, symmetrical and capable of diffraction. The next step will be to determine proper freezing conditions for our crystals in order to collect enough x-ray diffraction data for structure determination.

5.2 Involvement of PGAM5 in cell death pathways

Cell death plays an important role in development. Not only is cellular death important to destroy cells that become abnormal, cell death also plays a crucial role in normal growth and development [160]. Several types of cell death have been characterized, including apoptosis, necrosis, and autophagy [28, 47, 50, 55]. During the course of this work, there have been several other published reports suggesting one or more roles for PGAM5 in the regulation of cell death. The work reported in this dissertation provides important mechanistic insight into understanding the involvement of PGAM5 in cell death and suggest that PGAM5 may be a good target for the development of therapeutic strategies to manipulate cell death pathways in diverse diseases, including cardiovascular diseases, aging, and neurodegenerative diseases including Alzheimer's disease, Parkinson's disease, and Huntington's disease [1, 3, 4, 161].

5.2.1 PGAM5 and necrosis

Necrosis was originally thought to be an uncontrolled event that resulted from severe and sudden insult to a cell. Hallmarks of necrosis include membrane discontinuity, ATP depletion, and cell swelling and rupture [8]. Cell death by necrosis leads to an inflammatory response due to the release of pro-inflammatory factors upon cell rupture [44].

Necrosis is now becoming recognized as a controlled form of cell death that partially overlaps with the intrinsic apoptotic pathway. However, in contrast to apoptosis, which requires caspase activity for cell death, the pathway of programmed necrosis occurs independently of caspase activation. Indeed, inhibition of caspase activity is required for programmed necrosis to occur. Programmed necrosis is initiated by binding of TNF α to TNFR1, which induces oligomerization of TNFR1 on the plasma membrane. TRADD is recruited to TNFR1 through interactions between the death domains (DDs) found within both TRADD and TNFR1. The TNFR1/TRADD docking station recruits TRAF2, caspase-8, and RIPK1. Inhibition of caspase-8 allows the release of TRAF2/RIPK1 into the cytosol where they interact with RIPK3 and MLKL forming the necrosome [53]. The kinase activity of the necrosome is thought to be required for necrosis [50].

In a recent publication, Wang and coworkers proposed that PGAM5 is a target for phosphorylation by the necrosome [53]. In their model, phosphorylation of PGAM5 by the necrosome led to PGAM5 activation. Activated PGAM5 then recruited and dephosphorylates DRP1 at Ser-637, resulting in activation of DRP1 and subsequent

fission of mitochondria. However, in these studies, direct dephosphorylation of DRP1 by PGAM5 was not shown [53].

Our results do not support the suggestion of Wang and coworkers that the phosphatase activity of PGAM5 contributes to necrosis. First, we demonstrate that DRP1 phosphopeptides are poor substrates for PGAM5 when compared to other substrates tested against PGAM5. We tested PGAM5's phosphatase activity against several phosphopeptides and found DRP1-derived phosphopeptides to be relatively poor substrates, with a K_m of 400 μM for Ser-637 in DRP1. A different DRP1-derived phosphopeptide, containing Ser-548, was a better substrate for PGAM5, with a K_m of 113 μM . In contrast, phosphopeptides from BCL-XL and from ASK1 were found to have much lower K_m values, of approximately 25 μM . Taken together, these results suggest that Ser-637 of DRP1 is not likely to be a preferred target of PGAM5.

Second, our results demonstrate that the phosphatase activity of PGAM5 is dependent on the WDxNWD multimerization motif. Mutation or deletion of the WDxNWD motif caused the higher order complex of PGAM5 to shift completely to its dimeric form. Furthermore, overexpression of a A4-PGAM5 in COS1 cells results in mitochondrial fragmentation. In contrast, Wang et al. suggested that PGAM5's phosphatase activity was necessary to dephosphorylate and thereby activate DRP1, leading to fragmentation of mitochondria [53]. Since A4-PGAM5 is inactive as a phosphatase and is capable of causing mitochondrial fission when expressed in COS1 cells, further research is needed to determine if PGAM5 is directly or indirectly driving necrosis through DRP1 activation.

5.2.2 PGAM5 in apoptosis

Apoptosis is a caspase-dependent pathway that is mediated extrinsically through activation of death receptors or intrinsically through permeabilization of mitochondria [7, 27]. Extrinsically, ligand binding to death receptors induces receptor oligomerization and activation of DISC. This leads to activation of caspase-8, which activates the effector caspase-3 and results in apoptosis. Intrinsically, members of the BCL2 family regulate mitochondrial permeability. Stress, such as oxidative stress, results in an increase of BAX and BAK activation. BAX and BAK are thought to oligomerize and form pores in the mitochondrial membrane causing the release of apoptotic factors such as cytochrome c [37]. Once released into the cytosol, cytochrome c binds to APAF1 and pro-caspase-9, forming the apoptosome. Apoptosome formation leads to the cleavage and activation of caspase-9, which in turn cleaves and activates caspase-3, resulting in apoptosis [28]. Staurosporine is a general kinase inhibitor that is commonly used to induce apoptosis [27]. We show PGAM5-deficient MEFs are more sensitive to staurosporine-induced apoptosis when compared to wild-type MEFs. Reconstitution of PGAM5 in PGAM5-deficient MEFs partially rescued MEFs from increased staurosporine sensitivity. Furthermore, increased staurosporine-induced cell death in PGAM5-deficient MEFs was associated with a 2-fold increase in caspase-3/7 activity, as compared to that of wild-type MEFs. These results suggest that PGAM5 helps prevent staurosporine-induced apoptosis in cells.

Our staurosporine studies in MEFs suggest that PGAM5 provides protection against cell death by apoptosis, though the mechanism is not known. Given that PGAM5 alters mitochondrial morphology upon overexpression in cells, it may be the case that

changes in mitochondrial morphology determine the susceptibility of the outer mitochondrial membrane to permeability. Since PGAM5-deficient MEFs are more sensitive to staurosporine, examining PGAM5's ability to prevent release of apoptotic factors, such as cytochrome c, would provide insight into how PGAM5 is contributing to apoptosis.

Reconstitution of PGAM5 in PGAM5-deficient MEFs helps restore resistance to staurosporine-induced apoptosis. One experiment would be to see if reconstitution with A4-PGAM5 provides resistance to staurosporine treatment. If A4-PGAM5 reconstitution fails to increase resistance to staurosporine, then this would support the notion that multimerization and activation of PGAM5 is necessary for its protective function against apoptosis in cells.

5.2.3 PGAM5 in autophagy/mitophagy

Mitophagy is the controlled degradation of mitochondria, which serves to either break down and recycle cellular building blocks or eliminate damaged mitochondria [55]. Mitochondria actively maintain a membrane potential via oxidative phosphorylation [5]. Disruption of mitochondrial membrane potential (MMP) has been shown to activate the PINK1/PARKIN pathway, promoting degradation of mitochondria [57]. Loss-of-function mutations in either PINK1 or PARKIN is associated with early onset Parkinson's disease (PD) [126]. Under normal conditions, PINK1 is rapidly turned over. Uncoupling of mitochondria with CCCP results in the stabilization of PINK on the mitochondrial membrane. Stabilization of PINK1 promotes the recruitment of PARKIN to mitochondria. PARKIN is part of an E3 ligase complex, which promotes ubiquitination and degradation of mitochondrial associated proteins [56, 61, 67, 73].

In *Drosophila*, loss-of-function mutations in dPINK results in PD-like symptoms. These include loss of dopaminergic neurons, muscle degeneration that affects wing posture, reduced lifespan, and difficulties in climbing [125]. In *Drosophila*, dPGAM5 was identified as an interacting partner of dPINK1 [127]. In loss-of-function dPINK1 flies, symptoms of PD were partially alleviated in knockout dPGAM5 flies, while symptoms were enhanced in flies overexpressing dPGAM5 [127]. Knockout of dPGAM5 did not alleviate symptoms in dPARKIN-defective flies suggesting that PGAM5 was acting downstream of dPINK1 and upstream of PARKIN [127]. In another study, PINK1 was shown to be autophosphorylated upon uncoupling of mitochondria and that most disease-relevant mutations in PINK1 prevented this autophosphorylation [162]. The authors report that autophosphorylation occurs on PINK1-Ser-228 and PINK1-Ser-402, which is necessary for recruitment of PARKIN. It is possible that PGAM5 negatively acts on PINK1 by dephosphorylating PINK1 at Ser-228 and/or Ser-402.

In another study, the authors demonstrated that the rhomboid protease PARL differentially cleaves PINK1 and PGAM5, depending on the status of MMP [128]. In polarized mitochondria, PARL cleaves PINK1. CCCP treatment of cells and depolarization of mitochondria resulted in the stabilization of PINK1 and PARL-mediated cleavage of PGAM5 [128].

Western blot analysis of MEF lysates reveals that PGAM5 normally exists in two forms as indicated by the tight doublet observed when blotting for PGAM5. CCCP treatment of MEFs results in the complete shift of the upper band to the lower band, presumably as a result of PARL-mediated cleavage of PGAM5 [128]. We demonstrated

by SEC that PGAM5 exists in two pools in MEFs. One pool contains a higher order complex and one pool contains a lower order complex. CCCP treatment of MEFs depleted the higher order pool while the lower pool remained. We predict that the lower pool is indicative of the inactive-dimeric form of PGAM5.

It may be the case that in normal conditions, PGAM5 forms a higher order complex that is capable of dephosphorylating PINK1 at Ser-228 and/or Ser-402. Dephosphorylation of PINK1 results in PARL-mediated cleavage and ultimately degradation of PINK1. During mitochondrial depolarization, PARL associates with and cleaves PGAM5, promoting the inactive-dimeric form of PGAM5. This allows for accumulation of PINK1 phosphorylation, which mediates PARKIN recruitment to mitochondria, promoting mitophagy.

5.3 Future directions

Certain genes when disrupted in mice result in embryonic lethality, which makes characterizing a phenotype difficult. In some cases, gene disruption that results in embryonic lethality can be rescued by disrupting a second gene, a technique known as complementation. For instance, deletion of caspase-8 in mice results in embryonic death by E10.5 [163]. Deletion of caspase-8 increased assembly of the necrosome causing cells to die by necrosis [164]. Caspase-8 lethality was rescued by deleting RIPK3 in caspase-8 knockout mice [164]. It would be valuable to identify a gene that once disrupted would complement the lethality observed in PGAM5 gene-trap mice. Since PGAM5 is likely to be involved in regulating cell death, some candidates would include RIPK3, caspase-8, or caspase-3.

PINK1 phosphorylation at Ser-228 and Ser-402 was shown to be important in recruitment of PARKIN to mitochondria [162]. Since PGAM5 is a Ser/Thr phosphatase, we should investigate if PGAM5 is capable of dephosphorylating PINK1 and if PGAM5 dephosphorylation of PINK1 is dependent on mitochondrial membrane potential. We provided evidence that PGAM5 is a sequence specific phosphatase that prefers one or more negatively charged amino acid near the phosphorylation site. Both PINK1 Ser-228 and Ser-402 contain one or more negatively charged amino acid near the phosphorylation site.

We observed that PGAM5-deficient MEFs have increased caspase-3/7 activity, compared to that of wild-type MEFs, and that reconstitution of PGAM5 resulted in partial recovery. It would be informative to know if the resistance to staurosporine-induced cell death is dependent on multimerization of PGAM5. Furthermore, since overexpression of A4-PGAM5 cause fragmentation of mitochondria in cells, it would be useful to determine if the multimeric state of PGAM5 affects cytochrome c release. These results would help support the importance of PGAM5 multimerization in proper mitochondrial function and control of cell death.

Our results suggest that PGAM5 protects cells from apoptosis. Wang and coworkers showed that inhibition of caspases with z-VAD and activation of the necrosome with smac-mimetics resulted in activation of PGAM5, which caused cell death by necrosis [53]. It would be interesting to see if necrosis can be induced in PGAM5-deficient MEFs after inhibiting caspases with z-VAD and promoting necrosis with smac-mimetics. If we can induce necrosis, then we would demonstrate that necrosis can occur in a PGAM5-independent manner. However, if necrosis is blocked, then we

would help confirm that indeed necrosis is in part mediated through PGAM5. In either case, further investigation of downstream targets of PGAM5 is critical in understanding PGAM5's function in cells.

Though the exact function of PGAM5 remains to be determined, it is likely that PGAM5 plays an important role in regulating cell death. PGAM5 has been implicated in mitophagy, apoptosis, and necrosis, demonstrating that further research is needed to better understand the underlying role PGAM5 has in cells. Furthermore, elucidating the role of PGAM5 in cellular death may help lead to the discovery of new therapies, perhaps through the design of drugs that disrupt PGAM5 multimerization, that may be able to help treat cancer, cardiovascular diseases, and alleviate the symptoms of neurological disorders such as Parkinson's disease, Alzheimer's disease, and Huntington's disease.

Materials and Methods

Materials

The crystal screen kits Classics Suite, ComPAS Suite, JCSG Core I Suite, JCSG Core II Suite, MbClass Suite, MbClass II Suite, PACT Suite, and PEGs II Suite were purchased from Qiagen. The Additive Screen and Crystal Screen 1 and 2 were purchased from Hampton Research. The Precipitant Synergy and JBScreen Pentaerythritol HTS kits were purchased from Jena Bioscience.

The phosphopeptides END(pT)INASL, DDA(pT)VA, AAA(pT)VA, RRA(pT)VA, RRA(pS)VA, RRA(pY)VA, END(pY)INASL, DADE(pY)LIPQQG, RGRGS(pS)VGGGS, NPCTE(pT)FTGTL, ALSAG(pS)NEYLR, YLRSI(pS)LPVPV, NFEDH(pS)APPSP, HSAPP(pS)PEEKD, ESEME(pT)PSAIN, WHLAD(pS)PAVNG, SQLHI(pT)PGTAY, DPVAR(pT)SPLQT, PVART(pS)PLQTP, AGPAL(pS)PVPPV, QTPPV(pS)PAPQP, ASQEP(pS)PAASA, PIMPA(pS)PQKGH, VARKL(pS)AREQR, EVFCF(pS)QRRKE, FELIL(pS)PRSKE, and PEFPL(pS)PPKKK were purchased from GenScript. The phosphopeptides RRA(pT)VA, END(pY)INASL, and DADE(pY)LIPQQG were purchased from Promega.

The PGAM5 antibody was raised against human PGAM5 in chicken and was affinity purified. BCL-XL-pSer62 and TOM20 antibodies were purchased from Santa Cruz. Tubulin antibody was purchased from Sigma.

LipoD293 was purchased from SignaGen. Lipofectamine and PLUS reagents were purchased from Invitrogen.

Recombinant expression vectors for protein production

The PGAM5 expression vectors were generated by cloning PCR-derived fragments of PGAM5 into pET-15b (Novagen), pcDNA3 (Invitrogen), pCMV-Tag 4A (Sigma), or pWZL (Addgene) expression vectors. Single-point mutations of human PGAM5 were generated using PCR site-directed mutagenesis with standard overlap-extension techniques.

Protein purification

The pET-15b-PGAM5 expression vectors were transformed into Rosetta cells (BLP21) and grown in LB-media at 37C to an optical density of 0.5-0.6 (measured at absorbance 595nm). Temperature was reduced to 30C and expression of PGAM5 was induced by the addition of 1mM IPTG and 1mM PMSF for three hours. Bacterial cultures were pelleted at 4000rpm for ten minutes. The supernatant was removed and bacterial pellets were resuspended in lysis buffer (Lysis buffer: 500mM NaCl, 20mM Hepes pH 7.2, 10mM Imidazole, and protease inhibitor mix (Sigma)). The bacterial suspension was subjected to three freeze (-80C)/thaw (37C) cycles to lyse bacteria. Bacterial lysates were centrifuged at 15,500xg to remove cellular debris. Clarified lysates were passed over a Ni-NTA column and washed three times with lysis buffer (without protease inhibitors) followed by three washes with wash buffer (Wash buffer: 500mM NaCl, 20mM Hepes pH 7.2, 60mM Imidazole). PGAM5 protein was eluted off the Ni-NTA column with elution buffer (Elution buffer: 500mM NaCl, 20mM Hepes pH 7.2, and 500mM Imidazole). Eluted protein was desalted to 100mM NaCl, 20mM Hepes pH 7.2.

Drosophila selenomethionine-PGAM5

The pET-15b-drophila-PGAM5-V30-TGA construct was transformed in Rosetta cells (BLP21) using minimal media. Bacterial cultures were initially grown in M9 media (in 1L media add 12.8g Na₂HPO₄·7H₂O, 3g KH₂PO₄, 0.5g NaCl, 1g NH₄Cl, pH 7.2) at 37C until and OD 595nm of 0.5-0.6 was reached. An amino acid mix (100mg of K, F, and T, 50mg of I, L, and V, and 60mg of selenomethionine) was added to the bacterial culture and grown at 22C for 15 minutes. Expression of PGAM5 was induced with 1M IPTG and 1M PMSF for an additional 16-24 hours at 22C. Purification of dPGAM5 was carried out as described in Protein purification and FPLC sections.

Fast Protein Liquid Chromatography

We used fast protein liquid chromatography (FPLC, AKTA FPLC systems) to desalt and further purify protein eluted from the Ni-NTA column. To desalt, protein was loaded onto desalting columns (GE) and was exchanged into buffer containing 100mM NaCl and 20mM Hepes pH 7.2. For crystal trials, desalted protein was purified by cation exchange. Desalted protein was loaded onto a HiTrap SP HP column (GE). A salt gradient was established starting at 100mM NaCl and 20mM Hepes pH 7.2 and ending at 1M NaCl and 20mM Hepes pH 7.2 with PGAM5 eluting around 300-400mM NaCl. Protein eluted from the cation exchange column was desalted to 100mM NaCl and 20mM Hepes pH 7.2. Protein was detected using absorbance at 280nm.

For size exclusion chromatography, PGAM5 proteins eluted from Ni-NTA columns were separated on a HiLoad 26/60 Superdex 200 size exclusion column (GE). Running buffer contained 100mM NaCl and 20mM Hepes pH 7.2. Samples were run at 2.5ml/min. The standard curve for this column was generated using non-denatured

protein standards from Sigma under the same running conditions listed above. Protein was detected using absorbance at 280nm.

Crystal trials

PGAM5 protein was purified as described in the protein purification and FPLC sections. Purified PGAM5 protein was concentrated to the desired concentration using Amicon concentrators (Millipore) with a molecular weight cutoff of 10,000.

Concentrated protein was either used either immediately in crystal trials or frozen at -80C for future use. Trials were setup using the sitting drop method in 96-3 well INTELLI-plates (Art Robbins Instruments). Drops were setup at ratios of 1:3, 1:1, and 3:1 (protein:solution). In some cases, during optimization, drops were setup in alternate plates using the sitting drop method. All plates were sealed and stored at 18C during crystal growth periods. Crystals to be frozen in liquid nitrogen were picked from the drops and incubated in cryoprotectant for 15-30 seconds prior to submerging in liquid nitrogen. For diffraction collection, crystals were maintained in a nitrogen stream during x-ray diffraction collection, unless noted. Data collection was obtained on an R-Axis.

Phosphatase Assays

Phosphopeptide was suspended in reaction buffer (150mM NaCl, 10mM Hepes pH 7.4, and 0.5mM DTT) and reactions were started by the addition of PGAM5.

Phosphatase activity was determined using the malachite green assay (R&D Systems). Briefly, reactions were stopped by addition of sulfuric acid. Free-phosphate was detected with malachite green solution. Free-phosphate levels were determined by changes in absorbance at 620nm. Kinetic parameters were extrapolated using Kaleidagraph software.

Determination of molar mass

PGAM5 proteins were purified by size exclusion chromatography as described fast protein liquid chromatography. The eluent was monitored by refractive index to determine the protein concentration. The molar mass of PGAM5 was determined by light scattering.

Cell Fractionation

All steps were performed on ice or at 4°C. Five confluent 15cm plates of mouse embryonic fibroblasts were lysed in lysis buffer (50mM Hepes pH 8.0, 150mM NaCl, 1% Triton-X-100, 1% deoxycholate, 1mM DTT, and protease inhibitor mix (Sigma)) for ten minutes. Cell lysates were centrifuged at 15,500xg for ten minutes. The supernatant was separated on HiLoad 26/60 (GE) column (see FPLC section for details). Fractions were collected every 10mL from 100mL to 250mL (25 fractions) and were subjected to trichloroacetic acid (TCA) precipitation. Briefly, TCA was added to each 10mL fraction to a final of 20% TCA (v/v) and incubated for ten minutes. Precipitated protein was pelleted at 15,500xg for ten minutes. Supernatant was removed and pellets were washed with cold acetone. Protein was pelleted at 15,500xg and acetone was removed. Pellets were allowed to dry before resuspending in sample buffer. Samples were analyzed by western blot.

Immunofluorescence

Cells were plated onto glass coverslips and grown overnight. Cells were fixed with 4% paraformaldehyde at 37°C for 10min. Fixed cells were washed with PBS followed by permeabilization with 0.2% Triton-X-100 in PBS pH 7.4 for 10min. Cells were washed with PBS and incubated in primary antibody solution for one hour at room

temperature. Primary solution contained primary antibody, 10% FBS, and 1X PBS pH 7.4. The cells were washed twice for 15 minutes each in PBS followed by a one hour incubation in secondary solution. The secondary solution contained fluorescent dyes (Invitrogen), 10% FBS, and 1X PBS pH 7.4. Stained cells were washed once more in PBS and mounted using ProLong Gold (Invitrogen). Images were visualized on a Leica DMI6000B microscope.

Isolation of primary mouse embryonic fibroblasts (MEFs)

All mice were euthanized with standard protocols. Embryos were harvested around day 11.5. Under sterile conditions, the uterus was removed and cut in to sections separating individual embryos. Embryos were expelled from the uterus and washed with PBS. The umbilical was removed and the CNS (embryo head) was removed. Embryo bodies were minced and incubated in trypsin for three minutes. Trypsinized embryos were suspended in media and transferred to plates and allowed to grow.

Infections and transfections

Retroviral vectors used include pBabe-puro-SV40-LT, pWZL-hygro-empty vector, and pWZL-hygro-PGAM5-L-FLAG were constructed by subcloning the PCR-amplified human PGAM5-L-FLAG into the EcoRI and SalI sites. Virus was produced in 293FT cells. Primary MEFs were initially infected with pBabe-puro-SV40-LT for 24hrs and placed under selection with 1ug/mL puromycin. After puromycin selection was complete, Immortalized MEFs were infected with pWZL-hygro constructs for 24h, followed by selection with 200ug/mL hygromycin. For transfections we used pcDNA3.1-empty vector, pcDNA3.1-PGAM5, pcDNA3.1-ΔN55-PGAM5, pcDNA3.1-ΔN60-PGAM5, and pcDNA3.1-A4-PGAM5. PGAM5 was cloned into the AflIII and

BamHI sites. pcDNA3.1-HA-BCL-XL and pcDNA3.1-HA-BCL-XL were a gift from Dr. Chambers [165]. COS1 cells were transfected using Lipofectamine/PLUS reagents according to the manufacturer's instructions.

Cell death assays

MEF cells were plated in 96-well plates and grown overnight. Staurosporine was added to MEFs for 20 hours. Staurosporine was removed and MEFs were washed with PBS. Viability was measured using the XTT assay (Biotium). Briefly, XTT solution was added to cells and viability was measured by an absorbance shift at 475nm.

Caspase activity

MEFs were plated in 96-well plates and grown overnight. MEFs were treated with staurosporine for 20 hours. MEFs were washed with PBS and assayed for caspase activity using the Caspase-Glo 3/7 assay (Promega). Briefly, cells were lysed in assay buffer containing a substrate for active caspases-3/7. Cleavage of the substrate by caspases-3/7 releases aminoluciferin, which is used by luciferase. Caspase-3/7 activity is measured by the level of luciferase activity.

References:

1. Finkel, T. and N.J. Holbrook, *Oxidants, oxidative stress and the biology of ageing*. Nature, 2000. **408**(6809): p. 239-47.
2. Turrens, J.F., *Superoxide production by the mitochondrial respiratory chain*. Biosci Rep, 1997. **17**(1): p. 3-8.
3. Lin, M.T. and M.F. Beal, *Mitochondrial dysfunction and oxidative stress in neurodegenerative diseases*. Nature, 2006. **443**(7113): p. 787-95.
4. Ott, M., et al., *Mitochondria, oxidative stress and cell death*. Apoptosis, 2007. **12**(5): p. 913-22.
5. Hatefi, Y., *The mitochondrial electron transport and oxidative phosphorylation system*. Annu Rev Biochem, 1985. **54**: p. 1015-69.
6. Senior, A.E., S. Nadanaciva, and J. Weber, *The molecular mechanism of ATP synthesis by F1F0-ATP synthase*. Biochim Biophys Acta, 2002. **1553**(3): p. 188-211.
7. Kroemer, G., L. Galluzzi, and C. Brenner, *Mitochondrial membrane permeabilization in cell death*. Physiol Rev, 2007. **87**(1): p. 99-163.
8. Eguchi, Y., S. Shimizu, and Y. Tsujimoto, *Intracellular ATP levels determine cell death fate by apoptosis or necrosis*. Cancer Res, 1997. **57**(10): p. 1835-40.
9. Chen, Y., et al., *Mitochondrial electron-transport-chain inhibitors of complexes I and II induce autophagic cell death mediated by reactive oxygen species*. J Cell Sci, 2007. **120**(Pt 23): p. 4155-66.
10. Talalay, P., A.T. Dinkova-Kostova, and W.D. Holtzclaw, *Importance of phase 2 gene regulation in protection against electrophile and reactive oxygen toxicity and carcinogenesis*. Adv Enzyme Regul, 2003. **43**: p. 121-34.
11. Gao, X. and P. Talalay, *Induction of phase 2 genes by sulforaphane protects retinal pigment epithelial cells against photooxidative damage*. Proc Natl Acad Sci U S A, 2004. **101**(28): p. 10446-51.
12. Wasserman, W.W. and W.E. Fahl, *Functional antioxidant responsive elements*. Proc Natl Acad Sci U S A, 1997. **94**(10): p. 5361-6.
13. McMahon, M., et al., *The Cap'n'Collar basic leucine zipper transcription factor Nrf2 (NF-E2 p45-related factor 2) controls both constitutive and inducible expression of intestinal detoxification and glutathione biosynthetic enzymes*. Cancer Res, 2001. **61**(8): p. 3299-307.

14. Lee, J.M., et al., *NF-E2-related factor-2 mediates neuroprotection against mitochondrial complex I inhibitors and increased concentrations of intracellular calcium in primary cortical neurons*. J Biol Chem, 2003. **278**(39): p. 37948-56.
15. Lee, J.M., et al., *Identification of the NF-E2-related factor-2-dependent genes conferring protection against oxidative stress in primary cortical astrocytes using oligonucleotide microarray analysis*. J Biol Chem, 2003. **278**(14): p. 12029-38.
16. Itoh, K., et al., *Keap1 represses nuclear activation of antioxidant responsive elements by Nrf2 through binding to the amino-terminal Neh2 domain*. Genes Dev, 1999. **13**(1): p. 76-86.
17. Cullinan, S.B., et al., *The Keap1-BTB protein is an adaptor that bridges Nrf2 to a Cul3-based E3 ligase: oxidative stress sensing by a Cul3-Keap1 ligase*. Mol Cell Biol, 2004. **24**(19): p. 8477-86.
18. Zhang, D.D., et al., *Keap1 is a redox-regulated substrate adaptor protein for a Cul3-dependent ubiquitin ligase complex*. Mol Cell Biol, 2004. **24**(24): p. 10941-53.
19. Lo, S.C., et al., *Structure of the Keap1:Nrf2 interface provides mechanistic insight into Nrf2 signaling*. EMBO J, 2006. **25**(15): p. 3605-17.
20. Padmanabhan, B., et al., *Structural basis for defects of Keap1 activity provoked by its point mutations in lung cancer*. Mol Cell, 2006. **21**(5): p. 689-700.
21. Stewart, D., et al., *Degradation of transcription factor Nrf2 via the ubiquitin-proteasome pathway and stabilization by cadmium*. J Biol Chem, 2003. **278**(4): p. 2396-402.
22. Dinkova-Kostova, A.T., et al., *Direct evidence that sulfhydryl groups of Keap1 are the sensors regulating induction of phase 2 enzymes that protect against carcinogens and oxidants*. Proc Natl Acad Sci U S A, 2002. **99**(18): p. 11908-13.
23. Taguchi, K., H. Motohashi, and M. Yamamoto, *Molecular mechanisms of the Keap1-Nrf2 pathway in stress response and cancer evolution*. Genes Cells, 2011. **16**(2): p. 123-40.
24. Li, J. and J. Yuan, *Caspases in apoptosis and beyond*. Oncogene, 2008. **27**(48): p. 6194-206.
25. Walczak, H. and M.R. Sprick, *Biochemistry and function of the DISC*. Trends Biochem Sci, 2001. **26**(7): p. 452-3.

26. Budihardjo, I., et al., *Biochemical pathways of caspase activation during apoptosis*. Annu Rev Cell Dev Biol, 1999. **15**: p. 269-90.
27. Tang, D., J.M. Lahti, and V.J. Kidd, *Caspase-8 activation and bid cleavage contribute to MCF7 cellular execution in a caspase-3-dependent manner during staurosporine-mediated apoptosis*. J Biol Chem, 2000. **275**(13): p. 9303-7.
28. Yuan, S. and C.W. Akey, *Apoptosome structure, assembly, and procaspase activation*. Structure, 2013. **21**(4): p. 501-15.
29. Acehan, D., et al., *Three-dimensional structure of the apoptosome: implications for assembly, procaspase-9 binding, and activation*. Mol Cell, 2002. **9**(2): p. 423-32.
30. Zou, H., et al., *Apaf-1, a human protein homologous to C. elegans CED-4, participates in cytochrome c-dependent activation of caspase-3*. Cell, 1997. **90**(3): p. 405-13.
31. van Loo, G., et al., *The role of mitochondrial factors in apoptosis: a Russian roulette with more than one bullet*. Cell Death Differ, 2002. **9**(10): p. 1031-42.
32. Burlacu, A., *Regulation of apoptosis by Bcl-2 family proteins*. J Cell Mol Med, 2003. **7**(3): p. 249-57.
33. Korsmeyer, S.J., et al., *Pro-apoptotic cascade activates BID, which oligomerizes BAK or BAX into pores that result in the release of cytochrome c*. Cell Death Differ, 2000. **7**(12): p. 1166-73.
34. Kluck, R.M., et al., *The release of cytochrome c from mitochondria: a primary site for Bcl-2 regulation of apoptosis*. Science, 1997. **275**(5303): p. 1132-6.
35. Vander Heiden, M.G., et al., *Bcl-xL regulates the membrane potential and volume homeostasis of mitochondria*. Cell, 1997. **91**(5): p. 627-37.
36. Yang, J., et al., *Prevention of apoptosis by Bcl-2: release of cytochrome c from mitochondria blocked*. Science, 1997. **275**(5303): p. 1129-32.
37. Wei, M.C., et al., *Proapoptotic BAX and BAK: a requisite gateway to mitochondrial dysfunction and death*. Science, 2001. **292**(5517): p. 727-30.
38. Wolter, K.G., et al., *Movement of Bax from the cytosol to mitochondria during apoptosis*. J Cell Biol, 1997. **139**(5): p. 1281-92.
39. Kuwana, T., et al., *Bid, Bax, and lipids cooperate to form supramolecular openings in the outer mitochondrial membrane*. Cell, 2002. **111**(3): p. 331-42.

40. Letai, A., et al., *Distinct BH3 domains either sensitize or activate mitochondrial apoptosis, serving as prototype cancer therapeutics*. Cancer Cell, 2002. **2**(3): p. 183-92.
41. Grooten, J., et al., *Cell membrane permeabilization and cellular collapse, followed by loss of dehydrogenase activity: early events in tumour necrosis factor-induced cytotoxicity*. Cytokine, 1993. **5**(6): p. 546-55.
42. Vercammen, D., et al., *Dual signaling of the Fas receptor: initiation of both apoptotic and necrotic cell death pathways*. J Exp Med, 1998. **188**(5): p. 919-30.
43. He, S., et al., *Receptor interacting protein kinase-3 determines cellular necrotic response to TNF-alpha*. Cell, 2009. **137**(6): p. 1100-11.
44. Duprez, L., et al., *RIP kinase-dependent necrosis drives lethal systemic inflammatory response syndrome*. Immunity, 2011. **35**(6): p. 908-18.
45. Zhang, D.W., et al., *RIP3, an energy metabolism regulator that switches TNF-induced cell death from apoptosis to necrosis*. Science, 2009. **325**(5938): p. 332-6.
46. Wilson, N.S., V. Dixit, and A. Ashkenazi, *Death receptor signal transducers: nodes of coordination in immune signaling networks*. Nat Immunol, 2009. **10**(4): p. 348-55.
47. MacEwan, D.J., *TNF receptor subtype signalling: differences and cellular consequences*. Cell Signal, 2002. **14**(6): p. 477-92.
48. Lin, Y., et al., *Tumor necrosis factor-induced nonapoptotic cell death requires receptor-interacting protein-mediated cellular reactive oxygen species accumulation*. J Biol Chem, 2004. **279**(11): p. 10822-8.
49. Vercammen, D., et al., *Inhibition of caspases increases the sensitivity of L929 cells to necrosis mediated by tumor necrosis factor*. J Exp Med, 1998. **187**(9): p. 1477-85.
50. Li, J., et al., *The RIP1/RIP3 necrosome forms a functional amyloid signaling complex required for programmed necrosis*. Cell, 2012. **150**(2): p. 339-50.
51. Degterev, A., et al., *Identification of RIP1 kinase as a specific cellular target of necrostatins*. Nat Chem Biol, 2008. **4**(5): p. 313-21.
52. Cho, Y.S., et al., *Phosphorylation-driven assembly of the RIP1-RIP3 complex regulates programmed necrosis and virus-induced inflammation*. Cell, 2009. **137**(6): p. 1112-23.

53. Wang, Z., et al., *The mitochondrial phosphatase PGAM5 functions at the convergence point of multiple necrotic death pathways*. Cell, 2012. **148**(1-2): p. 228-43.
54. Fulda, S., *Autophagy and cell death*. Autophagy, 2012. **8**(8): p. 1250-1.
55. Levine, B. and D.J. Klionsky, *Development by self-digestion: molecular mechanisms and biological functions of autophagy*. Dev Cell, 2004. **6**(4): p. 463-77.
56. Vives-Bauza, C., et al., *PINK1-dependent recruitment of Parkin to mitochondria in mitophagy*. Proc Natl Acad Sci U S A, 2010. **107**(1): p. 378-83.
57. Jin, S.M., et al., *Mitochondrial membrane potential regulates PINK1 import and proteolytic destabilization by PARL*. J Cell Biol, 2010. **191**(5): p. 933-42.
58. Deas, E., et al., *PINK1 cleavage at position A103 by the mitochondrial protease PARL*. Hum Mol Genet, 2011. **20**(5): p. 867-79.
59. Takatori, S., G. Ito, and T. Iwatsubo, *Cytoplasmic localization and proteasomal degradation of N-terminally cleaved form of PINK1*. Neurosci Lett, 2008. **430**(1): p. 13-7.
60. Moriwaki, Y., et al., *L347P PINK1 mutant that fails to bind to Hsp90/Cdc37 chaperones is rapidly degraded in a proteasome-dependent manner*. Neurosci Res, 2008. **61**(1): p. 43-8.
61. Matsuda, N., et al., *PINK1 stabilized by mitochondrial depolarization recruits Parkin to damaged mitochondria and activates latent Parkin for mitophagy*. J Cell Biol, 2010. **189**(2): p. 211-21.
62. Kato, H., et al., *Tom70 is essential for PINK1 import into mitochondria*. PLoS One, 2013. **8**(3): p. e58435.
63. Harner, M., W. Neupert, and M. Deponte, *Lateral release of proteins from the TOM complex into the outer membrane of mitochondria*. EMBO J, 2011. **30**(16): p. 3232-41.
64. Lim, K.L., et al., *Parkin mediates nonclassical, proteasomal-independent ubiquitination of synphilin-1: implications for Lewy body formation*. J Neurosci, 2005. **25**(8): p. 2002-9.
65. Kahle, P.J. and C. Haass, *How does parkin ligate ubiquitin to Parkinson's disease?* EMBO Rep, 2004. **5**(7): p. 681-5.

66. Twigg, G., et al., *Fission and selective fusion govern mitochondrial segregation and elimination by autophagy*. EMBO J, 2008. **27**(2): p. 433-46.
67. Gegg, M.E., et al., *Mitofusin 1 and mitofusin 2 are ubiquitinated in a PINK1/parkin-dependent manner upon induction of mitophagy*. Hum Mol Genet, 2010. **19**(24): p. 4861-70.
68. Rojo, M., et al., *Membrane topology and mitochondrial targeting of mitofusins, ubiquitous mammalian homologs of the transmembrane GTPase Fzo*. J Cell Sci, 2002. **115**(Pt 8): p. 1663-74.
69. Chen, H., et al., *Mitofusins Mfn1 and Mfn2 coordinately regulate mitochondrial fusion and are essential for embryonic development*. J Cell Biol, 2003. **160**(2): p. 189-200.
70. Cai, Q. and Z.H. Sheng, *Moving or stopping mitochondria: Miro as a traffic cop by sensing calcium*. Neuron, 2009. **61**(4): p. 493-6.
71. Wang, X., et al., *PINK1 and Parkin target Miro for phosphorylation and degradation to arrest mitochondrial motility*. Cell, 2011. **147**(4): p. 893-906.
72. Weihofen, A., et al., *Pink1 forms a multiprotein complex with Miro and Milton, linking Pink1 function to mitochondrial trafficking*. Biochemistry, 2009. **48**(9): p. 2045-52.
73. Liu, S., et al., *Parkinson's disease-associated kinase PINK1 regulates Miro protein level and axonal transport of mitochondria*. PLoS Genet, 2012. **8**(3): p. e1002537.
74. Song, Z., et al., *Mitofusins and OPA1 mediate sequential steps in mitochondrial membrane fusion*. Mol Biol Cell, 2009. **20**(15): p. 3525-32.
75. Chen, H., A. Chomyn, and D.C. Chan, *Disruption of fusion results in mitochondrial heterogeneity and dysfunction*. J Biol Chem, 2005. **280**(28): p. 26185-92.
76. Ishihara, N., Y. Eura, and K. Mihara, *Mitofusin 1 and 2 play distinct roles in mitochondrial fusion reactions via GTPase activity*. J Cell Sci, 2004. **117**(Pt 26): p. 6535-46.
77. Knott, A.B., et al., *Mitochondrial fragmentation in neurodegeneration*. Nat Rev Neurosci, 2008. **9**(7): p. 505-18.
78. Koshiba, T., et al., *Structural basis of mitochondrial tethering by mitofusin complexes*. Science, 2004. **305**(5685): p. 858-62.

79. Delettre, C., et al., *Nuclear gene OPA1, encoding a mitochondrial dynamin-related protein, is mutated in dominant optic atrophy*. Nat Genet, 2000. **26**(2): p. 207-10.
80. Satoh, M., et al., *Differential sublocalization of the dynamin-related protein OPA1 isoforms in mitochondria*. Biochem Biophys Res Commun, 2003. **300**(2): p. 482-93.
81. Olichon, A., et al., *Mitochondrial dynamics and disease, OPA1*. Biochim Biophys Acta, 2006. **1763**(5-6): p. 500-9.
82. Delettre, C., et al., *Mutation spectrum and splicing variants in the OPA1 gene*. Hum Genet, 2001. **109**(6): p. 584-91.
83. Cipolat, S., et al., *OPA1 requires mitofusin 1 to promote mitochondrial fusion*. Proc Natl Acad Sci U S A, 2004. **101**(45): p. 15927-32.
84. Bossy-Wetzel, E., et al., *Mitochondrial fission in apoptosis, neurodegeneration and aging*. Curr Opin Cell Biol, 2003. **15**(6): p. 706-16.
85. Lee, Y.J., et al., *Roles of the mammalian mitochondrial fission and fusion mediators Fis1, Drp1, and Opa1 in apoptosis*. Mol Biol Cell, 2004. **15**(11): p. 5001-11.
86. Shin, H.W., et al., *Identification and subcellular localization of a novel mammalian dynamin-related protein homologous to yeast Vps1p and Dnm1p*. J Biochem, 1997. **122**(3): p. 525-30.
87. Zhu, P.P., et al., *Intra- and intermolecular domain interactions of the C-terminal GTPase effector domain of the multimeric dynamin-like GTPase Drp1*. J Biol Chem, 2004. **279**(34): p. 35967-74.
88. Smirnova, E., et al., *Dynamin-related protein Drp1 is required for mitochondrial division in mammalian cells*. Mol Biol Cell, 2001. **12**(8): p. 2245-56.
89. Yoon, Y., K.R. Pitts, and M.A. McNiven, *Mammalian dynamin-like protein DLP1 tubulates membranes*. Mol Biol Cell, 2001. **12**(9): p. 2894-905.
90. Wakabayashi, J., et al., *The dynamin-related GTPase Drp1 is required for embryonic and brain development in mice*. J Cell Biol, 2009. **186**(6): p. 805-16.
91. Suen, D.F., K.L. Norris, and R.J. Youle, *Mitochondrial dynamics and apoptosis*. Genes Dev, 2008. **22**(12): p. 1577-90.

92. Ishihara, N., et al., *Mitochondrial fission factor Drp1 is essential for embryonic development and synapse formation in mice*. Nat Cell Biol, 2009. **11**(8): p. 958-66.
93. Stojanovski, D., et al., *Levels of human Fis1 at the mitochondrial outer membrane regulate mitochondrial morphology*. J Cell Sci, 2004. **117**(Pt 7): p. 1201-10.
94. Gandre-Babbe, S. and A.M. van der Bliek, *The novel tail-anchored membrane protein Mff controls mitochondrial and peroxisomal fission in mammalian cells*. Mol Biol Cell, 2008. **19**(6): p. 2402-12.
95. Otera, H., et al., *Mff is an essential factor for mitochondrial recruitment of Drp1 during mitochondrial fission in mammalian cells*. J Cell Biol, 2010. **191**(6): p. 1141-58.
96. Billups, B. and I.D. Forsythe, *Presynaptic mitochondrial calcium sequestration influences transmission at mammalian central synapses*. J Neurosci, 2002. **22**(14): p. 5840-7.
97. Boldogh, I.R. and L.A. Pon, *Mitochondria on the move*. Trends Cell Biol, 2007. **17**(10): p. 502-10.
98. Baas, P.W., M.M. Black, and G.A. Banker, *Changes in microtubule polarity orientation during the development of hippocampal neurons in culture*. J Cell Biol, 1989. **109**(6 Pt 1): p. 3085-94.
99. Hirokawa, N. and Y. Noda, *Intracellular transport and kinesin superfamily proteins, KIFs: structure, function, and dynamics*. Physiol Rev, 2008. **88**(3): p. 1089-118.
100. Kanai, Y., et al., *KIF5C, a novel neuronal kinesin enriched in motor neurons*. J Neurosci, 2000. **20**(17): p. 6374-84.
101. Tanaka, Y., et al., *Targeted disruption of mouse conventional kinesin heavy chain, kif5B, results in abnormal perinuclear clustering of mitochondria*. Cell, 1998. **93**(7): p. 1147-58.
102. Scholey, J.M., et al., *Identification of globular mechanochemical heads of kinesin*. Nature, 1989. **338**(6213): p. 355-7.
103. Hirokawa, N., S. Niwa, and Y. Tanaka, *Molecular motors in neurons: transport mechanisms and roles in brain function, development, and disease*. Neuron, 2010. **68**(4): p. 610-38.

104. Gorska-Andrzejak, J., et al., *Mitochondria are redistributed in Drosophila photoreceptors lacking milton, a kinesin-associated protein*. J Comp Neurol, 2003. **463**(4): p. 372-88.
105. Glater, E.E., et al., *Axonal transport of mitochondria requires milton to recruit kinesin heavy chain and is light chain independent*. J Cell Biol, 2006. **173**(4): p. 545-57.
106. Guo, X., et al., *The GTPase dMiro is required for axonal transport of mitochondria to Drosophila synapses*. Neuron, 2005. **47**(3): p. 379-93.
107. Fransson, S., A. Ruusala, and P. Aspenstrom, *The atypical Rho GTPases Miro-1 and Miro-2 have essential roles in mitochondrial trafficking*. Biochem Biophys Res Commun, 2006. **344**(2): p. 500-10.
108. Smith, M.J., et al., *Mapping the GRIF-1 binding domain of the kinesin, KIF5C, substantiates a role for GRIF-1 as an adaptor protein in the anterograde trafficking of cargoes*. J Biol Chem, 2006. **281**(37): p. 27216-28.
109. Fransson, A., A. Ruusala, and P. Aspenstrom, *Atypical Rho GTPases have roles in mitochondrial homeostasis and apoptosis*. J Biol Chem, 2003. **278**(8): p. 6495-502.
110. King, S.M., *The dynein microtubule motor*. Biochim Biophys Acta, 2000. **1496**(1): p. 60-75.
111. Hirokawa, N., *Kinesin and dynein superfamily proteins and the mechanism of organelle transport*. Science, 1998. **279**(5350): p. 519-26.
112. Schroer, T.A., *Dynactin*. Annu Rev Cell Dev Biol, 2004. **20**: p. 759-79.
113. Vallee, R.B., et al., *Dynein: An ancient motor protein involved in multiple modes of transport*. J Neurobiol, 2004. **58**(2): p. 189-200.
114. Sweeney, H.L. and A. Houdusse, *Structural and functional insights into the Myosin motor mechanism*. Annu Rev Biophys, 2010. **39**: p. 539-57.
115. Quintero, O.A., et al., *Human Myo19 is a novel myosin that associates with mitochondria*. Curr Biol, 2009. **19**(23): p. 2008-13.
116. Jedrzejewski, M.J., *Structure, function, and evolution of phosphoglycerate mutases: comparison with fructose-2,6-bisphosphatase, acid phosphatase, and alkaline phosphatase*. Prog Biophys Mol Biol, 2000. **73**(2-4): p. 263-87.

117. Hammond, P.W., et al., *In vitro selection and characterization of Bcl-X(L)-binding proteins from a mix of tissue-specific mRNA display libraries*. J Biol Chem, 2001. **276**(24): p. 20898-906.
118. Lo, S.C. and M. Hannink, *PGAM5, a Bcl-XL-interacting protein, is a novel substrate for the redox-regulated Keap1-dependent ubiquitin ligase complex*. J Biol Chem, 2006. **281**(49): p. 37893-903.
119. Kobayashi, A., et al., *Oxidative stress sensor Keap1 functions as an adaptor for Cul3-based E3 ligase to regulate proteasomal degradation of Nrf2*. Mol Cell Biol, 2004. **24**(16): p. 7130-9.
120. Lo, S.C. and M. Hannink, *PGAM5 tethers a ternary complex containing Keap1 and Nrf2 to mitochondria*. Exp Cell Res, 2008. **314**(8): p. 1789-803.
121. Takeda, K., et al., *Mitochondrial phosphoglycerate mutase 5 uses alternate catalytic activity as a protein serine/threonine phosphatase to activate ASK1*. Proc Natl Acad Sci U S A, 2009. **106**(30): p. 12301-5.
122. Matsuzawa, A. and H. Ichijo, *Molecular mechanisms of the decision between life and death: regulation of apoptosis by apoptosis signal-regulating kinase 1*. J Biochem, 2001. **130**(1): p. 1-8.
123. Sturchler, E., et al., *Mechanism of oxidative stress-induced ASK1-catalyzed MKK6 phosphorylation*. Biochemistry, 2010. **49**(19): p. 4094-102.
124. Niture, S.K. and A.K. Jaiswal, *Inhibitor of Nrf2 (INrf2 or Keap1) protein degrades Bcl-xL via phosphoglycerate mutase 5 and controls cellular apoptosis*. J Biol Chem, 2011. **286**(52): p. 44542-56.
125. Munoz-Soriano, V. and N. Paricio, *Drosophila models of Parkinson's disease: discovering relevant pathways and novel therapeutic strategies*. Parkinsons Dis, 2011. **2011**: p. 520640.
126. Abudi, S., et al., *Parkinson's disease symptoms--patients' perceptions*. J Adv Nurs, 1997. **25**(1): p. 54-9.
127. Imai, Y., et al., *The loss of PGAM5 suppresses the mitochondrial degeneration caused by inactivation of PINK1 in Drosophila*. PLoS Genet, 2010. **6**(12): p. e1001229.
128. Sekine, S., et al., *Rhomboid protease PARL mediates the mitochondrial membrane potential loss-induced cleavage of PGAM5*. J Biol Chem, 2012. **287**(41): p. 34635-45.

129. Hoshino, A., et al., *p53-TIGAR axis attenuates mitophagy to exacerbate cardiac damage after ischemia*. J Mol Cell Cardiol, 2012. **52**(1): p. 175-84.
130. Du, C., et al., *Smac, a mitochondrial protein that promotes cytochrome c-dependent caspase activation by eliminating IAP inhibition*. Cell, 2000. **102**(1): p. 33-42.
131. Wang, L., F. Du, and X. Wang, *TNF-alpha induces two distinct caspase-8 activation pathways*. Cell, 2008. **133**(4): p. 693-703.
132. Chen, J., et al., *Caspase inhibition by Z-VAD increases the survival of grafted bone marrow cells and improves functional outcome after MCAo in rats*. J Neurol Sci, 2002. **199**(1-2): p. 17-24.
133. Sun, L., et al., *Mixed lineage kinase domain-like protein mediates necrosis signaling downstream of RIP3 kinase*. Cell, 2012. **148**(1-2): p. 213-27.
134. Chaikuad, A., Alfano, I., Picaud, S., Filippakopoulos, P., Barr, A., von Delft, F., Arrowsmith, C.H., Edwards, A.M., Weigelt, J., Bountra, C., Takeda, K., Ichijo, H., Knapp, S., *Crystal structure of human phosphoglycerate mutase family member 5 (PGAM5)*. 2010.
135. Oefner, C., et al., *Structure of human neutral endopeptidase (Neprilysin) complexed with phosphoramidon*. J Mol Biol, 2000. **296**(2): p. 341-9.
136. D'Arcy, A., et al., *Crystal engineering: a case study using the 24 kDa fragment of the DNA gyrase B subunit from Escherichia coli*. Acta Crystallogr D Biol Crystallogr, 1999. **55**(Pt 9): p. 1623-5.
137. Campbell, J.W., et al., *X-ray diffraction studies on enzymes in the glycolytic pathway*. Cold Spring Harb Symp Quant Biol, 1972. **36**: p. 165-70.
138. Doublet, S., *Preparation of selenomethionyl proteins for phase determination*. Methods Enzymol, 1997. **276**: p. 523-30.
139. Hendrickson, W.A., J.R. Horton, and D.M. LeMaster, *Selenomethionyl proteins produced for analysis by multiwavelength anomalous diffraction (MAD): a vehicle for direct determination of three-dimensional structure*. EMBO J, 1990. **9**(5): p. 1665-72.
140. Strub, M.P., et al., *Selenomethionine and selenocysteine double labeling strategy for crystallographic phasing*. Structure, 2003. **11**(11): p. 1359-67.
141. Brand, M.D., et al., *Mitochondrial superoxide: production, biological effects, and activation of uncoupling proteins*. Free Radic Biol Med, 2004. **37**(6): p. 755-67.

142. Lim, M.L., T. Minamikawa, and P. Nagley, *The protonophore CCCP induces mitochondrial permeability transition without cytochrome c release in human osteosarcoma cells*. FEBS Lett, 2001. **503**(1): p. 69-74.
143. Nicholls, D.G., *Mitochondrial membrane potential and aging*. Aging Cell, 2004. **3**(1): p. 35-40.
144. Linsinger, G., et al., *Uncouplers of oxidative phosphorylation can enhance a Fas death signal*. Mol Cell Biol, 1999. **19**(5): p. 3299-311.
145. Legros, F., et al., *Mitochondrial fusion in human cells is efficient, requires the inner membrane potential, and is mediated by mitofusins*. Mol Biol Cell, 2002. **13**(12): p. 4343-54.
146. Ishihara, N., et al., *Regulation of mitochondrial morphology through proteolytic cleavage of OPA1*. EMBO J, 2006. **25**(13): p. 2966-77.
147. Head, B., et al., *Inducible proteolytic inactivation of OPA1 mediated by the OMA1 protease in mammalian cells*. J Cell Biol, 2009. **187**(7): p. 959-66.
148. Ehses, S., et al., *Regulation of OPA1 processing and mitochondrial fusion by m-AAA protease isoenzymes and OMA1*. J Cell Biol, 2009. **187**(7): p. 1023-36.
149. Mikhailik, A., et al., *A phosphatase activity of Sts-1 contributes to the suppression of TCR signaling*. Mol Cell, 2007. **27**(3): p. 486-97.
150. Fujii, K., et al., *Negative control of apoptosis signal-regulating kinase 1 through phosphorylation of Ser-1034*. Oncogene, 2004. **23**(29): p. 5099-104.
151. Tobiume, K., M. Saitoh, and H. Ichijo, *Activation of apoptosis signal-regulating kinase 1 by the stress-induced activating phosphorylation of pre-formed oligomer*. J Cell Physiol, 2002. **191**(1): p. 95-104.
152. Schmitt, E., M. Beauchemin, and R. Bertrand, *Nuclear colocalization and interaction between bcl-xL and cdk1(cdc2) during G2/M cell-cycle checkpoint*. Oncogene, 2007. **26**(40): p. 5851-65.
153. Kharbanda, S., et al., *Translocation of SAPK/JNK to mitochondria and interaction with Bcl-x(L) in response to DNA damage*. J Biol Chem, 2000. **275**(1): p. 322-7.
154. Upreti, M., et al., *Identification of the major phosphorylation site in Bcl-xL induced by microtubule inhibitors and analysis of its functional significance*. J Biol Chem, 2008. **283**(51): p. 35517-25.

155. Stanford, W.L., J.B. Cohn, and S.P. Cordes, *Gene-trap mutagenesis: past, present and beyond*. Nat Rev Genet, 2001. **2**(10): p. 756-68.
156. Huang da, W., B.T. Sherman, and R.A. Lempicki, *Systematic and integrative analysis of large gene lists using DAVID bioinformatics resources*. Nat Protoc, 2009. **4**(1): p. 44-57.
157. Huang da, W., B.T. Sherman, and R.A. Lempicki, *Bioinformatics enrichment tools: paths toward the comprehensive functional analysis of large gene lists*. Nucleic Acids Res, 2009. **37**(1): p. 1-13.
158. Kanehisa, M. and S. Goto, *KEGG: kyoto encyclopedia of genes and genomes*. Nucleic Acids Res, 2000. **28**(1): p. 27-30.
159. Kanehisa, M., *Pathway databases and higher order function*. Adv Protein Chem, 2000. **54**: p. 381-408.
160. Zakeri, Z. and R.A. Lockshin, *Cell death during development*. J Immunol Methods, 2002. **265**(1-2): p. 3-20.
161. Lovas, J.R. and X. Wang, *The meaning of mitochondrial movement to a neuron's life*. Biochim Biophys Acta, 2013. **1833**(1): p. 184-94.
162. Okatsu, K., et al., *PINK1 autophosphorylation upon membrane potential dissipation is essential for Parkin recruitment to damaged mitochondria*. Nat Commun, 2012. **3**: p. 1016.
163. Varfolomeev, E.E., et al., *Targeted disruption of the mouse Caspase 8 gene ablates cell death induction by the TNF receptors, Fas/Apo1, and DR3 and is lethal prenatally*. Immunity, 1998. **9**(2): p. 267-76.
164. Kaiser, W.J., et al., *RIP3 mediates the embryonic lethality of caspase-8-deficient mice*. Nature, 2011. **471**(7338): p. 368-72.
165. Terrano, D.T., M. Upreti, and T.C. Chambers, *Cyclin-dependent kinase 1-mediated Bcl-xL/Bcl-2 phosphorylation acts as a functional link coupling mitotic arrest and apoptosis*. Mol Cell Biol, 2010. **30**(3): p. 640-56.

Vita

Jordan Wilkins was born on September 20, 1983 and grew up with his mother Jillian Wilkins and two brothers Joel and Justin Wilkins in White Bear Lake, Minnesota. He attended the University of Minnesota-Twin Cities as an undergraduate and graduated with a Bachelors of Science in Biochemistry in 2006. From 2003-2006, he worked as a technical aide at 3M company in the medical division. In 2006, Jordan was accepted into the University of Missouri-Columbia PhD program in Biochemistry. Jordan joined Dr. Mark Hannink's lab where he worked on the characterization of the protein PGAM5. He completed his PhD in Biochemistry in July of 2013.